Computational Screening of Zeolitic Imidazolate Framework/Polymer Mixed Matrix Membranes for Gas Separations

by

Gamze Yılmaz

A Thesis Submitted to the
Graduate School of Engineering
in Partial Fulfillment of the Requirements for
the Degree of

Master of Science
in
Chemical and Biological Engineering

Koç University

July 2013

Koç University

Graduate School of Sciences and Engineering

This is to certify that I have examined this copy of a master's thesis by

Gamze Yılmaz

and have found that it is complete and satisfactory in all respects,
and that any and all revisions required by the final
examining committee have been made.

Committee Members:

_____

Seda Keskin Avcı, Ph.D. (Advisor)

_____

Özlem Keskin Özkaya, Ph.D.

_____

Demircan Canadinç, Ph.D.

Date: _____

ABSTRACT

Metal organic frameworks (MOFs) are nanoporous inorganic-organic hybrid materials. Zeolitic imidazolate frameworks (ZIFs), composed of transition metal ions and imidazolate type organic linkers, are a subclass of MOFs. Many MOFs have been synthesized to date since these materials have been reported to be highly promising in gas separation applications. They are alternatives to traditional nanoporous materials which are used as adsorbents and membranes in gas separation processes. In this thesis, two structurally similar ZIFs, ZIF-11 and ZIF-12, which have not been examined as gas separation adsorbents and membranes yet, were studied for separation of H_2/CH_4, H_2/CO_2 and CO_2/CH_4 mixtures using atomically detailed simulations. Results showed that ZIF-11 and ZIF-12 outperform many nanoporous membranes and adsorbents for separation of CO_2 from CH_4 and H_2. Although MOFs are promising membranes, fabrication of defect free thin film MOF membranes is challenging. Mixed matrix membranes (MMMs) combine high selectivity and permeability of MOFs with processability of polymers. Gas permeability and selectivity of MOF-based MMMs for H_2/CH_4, H_2/CO_2, CO_2/CH_4 and CO_2/N_2 separations were examined combining atomically detailed simulations and theoretical permeation models. The results were compared with the available experimental data to test the accuracy of the calculation methods. After showing the good agreement between the predictions of theoretical methods and experiments, gas separation performances of 750 new MMMs composed of various polymers and MOFs were estimated. It was observed that MOF-based MMMs generally have higher gas permeabilities and selectivities compared to pure polymer membranes. Performances of MMMs containing two different types of fillers were also predicted using a new methodology introduced in this thesis. Effects of filler flexibility, filler loading and operation conditions on separation performance of MOF-based MMMs were also investigated.

ÖZET

Metal organik kafesler (MOF) organik-inorganik yapılı nanogözenekli malzemelerdir. Zeolit imidazolat kafesler (ZIF) MOFların alt grubudur ve geçiş metal iyonları ile imidazolat tipli organik bağlayıcılardan oluşmaktadır. MOFlar gaz ayırma işlemlerinde umut verici olduğu için şimdiye kadar çok sayıda MOF sentezlenmiştir. Bu malzemeler adsorban ve membran olarak sıklıkla kullanılan nanogözenekli diğer yapılara alternatiftir. Bu tezde şimdiye kadar gaz ayırma adsorbanı ve membranı olarak değerlendirilmemiş benzer yapıda olan iki ZIF, ZIF-11 ve ZIF-12, atomik detaylı simülasyonlar kullanılarak H_2/CH_4, H_2/CO_2 ve CO_2/CH_4 karışımlarının ayrımı için çalışılmıştır. Sonuçlar ZIF-11 ve ZIF-12'nin CO_2'i CH_4 ve H_2'den ayırma işlemlerinde birçok nanogözenekli membran ve adsorbana göre daha iyi olduğunu göstermiştir. MOFlar membran olarak umut verici olsalar da, hatasız ince film MOF membran üretimi oldukça zordur. Karışık yataklı membranlar (MMM) MOFların yüksek gaz geçirgenliği ve seçiciliği ile polimerik membranların işlenebilirliğini birleştirir. MOF dolgulu MMMlerin H_2/CH_4, H_2/CO_2, CO_2/CH_4 ve CO_2/N_2 ayırımı için gaz geçirgenliği ve seçiciliği atomik düzeyde detaylı simülasyonlar ile teorik geçirgenlik modelleri birleştirilerek hesaplanmıştır. Sonuçlar deneysel veri ile karşılaştırılarak kullanılan hesaplama tekniklerinin doğruluğu test edilmiştir. Teorik tahminlerin deneysel sonuçlarla uyumlu olduğu gösterilip, polimerler ve MOFlardan oluşan 750 adet yeni MMMnin gaz ayırma performansları tahmin edilmiştir. MMMlerin genellikle saf polimer membranlara göre daha yüksek gaz geçirgenliği ve seçiciliği gösterdiği gözlenmiştir. İki farklı çeşit dolgu içeren MMMlerin gaz ayırma performansları bu tezde tanıtılan yeni bir yöntem ile tahmin edilmiştir. Ayrıca, dolgu parçacıklarının yapı esnekliğinin, dolgunun polimerdeki miktarının ve membran işletim koşullarının MMMlerin ayırma performansına olan etkileri araştırılmıştır.

ACKNOWLEDGEMENTS

This thesis is dedicated to the most precious people in my life, my parents and my brother who have always supported, helped and believed me throughout my life.

I want to express my deeply-felt thanks to my advisor, Dr. Seda Keskin Avcı, for her endless support, motivation and patience since the first day of my thesis studies. The preparation of this study would not have been possible without her advises and valuable comments. I would like to thank my dissertation committee members, Dr. Özlem Keskin Özkaya and Dr. Demircan Canadinç for providing thoughtful comments and willingly sparing their precious time for my dissertation. I also thank all the other Chemical Engineering professors at Koç University and Izmir Institute of Technology (IZTECH) who teach and support me.

It is impossible not to mention the Nanomaterials, Energy and Molecular Modeling Research Group (NEMO) members, who were always with me whenever something went wrong or something disappointing occurred. With an ability to maintain an enthusiastic atmosphere, they always made me feel like home. My special thanks go to İlknur Eruçar, who has been like a sister more than a friend. I am also indebted to my many colleagues apart from group NEMO members for their friendship.

Last but not the least, I am most grateful to my best friend Ömer Buğra Kanargı for his endless care and support not only for my studies but for me, as well. My happiness and success will be with us during our journey of life that we are about to start together.

Finally, I gratefully acknowledge the financial support from the Scientific and Technological Research Council of Turkey (TÜBİTAK) National Young Researchers Career Development Programme (3501) through the grant number 111M314.

GAMZE YILMAZ

04.07.2013

TABLE OF CONTENTS

LIST OF TABLES

LIST OF FIGURES

NOMENCLATURE

AARE	average absolute relative error
c_i	concentration of species i at upstream side of membrane
$D_{self,i}$	self-diffusion coefficient of species i
$D_{o,i}$	corrected-diffusion coefficient of species i
$D_{t,i}$	transport-diffusion coefficient of species i
f_i	fugacity of species i
$IS_{(i/j)}$	ideal selectivity for species i over species j
J	steady state flux
l_I	interface thickness in MMM
MMM	mixed matrix membrane
MOF	metal organic framework
N	number of molecules
N*	number of experimental data points
P	permeability of MMM
$P_{d\text{-}pure,i}$	permeability of pure MOF or ZIF membrane for pure species i
$P_{d\text{-}mix,i}$	permeability of pure MOF or ZIF membrane for species i in mixture
P_m	permeability of continuous phase in MMM
P_{MMMw2F}	permeability of MMM having two different types of fillers
P_r	relative permeability of MMM
P_{eff}	effective permeability of pseudo insert phase in MMM
P_I	permeability of interface in MMM
P^{cal}	Permeability calculated by models (AARE equation)

P^{exp}	Permeability taken from experiments (AARE equation)
q_i	partial point charge of atom i
r_d	insert radius in MMM
$r_i(t)$	position vector of species i tracked in time t
$S_{ads(i/j)}$	adsorption selectivity for species i over species j
$S_{diff(i/j)}$	diffusion selectivity for species i over species j
$S_{perm(i/j)}$	permeation selectivity for species i over species j
TCF	thermodynamic correction factor
x_i	mole fraction of adsorbed component i
y_i	mole fraction of component i in bulk phase
ZIF	zeolitic imidazolate framework

Greek letters

β	reduced permeation polarizability
β^*	matrix rigidification factor
ε	Lennard Jones energy parameter
ε_0	dielectric constant
ϕ	volume fraction of filler particles
ϕ_I	volume fraction of the interface
ϕ_m	maximum packing volume fraction of particles
ϕ_s	volume fraction of dispersed phase in pseudo insert
λ_{dI}	permeability ratio of P_d/P_I
λ_{dm}	permeability ratio of P_d/P_m
λ_{lm}	permeability ratio of P_I/P_m
σ	Lennard Jones size parameter
δ	ratio of outer radius of interfacial shell core radius

Δp	pressure gradient between upstream and downstream sides of membrane
Δx_i	working capacity for species i
∇c	concentration gradient

Chapter 1

INTRODUCTION

Separation processes are necessary in industrial chemical plants since they are key operations used to manufacture high purity products after a number of chemical processes and treatments. For example, separation of CO_2 from CH_4, H_2 and N_2 and separation of CH_4 from H_2 are industrially important treatments. Separation of CO_2 from N_2 is crucial since flue gas emissions are responsible for 33-40% of the total CO_2 released to the atmosphere.[1] The anthropogenic carbon dioxide emissions have significant effects on global warming. By a more realistic view, average surface temperature (the average of near surface air temperature over land and sea surface temperature) rise is estimated to be between 1.4 and 5.8°C by 2100. CO_2/N_2 separations are needed in power plants before the discharge of flue gas emissions to the atmosphere.[2] CO_2 should be separated and captured from natural gas streams which is composed of mainly CH_4 (typically 75-90%) and CO_2 (5-10%) with minor gas impurities (nitrogen and heavier hydrocarbons). This separation is necessary for enrichment of natural gas and reduction of pipeline corrosion due to acidic nature of CO_2. CO_2/H_2 separations are required for hydrogen recovery from plants and refineries. Separation of CH_4 from H_2 to provide pure H_2 after steam reforming of natural gas is important since about 80% of H_2 is produced from steam reforming of natural gas.[3]

Separation technologies include adsorption and membrane-based separation together with traditional methods, such as distillation, absorption, extraction, crystallization and drying. Among many separation processes, it is important to choose the most feasible and economic one for desired separation application. Cryogenic distillation, absorption, adsorption and membrane separation are widely used for gas separation applications.[2, 4-6] Cryogenic distillation which requires high pressure and low temperature to separate gas mixtures depending on the boiling point difference of the components is the mostly used process for separation of gas mixtures. Demands of high capital cost to construct a series of heat exchangers and compressors and operational cost to satisfy energy requirement are the main problems associated with this process. Absorption depends on attachment of gas molecules into a solvent and it is widely applied in the natural gas and chemical industries for the capture of CO_2.[6] However, it suffers from cost as well as the difficulty of finding the appropriate solvent.

Adsorption-based gas separation has well developed with the synthesis of new adsorbent materials exhibiting high surface area, large pore volume and high porosity. For example, zeolites have played a major role in development of adsorption technology.[7] Conventional adsorbent materials used in industry are silica gel, activated carbon, activated alumina, zeolites and metal oxides. Metal organic frameworks (MOFs) are a recent group of crystalline, porous materials used in adsorption-based gas separation processes. Reaction of organic bridging ligands with metal ions builds up porous, crystalline MOF networks. MOFs generally have strong bonds that provide robustness, linking units that allow modification of chemical properties via organic synthesis and geometrically well-defined structures. It is possible to design a huge number of MOFs with a broad range of structural, chemical and catalytic properties from combinations of wide choice of metals and organic ligands. Zeolitic imidazolate frameworks (ZIFs), a subclass of MOFs, are tetrahedral networks constructed by linkage of transition metals (Zn, Co, Fe, Cu) and imidazolate (Im)

type linkers. ZIFs are synthesized by reaction of hydrated transition metal salt (usually nitrate) with ImH in an amide solvent. During this process, ImH deprotonates due to thermal degradation of the amide solvent and links to metal side.[8]. Combinations of transition metals with available imidazolate linkers allow synthesis of a large diversity of ZIFs. Besides the tunability, ZIFs exhibit chemical stability and permanent porosity. For example, ZIF-8 and ZIF-11 maintained fully crystallinity and found to be insoluble in solvents for at least 3 days when they were suspended into boiling benzene, methanol, water and aqueous sodium hydroxide.[9]

An ideal adsorbent for commercial applications should have high selectivity, high adsorption capacity, chemical and thermal stability, low cost and regenerability. Regenerability is a key property of an adsorbent. For regeneration, temperature swing adsorption (TSA) or pressure-swing adsorption (PSA) methods are employed. In the PSA process, the adsorbent is regenerated by applying low pressure desorption process after higher pressure adsorption process. If the desorption pressure is less than 1 bar, the process is vacuum swing adsorption (VSA). PSA is generally used in recovery of CO_2 from flue gas streams,[10-13] purification of H_2 after steam reforming of methane [14-16] and natural gas enrichment.[17] In the TSA process, regeneration is achieved by heating the adsorbent with the adsorbed gas product. The number of TSA cycles achievable at a given time is less than that of PSA since heating and cooling processes are slow. A much more rapid recycling is possible in PSA and larger quantities of impurities can be removed at a given time. PSA is more preferable than TSA due to lower energy demand and higher regeneration rate.[18] Based on the interactions between adsorbate and adsorbent material, adsorption can be categorized as physisorption and chemisorption. In physisorption, the interactions between adsorbate and adsorbent are weak and there is no chemical reaction whereas chemical bonds are formed in chemisorption.

Membranes are semipermeable thin barriers used to separate gases from their mixtures under a variety of driving forces, such as hydrostatic pressure difference, temperature difference, concentration difference, partial pressure difference or electrical potential gradient. Membrane-based separations have potential to save large amounts of energy since phase transition is not involved. They are also highly reliable (no moving parts) and environmentally friendly compared to conventional separation technologies. Efforts on development of efficient and economical membrane-based gas separation increase demands to fabricate membranes with high permeability, high selectivity and chemical and mechanical stability.

Performance of a membrane is mostly determined by two parameters, permeance and selectivity. Permeance is the rate of flow of a fluid per unit area of membrane per unit driving force across the membrane thickness. Selectivity is the ratio of permeation rates of the gas components. Both high permeance and high selectivity are required for an efficient and economic membrane separation process. If a membrane has high gas permeance, it requires less area and thus less capital cost. High selectivity means high purity, less complexity of membrane units and lower capital cost. Gas separation in a membrane depends on permeate molecule size and pore size and pore size distribution of membrane material. Membranes can be classified into two: non-porous (dense) and porous (microporous and macroporous) membranes. Dense membranes have pores which are generally less than a few Angstroms. Gas components must dissolve in membrane to be separated since they are not able to pass through otherwise. Microporous membranes contain interconnected pores in range of 10-100.000 Å diameter which are larger than dense membranes but much smaller than macroporous ones. Pores of microporous membranes generally have sizes similar to kinetic diameters of gas molecules thus microporous membranes are accepted as promising candidates due to their dominant size sieving property compared to dense and macroporous membranes. For example,

permeability of a molecule in a membrane whose pore size is smaller than kinetic diameter of the molecule is low. However, selectivity is high if the molecule is separated from another molecule whose kinetic diameter is smaller than pore size of the membrane. Macroporous membranes have large pores and they are generally used as support materials on thin dense and microporous membranes when any significant pressure difference in process conditions should be overcome to achieve reasonable output. Theoretical basis of transport through membranes depends on pores size of the membrane and kinetic diameter of the molecules. Figure 1.1 shows schematic representation of transport mechanisms in membranes. Convective fluid flow occurs when molecule's kinetic diameter is less than the pore diameter, as shown in Figure 1.1 (a). The convective flow is either Poiseuille or Knudsen type depending on the ratio of pore diameter to mean free path of the molecules. If the ratio is much less than one, Knudsen flow predominates. In the Knudsen-flow regime, molecules collide primarily with the pore walls rather than with other gas molecules.[19] Figure 1.1 (b) shows transport based on diffusion which can be described as random walk of molecules under chemical potential, concentration or partial pressure difference when bulk pressure is same on both sides of the membrane. Figure 1.1 (c) demonstrates molecular sieving mechanism in which a membrane's pore size is larger (smaller) than the kinetic diameter of small (large) gas molecules and only gas molecules with small kinetic diameter can pass through the pores. Convective flow and gas diffusion are predominant mechanisms for porous membranes whereas dense membranes allow access of the molecules through solution-diffusion mechanism which is shown in Figure 1.1 (d). In solution-diffusion mechanism, gas molecules dissolve and then diffuse through the membrane. Gas permeation through diffusion-solution mechanism is usually considered to consist of three steps: (1) adsorption upon the upstream boundary, (2) activated diffusion through the membrane and (3) dissolution or evaporation from the downstream

boundary.[20] Solution-diffusion mechanism is usually dominant in polymeric membranes while molecular sieving occurs in inorganic membranes.

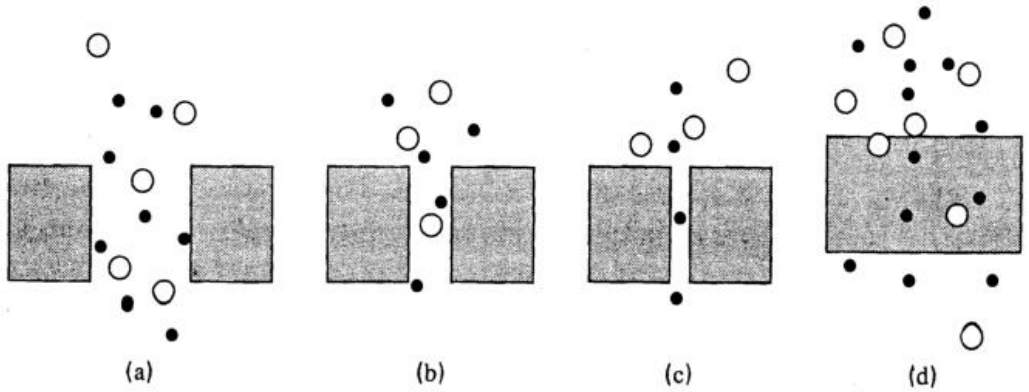

Figure 1.1: Transport mechanisms in membranes. (a) Convective flow through the pores; (b) diffusion through the pores; (c) molecular sieving; (d) solution-diffusion mechanism.[21]

Polymeric membranes are made of either natural or synthetic polymers. Natural polymers are naturally occurring polymers including wool, rubber and cellulose. Synthetic polymers are chemically synthesized by polymerization of a monomer by condensation (step reactions), addition (chain reactions) or copolymerization of two different monomers. Polymeric membranes are the most widely preferred membranes in gas separation processes due to their ease of fabrication, cost effectiveness, low energy requirement, high mechanical stability and easy scalability. They are used in industry for air separation, hydrogen separations (H_2/CH_4, H_2/CH_4 and H_2/CO separations in refineries), separation of CO_2 from CH_4 for natural gas purification and separation of CO_2 from N_2 for flue gas treatment.[22] Unfortunately, the most serious problem limiting the efficiency of polymeric gas separation membranes (polyimides, polysulfones, polyacetylenes, polypyrrolones and polymers of intrinsic microporosity) is trade-off relation between permeability and

selectivity which is valid for a large group of gas pairs including CO_2/CH_4, CO_2/N_2, H_2/CH_4, H_2/CO_2 and H_2/N_2 and O_2/N_2.[23] The limit of the performance was shown by Robeson et al. in 1991 and 2008.[23, 24] Robeson et al.[23, 24] represented gas separation performance of polymers by locating them on a plot having logarithmic axes of ideal selectivity of gas pair and permeability of more permeable gas. Permeability-selectivity data of gas pairs on Robeson's plot were collected from the experimental studies that tested the polymers on the same experimental conditions, in a temperature range of 25-35ºC under 2 bar. In 1991, Robeson et al. showed that [23] ideal selectivity of polymeric membranes generally decreases with increasing permeability of the more permeable gas component and a line determining the limit (upper bound) for the gas selectivity and permeability that can be achieved by polymeric membranes was set. The location of this upper bound was updated in 2008 by including new polymer membranes and it was reported that new upper bound positions have only minor shifts for many gas pairs.[24]

Polymers that are more permeable are generally less selective and vice versa. Polymers close to upper bound are generally glassy polymers. Glassy polymers have rigid chains and show molecular-sieving ability by allowing smaller gas molecules to diffuse rapidly than larger ones. Thus, they have high selectivity, but low permeability. On the other hand, rubbery polymers generally exhibit low selectivity but high permeability since they have flexible chains and allow non-selective passage of gas molecules through the membrane.

The trade-off penalty of the polymeric membranes has accelerated investigation of new materials that can improve efficiency of membrane separation processes. Inorganic membranes have been widely studied to separate gas mixtures due to higher permeabilities and selectivities as well as higher thermal and chemical stabilities compared to polymeric membranes. However, inorganic membranes suffer from high cost, low mechanical stability and complicated manufacturing procedures. MOFs having hybrid organic-

inorganic nature exhibits properties that are combination of the properties of both organic and inorganic porous materials. MOFs and ZIFs are mechanically less stiff and brittle and exhibit higher porosity and larger surface area than inorganic materials and they have higher selectivities and permeabilities than polymers.[25] Although they are shown to be promising materials for thin film membrane-based separations, they still have problems associated with scaling up and it is difficult to fabricate defect-free thin film MOF membranes.[26]

Recent studies have concentrated on development of new approaches to overcome the aforementioned deficiencies (e.g. low flux, selectivity, mechanical and chemical stability) of membranes and draw the required separation characteristics together. For example, two polymers have been blended together to take the advantage of different properties of polymers,[27] surface of membranes have been modified to adjust hydrophilicity, charge and roughness,[28] and polymers have been chemically cross-linked to improve chemical stability.[29] Another promising approach is addition of micro or nanoparticles into polymer matrix to form composite membranes. Composite membranes or mixed matrix membranes (MMMs) are heterogeneous materials that consist of molecular sieve type fillers dispersed into polymer matrix. MMMs combine the processability, low cost and mechanical stability of polymer phase (continuous phase) with the outstanding gas separation properties, thermal and mechanical stability of molecular sieving phase (dispersed phase). The first MMMs were prepared in the 1980s and have been increasingly investigated in recent years. Besides good separation properties, fabrication of MMMs is also practical once the polymer matrix and filler particles are available.

Morphology and separation performance of MMMs are affected from the materials that build up the MMM. Thus, it is fundamentally important to match the continuous phase with a proper dispersed phase. There are many polymers and molecular sieve type of fillers

that have been considered as membranes separately. However, combination of two creates a huge number of MMMs; thus, economical, time efficient and practical methods to screen this huge number of MMMs are needed.

The aim of the thesis is to provide molecular-level insights for adsorption and membrane-based separation of the gas mixtures. Atomically detailed simulations were used to evaluate two ZIFs, ZIF-11 and ZIF-12, as adsorbents and membranes. ZIF-11 and ZIF-12 were found to be very promising membranes and adsorbents for CO_2 separations. Exceptionally high membrane performance of these ZIFs aroused interest in testing these materials as filler particles in polymers. Therefore, a variety of ZIFs were screened as filler particles in MMMs for CO_2/CH_4, CO_2/H_2 and CH_4/H_2 separations. Moreover, more detailed separate study was performed for CO_2/N_2 separation using MOFs reported to have very high gas separation performance.

In Chapter 2, studies on adsorption and membrane separation performances of ZIFs were reviewed. MMM concept was explained in detail and experimental and theoretical literature on MMMs containing MOFs and ZIFs as filler particles were summarized.

In Chapter 3, MOFs, ZIFs and polymers for which the calculations were performed were presented. The molecular models used for adsorbate molecules, methodology used for adsorption and diffusion simulations and permeation models used for prediction of MMMs' permeability were described.

In Chapter 4, adsorption and membrane performances of ZIF-11 and ZIF-12 were examined and compared with other nanoporous materials.

In Chapter 5, the accuracy of permeation models described in 0 was tested for ZIF-based MMMs. After showing good agreement between experiments and simulations, a series of ZIF-based MMMs were evaluated for H_2/CH_4, CO_2/CH_4 and H_2/CO_2 separations.

In Chapter 6, permeability and selectivity of MOFs for CO_2/N_2 separation were presented. Effect of filler framework flexibility on permeability of MMMs was

investigated. Permeability of MMMs containing two different types of filler particles were predicted using a new methodology introduced in this thesis. The results of calculations were validated with experimental data.

Finally, in Chapter 7, outcomes of predictions in Chapter 4, Chapter 5 and Chapter 6 were summarized. Advantages of simulations and experimental efforts needed to complement limitations of simulations were discussed.

Chapter 2

LITERATURE REVIEW

Zeolites have been widely studied as adsorbents and membranes in purification and separation of gases.[30] There has been a long-standing challenge to synthesize a variety of zeolites using structure directing agents to orient the synthesis of zeolites toward a particular structure with higher acid-catalytic activity, sorption capacity and thermal and chemical stability.[31] However, 200 different structures could be synthesized with lack of development in chemical and physical properties.[32] The efforts for fabrication of materials with more promising properties directed researchers towards inclusion of metals with higher electronic and steric effects into frameworks to strengthen the interactions between the adsorbate and the crystal structure. Synthesis of the strongly bonded networks formed from self-assembly of metal ions and polyatomic organic bridging ligands is known as reticular synthesis and it allows the preparation of tunable MOF structures (see Figure 2.1) for which the composition, structure and functionality can be systematically varied. Theoretically infinite number of MOF structures having different physical and chemical characteristics can be synthesized. ZIFs are synthesized by combining highly polar imidazole linkers with transition metals and they are considered to be as promising materials for adsorption and membrane-based separations.[9, 32-34]

2.1. ZIFs as Adsorbents

A number of experimental and computational studies have been performed to evaluate the potential of ZIFs as adsorbents.

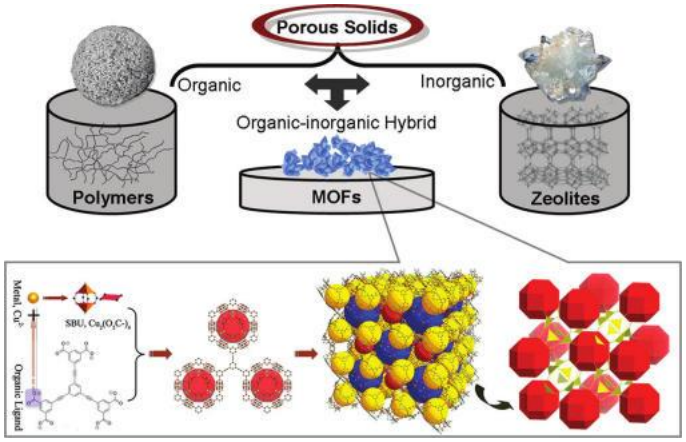

Figure 2.1: Classification of porous solids and general procedure for construction of MOFs.[35]

Park et al.[9] synthesized a group of ZIFs, ZIF-1 to ZIF-12, using Zn(II) (ZIF-1 to ZIF-4, ZIF-6 to ZIF-8 and ZIF-10 to ZIF-11) or Co(II) (ZIF-9 and ZIF-12) with imidazolate-type linkers and evaluated the performance of ZIF-8 and ZIF-11 as adsorbents for H_2 separation at 77 K. ZIF-8 was found to have lower H_2 uptake at low pressures (0-1 bar) whereas H_2 uptake in ZIF-8 was found to be close to that in ZIF-11 as pressure increases to 1 bar. The high H_2 uptake in ZIF-11 at low pressures was attributed to the benzene rings of the structure which create favorable hydrogen adsorption sites at low pressures. At higher pressures, physical properties such as surface area and pore volume dominantly affected H_2 adsorption and more H_2 molecules occupied the larger pores of ZIF-8. Huang et al.[36] investigated adsorption of pure CO_2, CO, CH_4 and N_2 in ZIF-8 and

estimated CO_2/CO, CO_2/CH_4, CO_2/N_2, CH_4/N_2 and CH_4/CO selectivities using Henry's law constants of the single component adsorption isotherms at 273, 298, 323 and 348 K. Selectivity was found to be strongly correlated with the differences of isosteric heat of adsorption (Q_{st}) between the two components: the larger the differences of Q_{st} between the two components, the bigger the selectivity. Binary gases having larger selectivity were more sensitive to temperature. Effect of temperature on adsorption of a component with large Q_{st} is more pronounced than the one with smaller Q_{st}. This difference leads to a larger effect of temperature on selectivity. Banerjee et al.[32, 34] focused on the effect of substituent groups on CO_2 adsorption in several studies. They synthesized, characterized and assessed CO_2 capture properties of a number of ZIFs having the same topology: ZIF-68, ZIF-69, ZIF-70, ZIF-78, ZIF-79, ZIF-80, ZIF-81 and ZIF-82. CO_2 capture capacity ranking of ZIFs was consistent with the ranking of the polarity of functional groups: $-NO_2$ (ZIF-78) > $-CN$, $-Br$, $-Cl$ (ZIF-82, ZIF-81, ZIF-69) $-C_6H_6$, $-Me$ (ZIF-68, ZIF-79) > $-H$ (ZIF-70). CO_2 capture performances of these materials were compared with an industrially used adsorbent, BPL carbon (an activated carbon) [37] and it was found that all ZIFs exhibit superior ability to store CO_2 compared to BPL carbon. Selectivities of ZIF-68, ZIF-69 and ZIF-70 for CO_2/CO (50/50:vol/vol) mixture were also reported to be higher than that of the BPL carbon for this mixture. Wang et al.[33] synthesized ZIF-95 and ZIF-100, measured CO_2, CH_4 and CO adsorption isotherms at room temperature and compared the results with the measurements of Banerjee et al.[32, 34]. They found that ZIF-95 and ZIF-100 show high CO_2 adsorption properties although CO_2 uptake of ZIF-100 is less than that of ZIF-69. One liter of ZIF-100 ($-C_6H_6$ linker) can hold up to 28.2 liter of CO_2 at 273 K whereas 1 liter of ZIF-69 stores 82.6 liter of CO_2 at 273 K. The equimolar mixture adsorption selectivities for CO_2 over CH_4, CO and N_2 of ZIF-100 (ZIF-95) were reported as 6, 17 and 25 (3, 8 and 11), respectively.

The number of computational studies is higher than the experimental studies on ZIF-based adsorption. Some of the computational studies reported effect of structural properties on gas adsorption. Guo et al.[38] investigated CH_4/H_2 separation in ZIF-3, ZIF-8, ZIF-10, ZIF-60 and ZIF-67 as well as IRMOF-1 (isoreticular metal organic framework-1) using Grand Canonical Monte Carlo simulations (GCMC). IRMOF-1 (also known as MOF-5) had the highest uptake for both H_2 and CH_4 due to its pore volume which is larger than the ZIFs', but CH_4 selectivity over H_2 of IRMOF-1 was found to be the less since it has nonselective pores compared to ZIFs. It was also shown that adsorption characteristic of ZIFs depends on the topology. ZIFs having the same topology have similar H_2 and CH_4 isotherms and similar CH_4/H_2 selectivities. (e.g., SOD topology: ZIF-8 and -67, MER topology: ZIF-10 and -60). Han et al.[39] investigated H_2 uptake in several ZIFs: ZIF-2, ZIF-3, ZIF-8, ZIF-10, ZIF-11, ZIF-68, ZIF-69, ZIF-70, ZIF-78 and ZIF-79 at 77 and 298 K up to 100 bar. ZIF-68, ZIF-69, ZIF-70, ZIF-78 and ZIF-79 have GME topology and they were studied to determine the influence of functional groups on H_2 adsorption. They observed that at low pressures (e.g., 10^{-2} bar), H_2 uptake is correlated with the type of functional groups since adsorption is affected by polarity of the functional group. The sequence of H_2 uptake in all ZIFs was found as follows: ZIF-78 (1.10 wt%) > ZIF-69 (0.81 wt%) > ZIF-79 (0.69 wt%) > ZIF-68 (0.64 wt%) > ZIF-70 (0.20 wt%) which is consistent with the findings of Banerjee et al.[32, 34]. At higher pressures H_2 uptake of ZIFs were found to be dependent on surface area and pore volume. They also underlined the fact that an ideal pore size does not guarantee high gas uptake as in ZIF-11 with pore aperture diameter of 3.0 Å that is very close to the kinetic diameter of H_2 (2.8 Å). It was concluded that H_2 adsorption at high (low) loadings is related with surface area and pore size (topology and functional groups) of ZIFs. Similarly, Chen et al.[40] studied H_2 adsorption in ZIF-68, ZIF-69, ZIF-78, ZIF-79 and ZIF-81 at 77 K under pressures 0.1 to 80 bar and 0.1 bar to 1 bar. They showed that at low (high) pressures, substituent groups (effective

porosity) cause differences in hydrogen uptake in ZIFs and the order of H_2 uptake is same with the one reported by Banerjee [32, 34] and Han et al.[39]. Effect of central metal ion on H_2 adsorption was also investigated. Chen and coworkers studied H_2 uptake of three groups of ZIFs having identical structural properties except the central metal atoms: (1) ZIF-7 and ZIF-9, (2) ZIF-11 and ZIF-12 and (3) ZIF-8 and ZIF-67; the first and second ZIFs in these groups have Zn and Co atoms, respectively. The H_2 adsorption isotherms of these groups were found to be very close to each other which shows that central metal atoms have nearly no effect on H_2 adsorption, at least in case of Zn and Co ions.

2.2. ZIFs as Thin Film Membranes

A handful of ZIFs were fabricated as thin film membranes. These are ZIF-7, ZIF-8, ZIF-22, ZIF-69, ZIF-78 and ZIF-90. Li et al.[41] prepared ZIF-7 membranes and tested their gas separation performance at 200°C and 1 bar. They reported permeance of H_2, CO_2, N_2 and CH_4 as pure components and in equimolar mixtures (H_2/CO_2, H_2/N_2 and H_2/CH_4). ZIF-7 (3.0 Å) was specifically chosen for separation of H_2 (2.9 Å) from larger gas molecules since ZIF-7 could show molecular-sieving effect due to its pore size which is slightly larger than the kinetic diameter of H_2 but smaller than the kinetic diameter of other gases. ZIF-7 membranes were reported to have good thermal and hydrothermal stabilities. H_2/CO_2, H_2/N_2 and H_2/CH_4 separation factors were found as 13.6, 18.0 and 14.0, respectively. Separation factor is defined as the molar ratio of components in the permeate side divided by the molar ratio of components in the retentate side. CO_2, N_2 and CH_4 did not block ZIF-7 pores and permeance of H_2 as a single component was found to be slightly higher than permeation of H_2 in the presence of other gas molecules. This was attributed to the competition between the molecules in binary mixtures. Bux et al.[42] fabricated ZIF-8 membranes and measured permeance of CO_2, O_2, N_2 and CH_4 as single gases and permeance of H_2 and CH_4 in equimolar mixture through ZIF-8 membrane at room temperature. H_2/CH_4 separation factor was 11.2 which is higher than the separation factor

of CuBTC (BTC=benzene-1,3,5-tricarboxylate) (also known as HKUST-1) membrane measured at the same conditions.[43] Comparison of single-gas permeance of H_2 with the mixed-gas one showed that pure H_2 permeance is slightly higher than the permeance of mixed gas and this experimental finding was consistent with the study of Li et al.[41]. Permeation of mobile H_2 molecules slowed down due to presence of slower CH_4 molecules. Huang et al.[44] reported permeance of pure H_2, CO_2, N_2 and O_2 and selectivities of 1:1 mixtures of H_2 with CO_2, N_2 and O_2 through ZIF-22 membrane at 323 K under atmospheric pressure. Separation factors were measured as 7.2, 6.4, 6.4 and 5.2 for H_2/CO_2, H_2/O_2, H_2/N_2 and H_2/CH_4, respectively. Separation factors of ZIF-22 membrane were reported to be high among separation factors of MOF and zeolite membranes. Dong et al.[45] fabricated ZIF-78 membrane and measured permeance of pure H_2, CO_2, N_2 and CH_4 and separation factors of H_2/CO_2, H_2/N_2 and H_2/CH_4. Order of single gas permeance was reported as: $H_2 > N_2 > CH_4 > CO_2$. This order is same with the kinetic diameter order. Relatively low permeance of CO_2 was attributed to strong interaction between CO_2 molecules and the functional linker of ZIF-78 which led to very low diffusivity. Separation factors of H_2/CO_2, H_2/N_2 and H_2/CH_4 were reported as 9.5, 5.7 and 6.4, respectively. H_2/CO_2 separation performance (with a H_2 permeability of 7.2×10^3Barrers) of ZIF-78 was found to be above the upper bound of the Robeson plot.[24]

The importance of choice of membrane fabrication method and the difficulty of fabrication of defect-free thin layer membranes were highlighted in several studies. Huang et al.[46] developed a new method to prepare continuous ZIF-90 membrane using a covalent linker between ZIF-90 layer and support. They measured permeance of pure H_2, CO_2, CH_4 and C_2H_4 and separation factors of H_2/CO_2, H_2/N_2, H_2/CH_4 and H_2/C_2H_4. For 1:1 binary mixtures, separation factors of H_2/CO_2, H_2/N_2, H_2/CH_4 and H_2/C_2H_4 were 7.3, 11.7, 15.3 and 62.8, respectively at 200°C and 1 bar. Effect of temperature on H_2 permeation and H_2/CH_4 selectivity were also investigated. H_2 permeance in H_2/CH_4 mixture was reported

to increase from 1.32×10^{-7} to 2.85×10^{-7} mol·m^{-2}·s^{-1}·Pa^{-1} when temperature increased from 25 to 225°C at 1 bar while H_2/CH_4 selectivity increased from 7.0 to 16.4 under the same conditions. The pronounced selectivity increase is related with the adsorption-diffusion mechanism. At lower temperatures, CH_4 molecules blocked the pores of ZIF-90 and prevented the passage of H_2 molecules whereas at high temperatures, less CH_4 molecules were adsorbed thus H_2 molecules were able to diffuse and larger H_2 permeation observed compared to CH_4 permeation. The same group [47] fabricated ZIF-90 membranes and studied H_2/CO_2 separation. They used covalent post-functionalization method to prepare ZIF-90 membranes in order to reduce non-selective transport through invisible intercrystalline defects which they faced in their earlier study.[44] Huang and coworkers measured H_2/CO_2 separation factor as 16.2 which is better from the previously measured one. Liu et al.[48, 49] fabricated and tested ZIF-69 membranes using in situ solvothermal [48] and seeded growth [49] method. In their first study, they performed experiments to measure permeation of pure H_2, CO, CH_4 and SF_6 and selectivity of equimolar binary mixture of CO_2/CO in ZIF-69 membranes fabricated using in situ solvothermal method. In their second study, they used the seeded growth method to compare separation performances of ZIF-69 fabricated by two different methods. The seeded growth method requires application of a layer of seeds and a synthesis solution on a support surface to carry out the continuous growth of the membrane. The permeance of pure CO_2, N_2, CO and CH_4 were measured as 23.6×10^{-9}, 10.6×10^{-9}, 8.2×10^{-9} and 8.6×10^{-9} mol·m^{-2}·s^{-1}·Pa^{-1} at 298 K under 1 bar, respectively. Separation factor of CO_2 over N_2, CO and CH_4 for equimolar binary mixtures were reported as 6.3, 5.0 and 4.6, respectively. It was concluded that under the same experimental conditions, CO_2/CO separation factor increases from 3.5 to 5.0 and permeance of CO_2 in CO_2/CO mixture increases from 3.6×10^{-8} to 1.0×10^{-7} mol·m^{-2}·s^{-1}·Pa^{-1} when membrane fabrication method is changed from situ solvothermal to seeded growth method.

A reasonable method for identifying the most promising membrane materials is using molecular simulations. Keskin et al.[50] used atomically detailed simulations to evaluate ZIF-3 and ZIF-10 as membranes for separation of CO_2/CH_4, CH_4/H_2 and CO_2/H_2 mixtures. Gas selectivity and permeability of membranes were compared with other nanoporous materials. ZIF-3 and ZIF-10 membranes were found to have promising CH_4/H_2 separation properties. However, it was reported that using these ZIFs as adsorbents is more efficient than using them as membranes. Atci et al.[51] assessed membrane-based separation performance of a number of ZIFs: ZIF-2, ZIF-3, ZIF-6, ZIF-8, ZIF-10, ZIF-60, ZIF-65, ZIF-67, ZIF-69, ZIF-79, ZIF-81 and ZIF-90. They compared CO_2/CH_4, CH_4/H_2 and CO_2/H_2 separation performance of ZIFs with zeolite and MOF membranes. ZIF-2 and ZIF-79 were found to have the highest CH_4/H_2 selectivity (10.63 and 9.19) and CH_4 permeability (3×10^5 and 1.6×10^5 Barrers, respectively) among all ZIFs. ZIF-90 was identified as a promising candidate for CO_2/CH_4 separations since CO_2 permeability and CO_2/CH_4 selectivity of ZIF-90 membrane are located above the Robeson upper bound.[24] For CO_2/H_2 separations, ZIF-2 was found to have very high permeability and selectivity compared to CuBTC, MOF-177, CHA, DDR and MFI.

2.3. Mixed Matrix Membranes

Incorporation of fillers within polymers resulted in MMMs that have better gas separation performance than pure polymers. Many porous materials have been used as filler particles in MMMs, including silica,[52] carbon molecular sieves,[53-57] zeolites [58-64] and carbon nanotubes.[65] The major challenge in fabrication of MMMs is associated with poor compatibility of the continuous (polymers) and dispersed phases (fillers).[66, 67] For example, nonselective void formation was observed in several studies due to low affinity of polymer phase for the filler phase on the polymer-additive interface.[68, 69] MMMs can be classified into two depending on the morphology: ideal and non-ideal MMMs. Figure 2.2 shows schematic diagram of an ideal MMM structure.

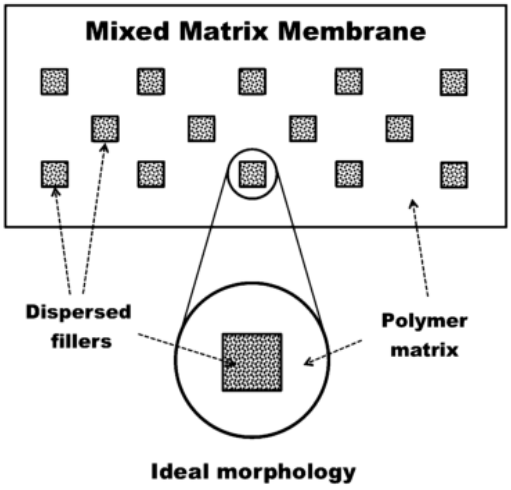

Figure 2.2: Schematic diagram of an ideal MMM structure.[70]

The interface between continuous and dispersed phase is defect free in an ideal MMM structure. Non ideal morphology is generally common since interaction between the polymer and filler phase can change the physical structure of the interface. There are three main interface defects: interfacial voids, rigidified polymer chain and blockage of filler pores. These defects are represented in Figure 2.3. Poor polymer-filler adhesion, repulsive forces between two phases, different thermal expansion coefficients, disruption of polymer chains by filler particles and solvent removal are the major causes for the formation of interfacial voids.[70] The performance of a membrane can be enhanced depending on the size of voids and gas molecules. Polymer chain rigidification occurs if strong adhesion between the polymer and filler phase exists.[71] The rigidified polymer chains have lower mobility than the original structure and it was shown that this effect generally increases selectivity while decreasing permeability.[72-76] Pore blockage occurs when filler's pores are blocked by a solvent, contaminant or minor component in feed gas or polymer chains.[66, 74, 77, 78] The pores can be blocked either totally or partially. Partial blockage

can enhance selectivity of the membrane depending on the blocked pore size of the membrane and kinetic diameter of the gas molecules. Total pore blockage causes non-selective membranes since molecules cannot pass through the membrane.

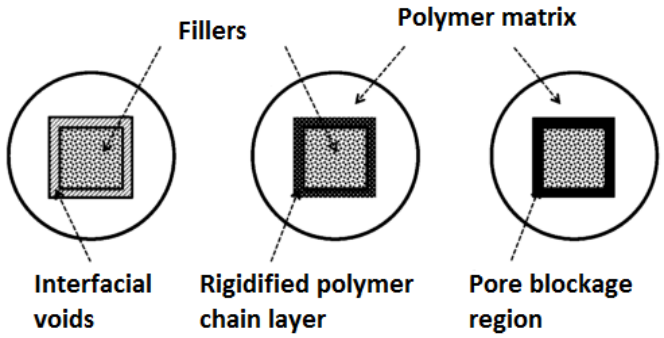

Figure 2.3: Schematic diagram of interface defects of non-ideal MMMs structures.[70]

Proper filler and polymer selection is fundamentally important. Recently, it was reported that MOFs and ZIFs have better compatibility with polymers compared to zeolites since MOFs and ZIFs contain organic ligands which may facilitate interactions with the polymer phase.[79-81] Incorporation of compatible fillers with high separation performance into polymer matrix improves the gas separation performance of MMMs. ZIFs and MOFs are also promising candidates due to their high surface area, porosity and chemical and thermal stability. Gas separation performance of inorganic membranes, polymeric membranes and MMMs are schematically presented on the Robeson plot in Figure 2.4. Figure 2.4 shows that inorganic membranes exceed the upper bounds, organic polymers are below the lines whereas MMMs are located on above and below the line specified in 2008.

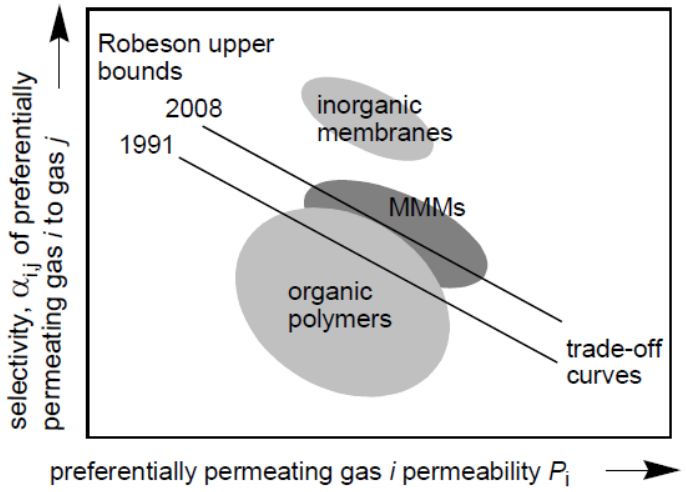

Figure 2.4: Comparison of gas separation performances of pure polymeric and inorganic membranes with MMMs on Robeson plot.[82]

2.3.1. MOF and ZIF-based MMMs

Yehia et al.[83] reported the first synthesized MOF-based MMMs that were fabricated using Cu(II)BPDC-TED (copper(II) biphenyl dicarboxylate triethylenediamine) as fillers and poly-3-acetoxyethylthiophene as polymer matrix. They measured permeability of pure CO_2 and CH_4 and reported that CO_2 (CH_4) permeability decreases (increases) with increasing filler loading. Liu and coworkers [84] reported the first patent on MOF-based MMMs, IRMOF-1 and HKUST-1 were incorporated into Ultem and Matrimid. They reported improvements in H_2, CO_2 and CH_4 permeability of MMMs relative to pure polymers while no improvement was found in H_2/CH_4 and CO_2/CH_4 ideal selectivity. Ideal selectivity is simply the ratio of pure gas permeabilities. Perez et al.[81] fabricated MOF-5/Matrimid MMMs and measured single gas (N_2, O_2, CH_4, CO_2 and H_2) permeability up to 30 wt% MOF-5 loading as well as mixed gas permeability and

selectivity [H_2/CO_2 (75/25, 50/50, 25/75: mol/mol), CH_4/N_2 (94/6, 50/50, 25/75: mol/mol) and CH_4/CO_2 (90/10, 50/50, 25/75: mol/mol)] at 30 wt% filler loading. They found that permeability of each pure gas increases with MOF-5 loading but ideal selectivity remains unchanged due to proportional increase in permeabilities of all gases as in the study of Liu et al.[84]. No improvement in H_2/CO_2 selectivity was observed whereas selectivity enhancement was reported for CH_4/N_2 and CH_4/CO_2 mixtures. Car et al.[85] prepared MMMs using CuBTC and $Mn(HCOO)_2$ (manganese (II) formate) as filler particles in polydimethylsiloxane (PDMS) and polysulfone (PSF) polymer matrix for separation of CO_2 from N_2 and CH_4. Slight improvements in ideal selectivity of CO_2 over N_2 (CO_2 over CH_4) in CuBTC/PDMS and $Mn(HCOO)_2$/PSF MMMs (CuBTC/PSF) were reported when loading of the filler particles is 10 wt% (5 wt%). Particle agglomeration caused decreases in selectivity of gas pairs with further increase in filler loading. Hu et al.[86] synthesized CuBTC crystals, incorporated them into polyimide (PI) at 3 and 6 wt% loading to prepare MMMs and tested permeance of pure H_2, CO_2, CH_4, N_2 and O_2 across CuBTC/PI MMMs. They observed that permeance of H_2 and ideal H_2 selectivity over N_2, O_2, CH_4, CO_2 increases with increasing CuBTC loading up to 6 wt%. However, decrease in permeability of N_2, O_2, CH_4 and CO_2 was reported. This result was attributed to the blockage of CuBTC pores by PI chains which restricted the penetration of larger gas molecules. Adams et al.[87] synthesized and characterized a MOF, copper terephthalic acid (CuTPA) and used it to fabricate CuTPA/polyvinyl acetate MMMs. Higher pure gas (He, O_2, N_2, CH_4, CO_2) permeabilities were reported for MMMs containing 15 wt% CuTPA compared to pure polymer matrix.

ZIFs are a subclass of MOFs and they are recently used in experimental MMM studies. A summarizing overview on experimental results of permeability of pure and mixed gases through various ZIF/polymer MMMs is provided in Table 2.1 and Table 2.2, respectively. The studies have investigated MMMs fabricated from ZIFs, such as ZIF-7,

ZIF-8, ZIF-20 and ZIF-90 and various polymers, including Matrimid, poly(1,4-phenylen ether-ether-sulfone) (PPEES), Ultem, 6FDA-DAM (6FDA: 2,2-bis (3,4-carboxy phenyl) hexafluoropropane dianhydride and DAM: diaminomesitylene), polybenzimidazole (PBI), PSF and poly (amide-b-ethylene oxide) (PEBAX). Almost every study reported improved permeability, sometimes coupled with enhanced selectivity for gas separation. As seen from Table 2.1 and Table 2.2, ZIF-8 has been the most extensively studied zeolitic imidazolate framework as filler particles in recent ZIF-based MMM experiments. Ordonez et al.[79] prepared and characterized ZIF-8/Matrimid MMMs containing fillers up to loadings of 80 wt% and tested permeability of H_2, CO_2, O_2, N_2, CH_4 and C_3H_8 and selectivity of H_2/CO_2 (50/50 mol%) and CO_2/CH_4 (10/90 mol%) mixtures in MMMs containing ZIF-8 up to loadings of 60 wt% since above this loading limit membranes were brittle and difficult to handle. They observed enhancements in permeability of pure gases through MMMs up to 40% (wt/wt) ZIF-8 loading which can be explained by the expansion in the polymer free volume due to disruption of polymer chains when filler particles are incorporated. At 50% (wt/wt) ZIF-8 loading, permeability of pure gases decreased because diffusion path length gets longer at higher ZIF-8 loadings and gas molecules follows a more tortuous path. Increasing loading up to 60% (wt/wt), a significant increase in permeability was observed for all gases since ZIF-8 particles aggregated and nonselective voids formed. Gas mixture selectivities enhanced with increase in ZIF-8 loading. Diaz et al.[88] incorporated ZIF-8 nanoparticles in PPEES and measured permeability of H_2, CO_2, O_2, N_2, CH_4, C_2H_6 and C_2H_4 through ZIF-8/PPEES containing 10, 20 and 30 wt% of ZIF-8. They observed improvements in gas permeability with addition of filler particles. This result is in agreement with the result of Ordonez et al.[79] which is related with polymer free volume increase. There are some studies that report no change in polymer free volume with increase in filler loading due to restricted motion of polymer chains resulting from strong interactions between polymer and filler.[66] They reported that there is no change in

glass transition temperature of MMMs with increase in filler loading. This observation suggests that ZIF-8 particles do not have very strong interactions with the polymer matrix that molecular mobility is not affected by the presence of ZIF-8. O_2/N_2 and H_2/N_2 separation performances of ZIF-8/PPEES at 30 wt% ZIF-8 loading were found to be close to the Robeson's upper bound line [24] while that of H_2/CH_4 and CO_2/CH_4 were below the line. Basu et al.[89] fabricated ZIF-8/Matrimid MMMs and tested CO_2/CH_4 and CO_2/N_2 mixture gas separation performance of membranes. CO_2 permeance and CO_2 selectivity over CH_4 and N_2 were found to increase with increasing filler loading. For example, they observed that CO_2 permeance (selectivity over CH_4 for CO_2/CH_4:35/65 (mol/mol)) increases 209% (15%) compared to pure Matrimid when ZIF-8 particles are added to Matrimid with a weight fraction of 0.3 at 35°C and 5 bar. Effect of composition of CO_2/CH_4 and CO_2/N_2 mixtures (CO_2/CH_4 and CO_2/N_2: 10/90, 35/65, 75/25 (mol/mol)) on CO_2 selectivity was investigated and it was found that selectivity of MMMs decreases with increasing CO_2 content in feed gas mixture. The decrease in CO_2 selectivity was attributed to the plasticization of the polymer matrix induced by CO_2 molecules. The plasticized polymer chains allowed the transport of larger CH_4 and N_2 molecules that had been previously restricted. Song et al.[90] fabricated and characterized ZIF-8/Matrimid membranes and tested pure gas (H_2, CO_2, O_2, N_2, CH_4) permeation in MMMs that contain 0-0.3 weight fractions of ZIF-8 in Matrimid. Permeability of all gases increased with the increment in ZIF-8 loading. For example, H_2 and CO_2 permeability was two times that of the pure polymer when ZIF-8 loading increased to 20 wt%. Nearly no improvement in ideal selectivities of CO_2/CH_4, CO_2/N_2 and O_2/N_2 were recorded while ideal selectivity of small H_2 molecules over N_2 and CH_4 decreased slightly in comparison to the pure polymer membrane. This result was supported with the positron annihilation lifetime spectroscopy (PALS) tests which indicated that free volume of the polymer increases with incorporation of ZIF-8 particles, thus gas permeability increases. However, selectivity of some gas pairs

decreases, including selectivity of a small highly permeable gas over a large less permeable one. Extra free volume allowed bulky, less permeable gas molecules to diffuse faster, but permeability increase in smaller molecules was not as pronounced as larger ones. The permeability of gases across ZIF-8/Matrimid MMM was predicted theoretically using Maxwell model. The predictions slightly underestimated the experimental permeability measurements of all gases and it was attributed to higher permeability in experiments due to increase in polymer free volume as proved by the PALS analysis. Dai and coworkers [91] synthesized asymmetric hollow fiber MMMs by embedding ZIF-8 fillers into Ultem polymer with a weight fraction of 0.13. Both higher CO_2 permeance and higher CO_2/N_2 ideal selectivity were observed in ZIF-8/Ultem MMMs compared to pure polymer fiber membranes. 85% and 20% improvement in CO_2 permeance and ideal selectivity were achieved, respectively. They found promising results for the ideal separation performance of hollow fiber ZIF-8/Ultem MMM compared to a zeolite-based MMM (HSSZ-13/ Ultem MMM) reported in their previous study,[68] since they had observed a slight decrease in CO_2/N_2 selectivity across HSSZ-13/Ultem MMM relative to pure polymer fiber membrane.

ZIF-7, ZIF-20 and ZIF-90 are other ZIFs that were incorporated in polymers and gas separation performances of these MMMs were measured. Bae et al.[80] synthesized ZIF-90 particles and added them into three different polyimides: Ultem, Matrimid and 6FDA-DAM with a ZIF-90 loading of 15 wt%. They recorded pure gas (CO_2 and CH_4) permeability across ZIF-90/Ultem, ZIF-90/Matrimid and ZIF-90/6FDA-DAM as well as selectivity of equimolar CO_2/CH_4 mixture for only ZIF-90/6FDA-DAM membranes at 25°C and 2 bar. They observed increases in CO_2 permeability of Ultem and Matrimid-based MMMs without any loss in CO_2/CH_4 ideal selectivity whereas significant enhancements in both CO_2 permeability and CO_2/CH_4 ideal selectivity were observed in 6FDA-DAM-based MMMs at 15 wt% ZIF-90 loading. CO_2 permeability (CO_2/CH_4 equimolar mixture selectivity) of pure 6FDA-DAM increased from 390 (24) Barrers to 72

Table 2.1: Pure gas permeability and ideal selectivity of synthesized ZIF-based MMMs.

Ref	ZIFs	Polymers	Loading (wt%)	Condition		Permeability (P) (Barrer)				Ideal selectivity (S)			
				T(K)	P (Bar)	CO_2	CH_4	H_2	N_2	CO_2/CH_4	CO_2/H_2	CO_2/N_2	H_2/CH_4
[79]	ZIF-8	Matrimid	20, 30*, 40, 50, 60	308	2	14.2	0.4	47.2	0.6	37.4	0.3	24.1	124.2
[88]	ZIF-8	PPEES	10, 20*, 30	283-313	1	18.1	0.8	32.7	0.6	24.1	0.5	28.3	43.6
[90]	ZIF-8	Matrimid	5, 10, 20*, 30	295	4	16.6	0.5	63.5	0.9	36.2	0.3	18.9	138.1
[91]	ZIF-8	Ultem	5*	308	6.9	1.8	-	-	0.04	-	-	44	-
		Ultem	15*	308	4.5	2.9	0.1	-	-	39	-	-	-
[80]	ZIF-90	Matrimid	15*	308	4.5	12.0	0.3	-	-	34.9	-	-	-
		6FDA-DAM	15*	298	2	804.5	29.6	-	-	27.2	-	-	-
[92]	ZIF-7	PBI	10, 25*, 50	308	3.5	1.3	-	15.4	-	-	11.8	-	-
[93]	ZIF-7	PEBAX	8, 22*, 34	293	3.75	111	-	-	-	30	-	97	-

*Permeability and ideal selectivity data are given for this condition.

Table 2.2: Mixed gas permeability and selectivity of synthesized ZIF-based MMMs.

Ref	MOFs	Polymers	Loading (wt%)	Conditions		Compositions	Permeability (P) (Barrer)				Mixture selectivity (S)			
				T (K)	P (bar)		CO_2	CH_4	H_2	N_2	CO_2/CH_4	H_2/CO_2	CO_2/N_2	H_2/CH_4
[80]	ZIF-90	6FDA-DAM	15*	298	2	50/50	720	-	-	-	37	-	-	-
[79]	ZIF-8	Matrimid	50*	308	3	CO_2/CH_4:10/90	-	-	-	-	89.2	3.5	-	-
			60*			H_2/CO_2: 50/50	-	-	-	-	80.1	7	-	-
[92]	ZIF-7	PBI	25*	308*-453	7	H_2/CO_2: 50/50	0.9	-	6.3	-	-	6.8	-	-
			50*				1.8	-	13.3	-	-	7.2	-	-

*Permeability and ideal selectivity data are given for this condition.

(37) Barrers when ZIF-90 was incorporated into 6FDA-DAM membrane and ZIF-90 nanoparticles were able to carry pure 6FDA-DAM above the Robeson upper bound.[24] They also tested CO_2/N_2 separation performance of ZIF-90/6FDA-DAM MMMs and found promising results. They reported that ZIF-90 shows good adhesion to 6FDA-DAM and the permeabilities of the MOF and the polymer matches well. Yang et al.[92] incorporated ZIF-7 particles into PBI polymer matrix and tested pure H_2 and CO_2 permeabilities at 35°C under 3.5 atm and permeabilities of equimolar H_2/CO_2 mixture at 35°C and 7 atm. Pure gas permeability, mixed gas permeability and CO_2/H_2 ideal selectivity increased with increasing ZIF-7 loading in MMM. For example, pure H_2 permeability (the ideal selectivity of H_2/CO_2) of pure PBI increased from 3.7 Barrers (8.7) to 26.2 Barrers (14.9) with addition of 50 wt% ZIF-7 into PBI polymer matrix. These results were explained by PALS and glass transition temperature analysis. Increase in polymer free volume proven by PALS analysis supported increase in permeability. Good interactions between PBI and ZIF-7 led an increase in glass transition temperature, polymer chain rigidification and molecular sieving effect; these results explained the reason for H_2/CO_2 selectivity enhancement. Li et al.[93] embedded ZIF-7 particles into PEBAX polymer and tested performance of the composite membranes by pure gas permeation measurements of CO_2, N_2 and CH_4 at low (8 wt%), medium (22 wt%) and high (34 wt%) filler loadings. ZIF-7/PEBAX MMMs showed higher CO_2 permeability and CO_2/CH_4 and CO_2/N_2 selectivity compared to the gas separation performances of MMMs which had been previously reported, such as ZIF-8/Matrimid and ZIF-8/Ultem.[89, 91] High performance of ZIF-7/PEBAX MMMs was attributed to polymer-penetrant interaction because polyethylene oxide (PEO) segments of the polymer have high affinity to polar CO_2 molecules. At medium and high loadings of ZIF-7, CO_2 selectivity increased but CO_2 permeability decreased because of polymer chain rigidification, but it was still higher than most of the ZIF-based MMMs at 34 wt% filler loading. Seoane et al.[94] fabricated ZIF-20/PSF MMMs and tested their O_2/N_2 separation

performance. They reported that ZIF-20/PSF MMMs in which ZIF-20 is 8 wt% have a better performance in separation of equimolar O_2/N_2 mixture than pure PSF.

Figure 2.5 shows the performances of ZIF-based MMMs that are close to the upper bound set by Robeson in 1991[23] and 2008 [24]. ZIF-90-based MMMs are above the Robeson's updated upper bound while ZIF-7 and ZIF-8 are above and/or close to the 1991 upper bound. This result underlines the fact that MMMs fabricated using ZIFs are attractive candidates for membrane-based separation applications. Although many ZIFs were synthesized as crystals, gas separation performance of MMMs composed of just one or two different types of ZIFs could be investigated in an experimental study. An extensive study is required for testing the gas separation performance of MMMs composed of a large collection of ZIFs as filler particles. Experimental efforts to fabricate and test such a large collection of ZIF-based MMMs are disadvantageous, but computational methods are very useful for screening purposes to determine appropriate ZIF-polymer pairs. We [95] studied fifteen different ZIFs: ZIF-2, ZIF-3, ZIF-6, ZIF-8, ZIF-10, ZIF-11, ZIF-12, ZIF-60, ZIF-65, ZIF-67, ZIF-69, ZIF-78, ZIF-79, ZIF-81 and ZIF-90 as fillers in polymers in this thesis. The performances of 360 new ZIF-based MMMs for separation of CO_2/CH_4, H_2/CH_4 and H_2/CO_2 were predicted using molecular simulations and permeation models. ZIF-11, ZIF-90 and ZIF-65 were found to be promising filler candidates for CO_2/CH_4, H_2/CH_4 and H_2/CO_2 separations, respectively. The details of this study will be discussed in Chapter 5.

2.4. Filler1/Filler2/Polymer and Filler/Polymer1/Polymer2 MMMs

MMMs composed of three systems having different nature have been synthesized to enhance separation performance of MMMs. These MMMs are formed from either combination of two different fillers in one type of polymer or incorporation of one type of filler into a polymer blend which is composed of two types of polymer.

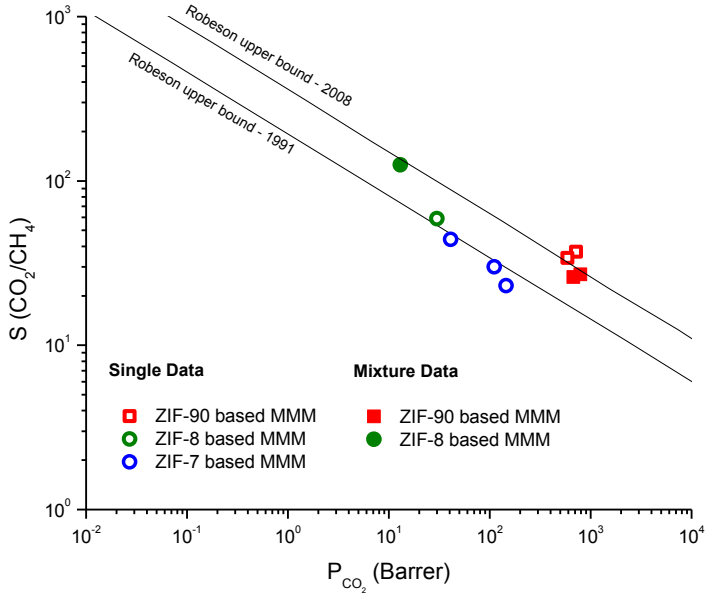

Figure 2.5: Experimental data of ZIF-based MMMs that are close to the Robeson upper bound.[79, 80, 93]

Combination of two different types of porous fillers in a polymer matrix is a relatively new idea that a limited number of experiments have been conducted to investigate separation performance of that kind of MMMs to date. For example, Zornoza et al.[96] incorporated two different kinds of filler particles in a polymer matrix to increase dispersion and disaggregation of filler particles since fillers having different nature can have complementary interaction and have less tendency to come together whereas filler particles having the same nature may agglomerate. They used silicalite-1 (S1C) and ZIF-8 or CuBTC together in PSF to combine good interaction of S1C with polymer and compatibility of MOFs and ZIFs with polymer due to their organic nature. Scanning electron microscopy (SEM) images proved homogeneous dispersion and intimate filler-polymer interaction as can be seen from Figure 2.6. They reported improvements in CO_2

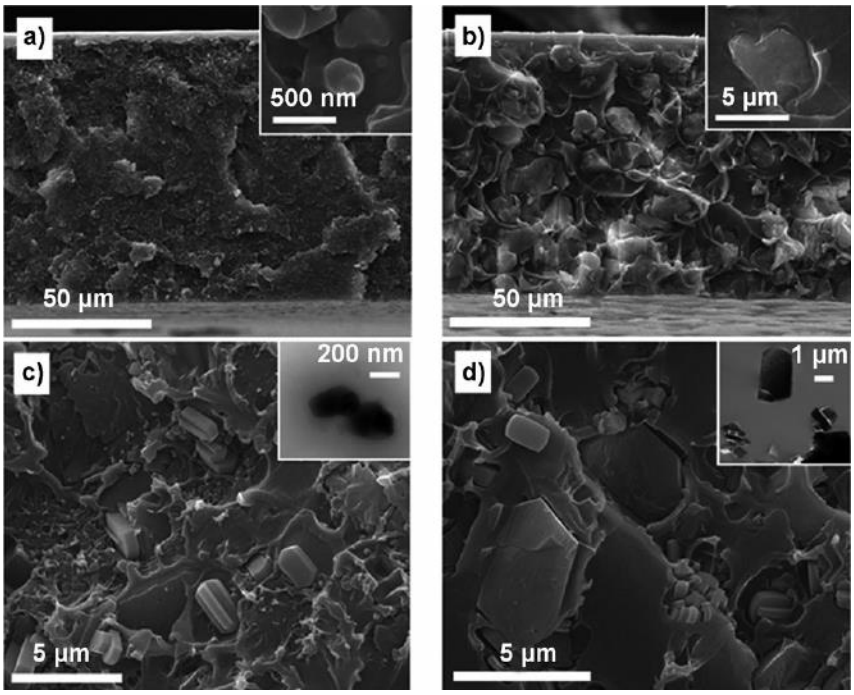

Figure 2.6: SEM images of MMMs. (a) 16 wt% ZIF-8/PSF, (b) 16 wt% HKUST-1/PSF, (c) 8 wt% ZIF-8+8 wt% S1C/PSF, (d) 8 wt% HKUST-1+8 wt% S1C/PSF.[96]

permeability across both CuBTC/S1C/PSF and ZIF-8/S1C/PSF membranes compared to pure PSF; this was explained by the increase in polymer's free volume with addition of filler particles. Combination of CuBTC with S1C in PSF gave the highest CO_2/N_2 and CO_2/CH_4 selectivity whereas ZIF-8/S1C/PSF MMMs were found to be promising for mixtures that are separated based on diffusion differences, such as O_2/N_2 and H_2/CH_4. Galve et al.[97] combined high H_2 permeability of mesoporous silica MCM-41 (2-3 nm pores) with high H_2/CH_4 selectivity of a microporous titanosilicate JDF-L1 (0.3 nm pores) at a total loading of 12 wt% in 6FDA-copolyimide polymer matrix to separate H_2 from CH_4. They observed that incorporation of MCM-41 (JDF-L1) particles to the polymer decreases (increases) H_2/CH_4 selectivity but increases (decreases) H_2 permeability through

MCM-41/JDF-L1/6FDA-copolyimide MMMs. The MMMs were located between the Robeson's upper bounds set in 1991 [23] and 2008 [24] for H_2/CH_4 separation. Besides good H_2/CH_4 separation performance of MMMs, good dispersibility of fillers in polymer phase and good interaction between fillers and polymer were observed.

There have been many studies on fabrication of polymeric membranes made of polymer blend to achieve enhancement in permeability and selectivity.[98-104] Recently, several groups have concentrated on incorporation of nanoporous materials into polymer blends. Basu and coworkers [105] embedded CuBTC into Matrimid and Matrimid/PFS (3/1) blend. They investigated CO_2, CH_4 and N_2 permeance across the membranes and selectivities of CO_2/CH_4 and CO_2/N_2 at 35°C and 10 bar under various effects: (1) addition of PSF into pure Matrimid, (2) addition CuBTC in Matrimid and Matrimid/PFS (3/1) blend, (3) increase in CO_2 feed composition (10, 35 and 75 mol%). Reason for addition of PSF into Matrimid is to reduce the tendency of plasticization of Matrimid and provide superior separation properties which are suitable for MMMs. PSF is highly resistant to plasticization while Matrimid is quite susceptible to plasticization in CO_2 environment although it has promising gas separation properties. Plasticization of Matrimid accelerates permeation of larger molecules, thus plasticization causes loses in selectivity. CO_2/CH_4 and CO_2/N_2 selectivities in CuBTC-Matrimid/PFS MMMs were found to be lower than CuBTC/Matrimid MMMs at any CO_2 content and filler loading due to lower CO_2 selectivity of PSF. They observed that CO_2/CH_4 and CO_2/N_2 selectivity of both non-blend Matrimid and Matrimid/PSF blend increases (decreases) with increasing filler loading (CO_2 content of the feed), irrespective of the CO_2 content of the feed (CuBTC loading). Decrease in CO_2/CH_4 and CO_2/N_2 selectivity with increasing CO_2 content of the feed mixture was attributed to strong interaction between Matrimid and CO_2 which causes plasticization of polymer matrix and increase in the diffusion of the better retained CH_4 and N_2 molecules. It was shown that a relatively moderate decrease occurs in CO_2/CH_4 and CO_2/N_2 selectivity

in CuBTC/Matrimid/PFS MMMs (compared to CuBTC/Matrimid MMMs) with increase in CO_2 content of the feed which underlines the fact that plasticization of Matrimid decreases when PSF is added to Matrimid. Thus, in gas mixtures containing high CO_2, the same selectivity as pure Matrimid can be achieved using Matrimid/PSF blend which is economically more attractive. Dorosti et al.[106] fabricated PI/PSF-based MMMs filled with zeolite ZSM-5 particles and tested CO_2, CH_4, N_2 and O_2 permeabilities across 100 wt% PSF, 70/30 (PSF/PI), 50/50 (PSF/PI), 30/70 (PSF/PI) (wt/wt) and 100 wt% PI membranes with ZSM-5 between 0 and 20 wt% loadings. Gas permeability decreased with addition of polyimide to polysulfone at constant zeolite loading. This was attributed to the stiff chains and high glass transition temperature of polyimide. Enhancement in gas permeability was observed with addition of zeolite at constant polymer loading due to increase in polymer free volume in presence of fillers. Thermal stability of ZSM-5/PI/PSF MMMs increased at the expense of uncontrollable void formation after zeolite loadings of 20 wt%. Rafiq et al.[107] made MMMs by incorporating inorganic silica nanoparticles into PI/PSF (1/4) blend and tested pure CO_2 and CH_4 permeance as well as selectivity of CO_2/CH_4 mixture with compositions of 25/75, 50/50 and 25/75 (vol/vol) at 25°C under 1-20 bar. Improvements in CO_2 and CH_4 permeance through silica-PSF/PI MMMs with increasing filler loading (5, 10, 15, 20 wt%) were reported. They observed decreases in CO_2 permeance with increasing pressure which indicates absence of plasticization in polymer matrix since membranes exhibit higher permeance values in the presence of plasticization. It was also found that CO_2/CH_4 selectivities do not change with composition of the feed gas mixture. This result was contrary to the results of Basu et al.[105] because amount of PSF which is 33 wt% in polymer blend was not enough to prevent plasticization whereas in the study of Rafiq et al.[107] the blend was composed of 80 wt% PSF.

In literature, there is no theoretical study that uses simulations and models to predict gas permeability and selectivity of MMMs composed of two different types of fillers in one type of polymer or MMMs containing one type of filler into a polymer blend.

Chapter 3

COMPUTATIONAL DETAILS

3.1. Materials

3.1.1. MOFs and ZIFs

Atomically detailed simulations were used to assess adsorption-based and membrane-based gas separation performances of ZIF-11 and ZIF-12. ZIF-11, having zinc (Zn) as metal atom and benzimidazolate (blm) as linker, is a cubic structure with unit cell dimensions of 28.76×28.76×28.76 Å. ZIF-12 consists of the same type of linker, unit cell dimensions and structure as ZIF-11, but it has cobalt (Co) as central metal atom. Both ZIF-11 and ZIF-12 have 3.3 Å pores in diameter with 14.9 Å pore apertures.[108] Because ZIF-11 and ZIF-12 are identical except the central metal atoms, they are good candidates to study the effect of central metal atom on the gas separation performance of ZIF-based adsorbents and membranes. The structural representation of ZIF-11 and ZIF-12 are schematically shown in Figure 3.1 and atomic representation of ZIFs is provided in Figure A1.

Several MOFs and their subclass ZIFs were evaluated as filler particles in MMMs. These MOFs are BACMOH-10, BAHGUN, FOHQUO, JASNEX, MABJOP, MABJUV-01, MIHHOA, MIHHUG, MMIF, UFUNAK, UFUMUD-01, UGEPEB and YOPMAS and ZIFs are ZIF-2, ZIF-3, ZIF-6, ZIF-8, ZIF-10, ZIF-11, ZIF-12, ZIF-60, ZIF-65, ZIF-67,

ZIF-69, ZIF-78, ZIF-79, ZIF-81 and ZIF-90. The structural properties of ZIFs are listed in Table 3.1.

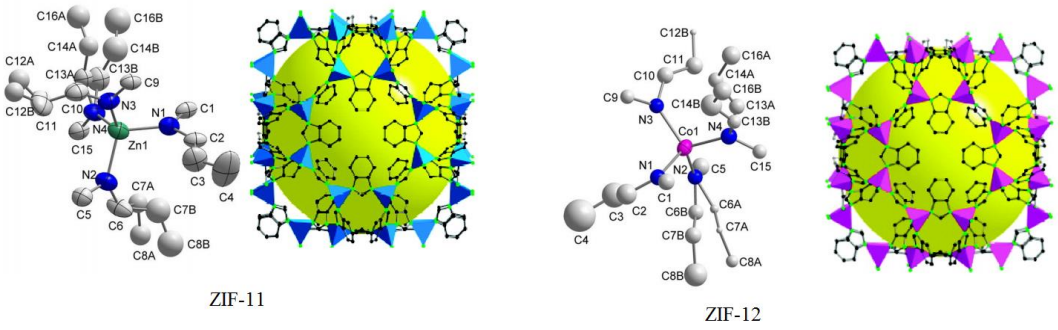

Figure 3.1: Unit cell atoms [9] and crystal structures [8] (carbon (C) atom, nitrogen (N) atom, ZnN_4 polyhedral and CoN_4 polyhedral are in black, green, blue and pink, respectively.) of ZIF-11 and ZIF-12.

3.1.2. Polymers

In MMM calculations, groups of polymers that were specified by Robeson et al.[22] for desired gas separation were used. 12 polymers for CO_2/CH_4, 7 for H_2/CH_4, 5 for H_2/CO_2 and 15 for CO_2/N_2 separations were considered in this thesis. These polymers and their gas permeabilities and selectivities for CO_2/CH_4, H_2/CH_4 and H_2/CO_2 and CO_2/N_2 separations are given in Table C1, Table C2, Table C3 and Table C4, respectively. The data in these tables include experimental permeability measurements of polymers at 25-35˚C and 2 bar.

Table 3.1: Structural properties of ZIFs.

Material	Composition	Porosity (%) [80, 109, 110]	Density (g/cm^3)	Pore size (Å) [8, 111]	Volume ($Å^3$)	Cell Dimensions (a, b, c) (Å) Cell Angles (α, β, γ) (^{o})	Topology
ZIF-2	$Zn_2(Im)_4$	49.20	0.929	6.4/6.9	5707	9.679×24.114×24.450 90, 90, 90	BCT
ZIF-3	$Zn_2(Im)_4$	57.80	0.880	4.6/6	6024	18.9701×18.9701×16.740 90, 90, 90	DFT
ZIF-6	$Zn(Im)_2$	62.70	0.764	8.2/8.8	6940	18.515×18.515×20.245 90, 90, 90	GIS
ZIF-8	$Zn(mIm)_2$	43.30	0.924	3.4/11.6	4905	16.9910×16.9910×16.9910 90, 90, 90	SOD
ZIF-10	$Zn(Im)_2$	65.00	0.746	8.2/12.12	14210	27.0608×27.0608×19.406 90, 90, 90	MER
ZIF-11	$Zn(bIm)_2$	58.78	1.003	3.00/14.6	23787	28.7595×28.7595×28.7595 90, 90, 90	RHO
ZIF-12	$Co(bIm)_2$	58.78	0.981	3.00/14.6	23787	28.7595×28.7595×28.7595 90, 90, 90	RHO
ZIF-60	$Zn_2(Im)_3(mIm)$	70.82	0.769	7.2/9.4	14270	27.2448×27.2448×19.2254 90, 90, 90	MER
ZIF-65	$Co(nIm)_2$	67.90	1.095	3.4/10.4	5152	17.2715×17.2715×17.2715 90, 90, 90	SOD
ZIF-67	$Co(mIm)_2$	62.27	0.904	3.4/11.6	4877	16.9589×16.9589×16.9589 90, 90, 90	SOD
ZIF-69	Zn(cbIm)(nIm)	57.41	1.145	4.4/7.8	11436	26.0840×26.0840×19.4082 90, 90, 120	GME
ZIF-78	Zn(nbIm)(nIm)	55.38	1.176	3.8/7.1	11514	26.1174×26.1174×19.4910 90, 90, 120	GME
ZIF-79	Zn(mbIm)(nIm)	56.87	1.075	4.0/7.5	11441	25.9263×25.9263×19.6532 90, 90, 120	GME
ZIF-81	Zn(brbIm)(nIm)	56.65	1.292	3.9/7.4	11527	25.9929×25.9929×19.6997 90, 90, 120	GME
ZIF-90	$Zn(Ica)_2$	60.40	0.974	3.5/11.2	5233	17.3612×17.3612×17.3612 90, 90, 90	SOD

3.2. Molecular Models

A reliable simulation depends on well description of both gas-gas and gas-adsorbent interactions. H_2 was modeled as a spherical, single site molecule (so-called united atom model) with 12-6 Lennard-Jones (LJ) potential (σ=0.296 nm, ε/k_B=34.2 K) centered on the sphere. This model was proposed by Buch et al.[112] and it is known to reproduce experimental bulk equation of state accurately. There are also two and three site models in literature to describe H_2 using quadrupolar electrostatic terms, these models have been shown to be more accurate in modeling hydrogen interactions in complex and heterogeneous condensed phase systems.[113, 114] The simulations considered in this thesis do not include complex and condensed systems which require more detailed calculations, thus Buch potential was used to model H_2 to save computational time. CH_4 was modeled using TraPPE force field (σ=0.373 nm, ε/k_B=148.0 K) based on the united-atom description.[115] The TraPPE force field was validated to reproduce the experimental vapor-liquid coexistence curves and critical properties of linear alkanes from methane to dodecane and results showed high accuracy.[115] CO_2 was represented as a linear triatomic molecule. CO_2 potential consists of three LJ sites which were located on C atom (σ=0.280 nm, ε/k_B=27.0 K) and two O atoms (σ=0.305 nm, ε/k_B=79.0 K) with partial point charges centered at each site (q_C=0.70e and q_O=−0.35e).[116] The accuracy of this model was tested by reproducing vapor-liquid equilibria (VLE) of pure CO_2 and mixtures containing CO_2 and it was found that calculations using this model yields results that are in a good agreement with the experimental data.[116] N_2 was modeled as a three site molecule with two LJ sites located at two N atoms (σ=0.331 nm, ε/k_B=36.4 K) with partial point charges (q_N=-0.404e) and the third LJ site (σ=0.331 nm, ε/k_B=0.0 K) located at its center of mass (COM) with a partial point charge (q_{COM}=0.809e).[117]

Crystallographic structures of MOFs were taken from Cambridge Structural Database (CSD) which is a large archive presenting experimental X-ray diffraction data of

more than 35,000 MOF structures.[118] Solvent-free rigid structures (atoms are fixed at their crystallographic positions) were used in all simulations. The rigid framework assumption provides large computational time savings compared to time consumed in simulations performed using flexible framework structures although inclusion of lattice motion allows more accurate description of molecular dynamic simulations. The assumption of rigid framework is also reasonable due to the lack of a reliable force field for modeling flexible frameworks. Flexibility should take into consideration when pore of the material is smaller than the kinetic diameter of gas components. The LJ parameters of the framework atoms were assigned from universal force field (UFF) that has been widely used in adsorption and diffusion simulations of porous materials.[119-122] The results of the simulations employing UFF were found to be in a good agreement with the results experiments.[38, 121] DREIDING force field parameters were also used in some cases to observe the effects of force fields on molecular simulations. DREIDING force field was proposed by Mayo et al.[123] and the parameters of the force field were estimated using general force constants and geometry parameters based on simple hybridization considerations. For simulation of gas molecules with quadruple moment (CO_2 and N_2), the atomic partial charges of frameworks, except ZIF-90, were estimated using the approach known as connectivity based atom contribution (CBAC) method proposed by Xu et al.[124] Assignment of charges to the framework atoms using CBAC was performed based on the idea that the atoms having the same bonding environment have identical charges regardless of identity of MOF. The method was tested on 43 MOFs and it was found that adsorption isotherms computed using CBAC charges agree well with those predicted using quantum mechanical (QM) charges and agree well with the experimental data.[124] The atomic partial charges of ZIF-90 were assigned from REPEAT charges of Watanabe et al.[125]. Watanabe and coworkers tested REPEAT charges to reproduce experimental CO_2 adsorption isotherm in ZIF-90 and showed that CO_2 adsorption isotherm computed using

REPEAT charges was the most accurate one among the CO_2 adsorption isotherms computed using QM calculation-based point charges when compared with the experimental measurements.

Total potential energy of the system was calculated using LJ and Coulomb potentials. Pairwise non-bonded repulsive and attractive interactions between adsorbate-adsorbate and adsorbate-adsorbent atoms were computed using LJ parameters of adsorbate and adsorbent atoms:

$$U_{LJ}(r_{ij}) = 4\varepsilon_{ij}\left[\left(\frac{\sigma_{ij}}{r_{ij}}\right)^{12} - \left(\frac{\sigma_{ij}}{r_{ij}}\right)^{6}\right] \quad (3.1)$$

Here, U_{LJ} represents LJ potential energy, ε_{ij} and σ_{ij} are the energy and size parameters of the LJ potential for particles i and j and r_{ij} is the distance between two particles. The former part of the equation, $(\sigma_{ij}/r_{ij})^{12}$ describes the repulsive forces between particles while the latter part of the equation, $(\sigma_{ij}/r_{ij})^{6}$ denotes attraction. When the interatomic separation is small (large) r^{12} (r^6) term dominates and the potential becomes repulsive (attractive). For the Lennard-Jones interactions between unlike sites, Lorentz−Berthelot combining rules were used. According to Lorentz−Berthelot rules:

The size parameter (σ_{ij}) is determined by the arithmetic mean of σ_i and σ_j:

$$\sigma_{ij} = \frac{\sigma_i + \sigma_j}{2} \quad (3.2)$$

- The cross energy well depth (ε_{ij}) is calculated as the geometric mean of the energy parameters ε_i and ε_j:

$$\varepsilon_{ij} = \sqrt{\varepsilon_i . \varepsilon_j} \quad (3.3)$$

Coulomb potential energy (U_C) contribution to the total energy in case of interaction between two charged atoms was calculated using the following equation:

$$U_C(r_{ij}) = \frac{q_i q_j}{4\pi\pi_0 r_{ij}^2} \quad (3.4)$$

Here, q_i and q_j are charges of atoms i and j and ε_0 is permittivity of free space (8.854×10^{-12} $C^2J^{-1}m^{-1}$).

Total energy (U_T) was calculated as the sum of LJ and coulomb potential energy:

$$U_T = U_{LJ} + U_C \quad (3.5)$$

3.3. Simulation Methodology

3.3.1. Molecular Simulation of Adsorption

Grand Canonical Monte Carlo (GCMC) simulations were employed to determine amount of gas adsorbed into porous materials as a function of pressure. In the grand canonical ensemble; chemical potential (μ), temperature (T) and volume (V) are fixed while number of particles is allowed to fluctuate during simulation.[126] For pure gases, four types of trial moves, attempts to translate a molecule, attempts to rotate a molecule, attempts to create a new molecule and attempts to delete an existing molecule were included. For mixtures, an additional attempt to exchange molecular identity was included. Periodic boundary conditions were used to mimic infinite bulk surrounding and eliminate surface effects. The use of periodic boundary conditions allows each particle in simulation box to interact with the other particles in the box and with their images in periodic box. Therefore, the number of interacting pairs increases enormously. Cut-off distance (less than half diameter of the box) is applied to prevent this inconvenience and save computational time. Cut-off distance was set as 13 Å and 25 Å in calculation of LJ and coulomb interactions, respectively. 2×2×2 unit cell simulation box was used in all GCMC simulations. Simulations included 1.5×10^7 equilibration steps with a 1.5×10^7 production steps used for data collection. Simulations at the lowest fugacity for each system were started from an empty matrix and each subsequent simulation at higher fugacity was started

from the final configuration of the previous run. In all calculations, gases were assumed to be ideal gas, thus fugacity and pressure corresponds to the same value. Ideal gas assumption is reasonable since, differences between fugacity and pressure are small for H_2 and CH_4 at the conditions that are considered in this thesis. For CO_2 and N_2 deviations from ideal gas behavior at high pressures (>35 bar) are not significant.

3.3.2. Molecular Simulation of Diffusion

Equilibrium Molecular Dynamics (EMD) simulations were used to compute self and corrected-diffusion coefficients of gases in the canonical ensemble with a Nose-Hoover thermostat.[127] The number of particles that would be included in MD was determined from GCMC simulations. Initial states of the particles were created using GCMC and initial velocities were assigned from Maxwell-Boltzmann distribution. The system was equilibrated with EMD prior to taking data by solving the Newton's equation of motion until the properties no longer change with time. Newton's equation of motion was integrated using Verlet algorithm. The simulation box was enlarged to 4×4×4 unit cells in cases to accommodate enough adsorbates to guarantee the simulation accuracy at the lowest loadings.

Diffusion coefficients used in this thesis are:

Self-diffusion coefficient describes the motion of individual, tagged particles and is defined as:

$$D_{self,i} = \lim_{t\to\infty} \frac{1}{6t} \left\langle \frac{1}{N_t} \sum_{i=1}^{N} [r_i(t) - r_i(0)]^2 \right\rangle \qquad (3.6)$$

where, N is the number of molecules, $r_i(t)$ is position vector of species i tracked in time t and the angular brackets denote that the ensemble average.

Corrected-diffusion coefficient describes the collective motion of adsorbed molecules and is defined as:

$$D_{o,i} = \lim_{t\to\infty} \frac{1}{6Nt} \left\langle \left(\sum_{i=1}^{N} \left[r_i(t) - r_i(0) \right] \right)^2 \right\rangle \tag{3.7}$$

The diffusivities coincide in low adsorbate concentrations limit at which the self and corrected diffusivities are equal.[128]

3.4. Detailed Calculations for Performance Predictions of MOFs

Adsorption selectivity is the main factor to evaluate the performance of MOF adsorbents. Adsorption selectivity (S_{ads}) is defined as:

$$S_{ads(i/j)} = \frac{x_i / x_j}{y_i / y_j} \tag{3.8}$$

Here, x_i (x_j) represents mole fraction of adsorbed component i (j) in total adsorbed gas mixture and y_i (y_j) is the mole fraction of component i (j) in the bulk phase. The other important factor that determines the efficiency of the adsorption-based separations is working capacity (or delta loading). Working capacity (Δc_i) for CO_2, CH_4 and H_2 was evaluated at adsorption and desorption pressures of 10 and 1 bar, respectively:

$$\Delta c_i = c_i^{ads} - c_i^{des} \tag{3.9}$$

where c_i^{ads} and c_i^{des} are the adsorbed loadings at 10 and 1 bar, respectively. They are generally expressed in terms of mmol adsorbed gas/gram material.

Diffusion selectivity (S_{diff}) is defined as the ratio of self-diffusion coefficients of components in mixture:

$$S_{diff\,(i/j)} = \frac{D_{self,i}}{D_{self,j}} \tag{3.10}$$

Permeation selectivity is the main factor to evaluate the performance of MOF membranes. Permeation selectivity is the product of adsorption and diffusion selectivities:

$$S_{perm_{(i/j)}} = S_{ads(i/j)} \times S_{diff\,(i/j)} \tag{3.11}$$

This equation is an approximation introduced by Keskin and Sholl [129] to predict the gas mixture separation performance of MOF membranes under conditions where the permeate side is vacuum. This relation is known to fail in systems with strongly heterogeneous potential energy surfaces.

3.4.1. Ideal Adsorbed Solution Theory (IAST)

Ideal adsorbed solution theory (IAST) is a useful approach to make predictions about adsorption isotherms of components in a gaseous mixture using only pure component adsorption isotherms at the same temperature and on the same adsorbent. This theory is known to work accurately in many nanoporous materials except in materials which have strong energetic or geometric heterogeneity.[130] IAST was used to predict multicomponent adsorption isotherms of CH_4/H_2, CO_2/CH_4 and CO_2/H_2. IAST was applied by fitting pure component adsorption isotherms using dual-site Langmuir (Langmuir-Freundlich) isotherm model for H_2 and CH_4 (CO_2).

Dual-site Langmuir isotherm model:

$$c_i = \frac{a_i P}{b_i + P} + \frac{c_i P}{d_i + P} \tag{3.12}$$

Langmuir-Freundlich isotherm model:

$$c_i = \frac{a_i P^{c_i}}{b_i + P^{c_i}} \tag{3.13}$$

where a_i, b_i, c_i and d_i are fitting parameters of species i (H_2, CH_4 and CO_2). P is the pressure (bar) and c is the adsorbed amount of pure gas (molecules/unit cell).

3.5. Detailed Calculations for Performance Predictions of MOF-based MMMs

3.5.1. Prediction of Pure Gas Permeability through MOFs

Membrane-based gas separation performance of a material depends on both of adsorption and diffusion of the gases in the material. Gas flux (J) is defined in terms of transport diffusion coefficient (D_t) and concentration gradient (∇c) by Fick's law:

$$J = -D_t(c) \cdot \nabla c \tag{3.14}$$

∇c depends on the difference between adsorbed loadings at feed and permeate side pressures of the membrane and membrane thickness, $\nabla c = \left(c^{permeate} - c^{feed}\right)/L$. The transport diffusion coefficient (D_t) is determined using corrected diffusion coefficient (D_o) calculated from equilibrium molecular dynamic (EMD) simulations. The corrected diffusivities for the adsorbed components are assumed to be constant throughout the membrane and they are evaluated at the average of feed and permeate side concentrations. D_t can be computed using following expression:

$$D_t(c) = D_o(c) \cdot \frac{\partial \ln f}{\partial \ln c} \tag{3.15}$$

Here, the second term is the thermodynamic correction factor (TCF) which can be predicted once single component adsorption isotherms are known and TCF relates the adsorbate concentration, c and bulk phase fugacity, f. Gas permeability is a pressure normalized quantity and can be defined as:

$$P_{d-pure,i} = \frac{J}{\Delta p / L} \tag{3.16}$$

where Δp is the pressure drop, the difference between the feed and permeate side pressures.[131]

3.5.2. Prediction of Mixture Gas Permeability through MOFs

Permeability of a gas component in a mixture is affected from adsorption and diffusion behavior of the other gas component in the mixture, thus a different formulation is needed to predict mixture gas permeability through MOFs. van Baten and Krishna's formulation[132] was used to predict mixture permeability as a function of concentration of gas species at the upstream side of the membrane c_i (mol/m^3), self-diffusivity of species D_{self} (m^2/s), bulk phase partial fugacity of the species f_i (Pa) and the fractional pore volume of the crystalline material θ (fractional pore volumes of ZIFs are listed in Table 3.1):

$$P_{d-mix,i} = \frac{\theta \cdot D_{i,self} \cdot c_i}{f_i} \tag{3.17}$$

$P_{d\text{-}mix,i}$ (mol m^{-1}Pa^{-1}s^{-1}) is permeability of gas in mixture conditions. Since membrane research community uses Barrers to report gas permeability, permeability in mol/m/Pa/s was converted to Barrers. (1 Barrer=3.348×10^{-16} mol m^{-1}Pa^{-1}s^{-1})

For mixed matrix membranes ideal selectivity, $IS_{(i/j)}$, is defined as the ratio of the permeability of the two gas components where P_i and P_j can be pure ($P_{d\text{-}pure}$) or mixture ($P_{d\text{-}mix}$) gas permeability:

$$IS_{(i/j)} = \frac{P_i}{P_j} \tag{3.18}$$

3.5.3. Prediction of Gas Permeability through MMMs with One Type of Fillers

Gas transport through MMMs can be predicted using several mathematical models which are adaptations of thermal and electrical conductivity models since there is an analogy between thermal and electrical conduction in composite materials and permeation of species through such materials.[133] The basic parameters used in models to predict permeability of gaseous species through MMM are permeabilities of continuous and dispersed phases as well as volume fraction of the dispersed phase for MMMs having ideal

morphology. Additional parameters are included in the MMM permeation models if MMM's morphology is non-ideal. Gas permeability through MMMs was determined using four different gas permeation models: Maxwell, extended Maxwell and modified Maxwell and modified Felske in this thesis.

Maxwell model [134] is the simplest and most common model used to predict permeability in MMMs. It was derived based on ideal morphology of MMMs. It is applicable to a dilute suspension of fillers up to a filler loading of 0.2 since this model was developed based on the assumption that the streamlines around the particles are not affected by the presence of nearby particles. This model does not consider packing limit of particles, the effect of particle size distribution. The relative permeability (P_r) of gas species in MMMs is predicted by Maxwell model as follows:

$$P_r = \frac{P}{P_m} = \left[\frac{2(1-\phi) + (1+2\phi)\lambda_{dm}}{(2+\phi) + (1-\phi)\lambda_{dm}} \right] \tag{3.19}$$

In this model, λ_{dm} is the permeability ratio (P_d/P_m), P_d is the permeability of dispersed phase, P_m is the permeability of continuous phase, P is the permeability of MMM and ϕ is the volume fraction of filler particles.

Chiew and Glandt [135] presented an extension of the Maxwell model:

$$P_r = \frac{P}{P_m} = 1 + 3\beta\phi + K\phi^2 + O\left(\phi^3\right) \tag{3.20}$$

$$\beta = \frac{P_d - P_c}{P_d + 2P_c} \tag{3.21}$$

$$K = a + b\phi^{3/2} \tag{3.22}$$

$$a = -0.002254 - 0.123112\beta + 2.93656\beta^2 + 1.690\beta^3 \quad (3.23)$$

$$b = 0.0039298 - 0.80349\beta - 2.1620\beta^2 + 6.4829\beta^3 + 5.2719\beta^4 \quad (3.24)$$

In these equations, β is the reduced permeation polarizability and bounded by $-0.5 < \beta < 1$, where the lower and upper limits correspond to totally non-permeable filler particles ($P_d = 0$) and to perfectly permeable filler particles ($P_c = 0$), respectively. The difference of extended Maxwell model from the original Maxwell is the inclusion of particle-particle interactions which are not described in original Maxwell model since the particle size is neglected compared to the mean distance between particles. The extended Maxwell model accounts for the correction of the interactions between particles by K which is estimated by parameters a and b as a function of the reduced permeation polarizability. Using K, reduced permeation polarizability and the volume fraction of the filler, one can predict gas permeability of MMMs by equation (3.20) and $O(\varphi^3)$ term is negligible compared to the other terms. The extended Maxwell model is valid for MMMs with ideal morphology. It gives the same results as original Maxwell model if particle loading is too low.

Modified Maxwell model [66] predicts separation performance of MMMs based on non-ideal morphology which includes the effects of the rigidification of the polymer chains at the polymer-sieve interface. This model consists of properties of two phases, polymer matrix as one phase and pseudo-insert phase as the other phase. Interfacial defect and dispersed phase together are taken as the pseudo-insert phase. Like the original Maxwell model, Modified Maxwell model is valid for low to moderate values of filler concentration and particle size distribution, particle shape and aggregation of the particles are not accounted. Modified Maxwell model can be used to estimate permeability of the MMM by the following expression:

$$P_{eff} = P_I\left[\frac{2(1-\phi_s)+(1+2\phi_s)(P_d/P_I)}{(2+\phi_s)+(1-\phi_s)(P_d/P_I)}\right] \quad (3.25)$$

In this model, P_{eff} is the effective permeability of the pseudo insert phase, P_I is the permeability of the interface (P_m/β^*) and ϕ_s is the volume fraction of the dispersed phase in the pseudo insert phase. ϕ_s was reported to be ~50% for the zeolites and ~68% for the CMS particles by Moore et al.[66] Since MOFs have more favorable interactions with polymers than CMS and zeolites, pseudo insert phase of MOF/polymer MMMs was assumed to be thinner than that of CMS/polymer MMMs. Thus, ϕ_s values between 0.7 and 0.9 were screened and the one (0.75) giving the closest permeability prediction to the experimental data was chosen. If the thickness of the interface layer is known, ϕ_s can be estimated as follows,

$$\phi_s = \frac{\phi}{\phi+\phi_I} = \frac{r_d^{\,3}}{(r_d+l_I)^3} \quad (3.26)$$

$$P_l = \frac{P_d}{\beta^*} \quad (3.27)$$

where ϕ_I is the volume fraction of the interface, r_d is the insert radius, l_I is the interface thickness and β^* is the matrix rigidification factor. The permeability of the polymer in the interphase P_I is assumed to be decreased by a chain immobilization factor. β^* was chosen as 3 which is an approximate value in the range of typical gas penetrants in semi-crystalline polymers.[136] After calculation of P_{eff}, gas permeability of the MMMs can be predicted using the following equation:

$$P_r = \frac{P}{P_m} = \left[\frac{2(1-\phi)+(1+2\phi)(P_{eff}/P_m)}{(2+\phi)+(1-\phi)(P_{eff}/P_m)}\right] \quad (3.28)$$

Modified Felske model is an expression for the permeability of MMMs accounting for core particles surrounded by interfacial shell layer (rigidified layer or voids or particle pore blockage) and polymer matrix. It considers the morphology and packing factor of particles:

$$P_r = \frac{P}{P_m} = \left[\frac{1+2((\beta-\gamma)/(\beta+2\gamma))\phi}{1-((\beta-\gamma)/(\beta+2\gamma))\phi\varphi}\right] \tag{3.29}$$

$$\begin{aligned}\beta &= (2+\delta^3)\lambda_{dm} - 2(1-\delta^3)\lambda_{Im}\\ \gamma &= (1+2\delta^3) - (1-\delta^3)\lambda_{dI}\\ \varphi &= 1+\left(\frac{1-\phi_m}{\phi_m{}^2}\right)\phi\end{aligned} \tag{3.30}$$

In this model, ϕ_m is the maximum packing volume fraction of particles and it was taken to be 0.64, corresponding to the random close packing of uniform spheres. δ is the ratio of outer radius of interfacial shell to core radius and it was taken as 1.18 which is proposed by Shimekit et al.[137] λ_{dm} is the ratio of P_d/P_m, λ_{Im} is the ratio of P_I/P_m, P_I is interface permeability and λ_{dl} is the ratio of P_d/P_I. If both ϕ_m and δ are equal to 1, this model reduces to Maxwell model.

3.5.4. Prediction of Gas Permeability through MMMs with Two Different Types of Fillers

Gas permeability and selectivity of MMMs composed of two different types of fillers and one type of polymer was also predicted in this study. First, gas permeabilities through first filler/polymer (P_1) and second filler/polymer (P_2) systems were computed using the original Maxwell model. Then, the permeabilities of two systems were combined in the following expression:

$$\log P_{MMMw2F} = \phi_1 \log P_1 + \phi_2 \log P_2 \quad (3.31)$$

Here, P_{MMMw2F}, is the gas permeability of the MMM having two different type of fillers, ϕ_1 and ϕ_2 represent the volume fractions of the first filler/polymer system and second filler/polymer system, respectively.

Chapter 4

PREDICTING PERFORMANCES of ZIF-11 and ZIF-12 in GAS SEPARATIONS

Atci et al.[51] assessed performances of ZIF-2, ZIF-3, ZIF-6, ZIF-10, ZIF-60, ZIF-65, ZIF-69, ZIF-79, ZIF-81 and ZIF-90 as adsorbents and membranes for CH_4/H_2, CO_2/CH_4 and CO_2/H_2 separations using molecular simulations. They reported that some of the ZIFs outperform traditional porous adsorbent and membrane materials. In this chapter, two new ZIFs, ZIF-11 and ZIF-12, which were not considered in the previous study, were examined. Adsorption, diffusion and permeation performances of ZIF-11 and ZIF-12 for CH_4/H_2, CO_2/CH_4 and CO_2/H_2 mixtures were assessed using computational methods and compared with zeolites, MOFs and other ZIFs.

The accuracy of molecular simulations was tested by comparing the predictions of simulations in this study with the previous simulations performed in the literature. H_2 adsorption isotherm of ZIF-11 at 77 K has been reported in several theoretical studies.[39, 40, 138] Only one simulation study [40] reported the adsorption isotherm of ZIF-12. GCMC simulations were performed to compute H_2 adsorption isotherms of ZIF-11 and ZIF-12 at the same conditions with the simulations reported in the literature. Both UFF and DREIDING force fields were tested. Results of GCMC simulations for ZIF-11 and ZIF-12 were compared with the H_2 adsorption isotherms presented in the literature [39, 40, 138] as shown in Figure 4.1 (a) and Figure 4.1 (b), respectively. H_2 adsorption isotherm of ZIF-11 which was computed using UFF parameters agrees well with the adsorption isotherm

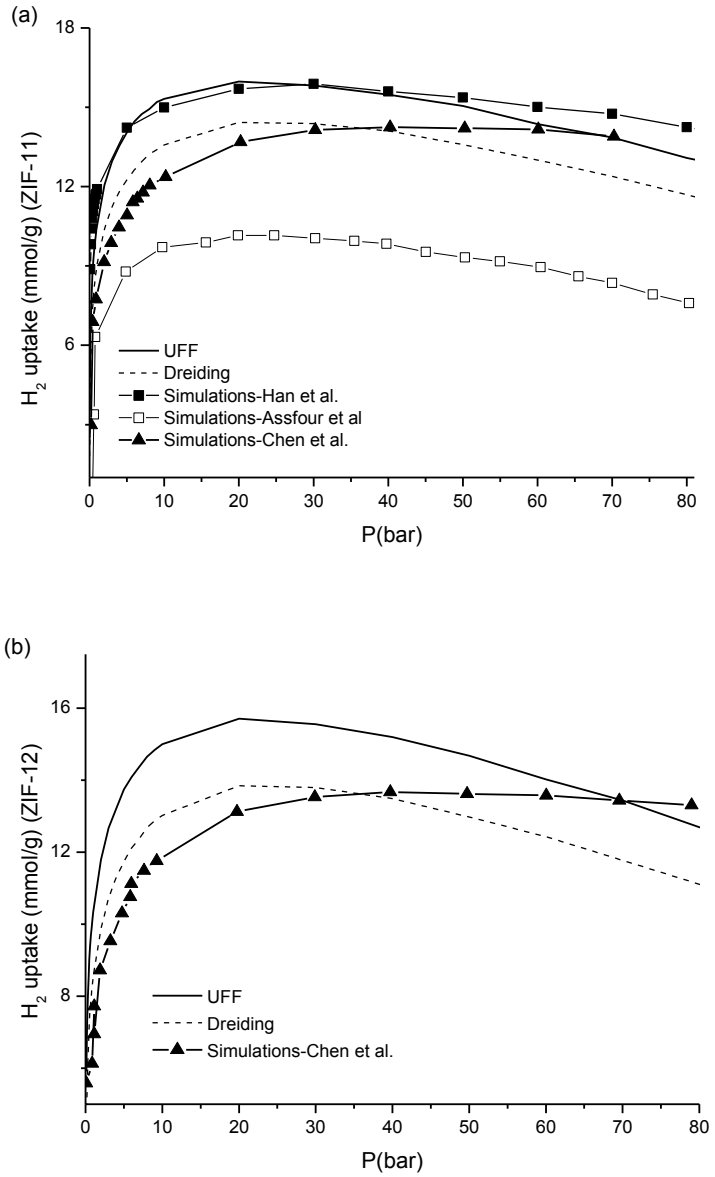

Figure 4.1: Comparison of results of simulations in this study with other simulations in the literature [39, 111, 138] for excess H_2 uptake in (a) ZIF-11 and (b) ZIF-12 at 77 K.

reported by Han et al.[39] Adsorption isotherms of ZIF-11 and ZIF-12 which were computed using UFF are closer to the predictions of Chen et al.[40] at higher pressures. Simulations performed using UFF give better results compared to predictions of simulations in which DREIDING force field is used. However, we performed most simulations using both force fields to understand the effect of force field on predicting the separation performance of ZIFs.

4.1. Adsorption-Based Separation in ZIF-11 and ZIF-12

Figure 4.2 shows single component and equimolar binary mixture adsorption isotherms of H_2, CH_4 and CO_2 at 298 K as a function of bulk pressure. UFF was used in these simulations. Single component gas adsorption amounts are larger than the mixture adsorptions for all gases. This is attributed to the competition of two different gas molecules in mixture adsorption. For example, ZIF-11 adsorbs 34 molecules H_2/unit cell of ZIF-11 (m/uc) when H_2 is pure whereas 2 molecules H_2/unit cell of ZIF-11 is adsorbed when H_2 is together with CO_2 (CO_2/H_2:50/50) at 70 bar 298 K. As can be seen in Figure 4.2(a) and Figure 4.2(d), CH_4 is preferentially adsorbed over H_2 in both ZIF-11 and ZIF-12 because CH_4 has stronger interactions with ZIF atoms and excludes H_2 molecules in the pores. Adsorption strongly favors CO_2 over CH_4 (H_2) in CO_2/CH_4 (CO_2/H_2) since CO_2 has a quadruple moment that leads to electrostatic interactions with ZIF atoms. One striking feature of Figure 4.2 is that the central metal ions, Zn and Co, play a significant role in gas adsorption in ZIF-11 and ZIF-12. ZIF-11 has a higher affinity toward H_2, CH_4 and CO_2 both in pure gas and mixed gas adsorptions compared to ZIF-12 due to the stronger interaction of Zn with the gases compared to Co. This is reflected in simulations where energy parameter of Zn (ε/k_B =62.4 K) is higher than that of Co (ε/k_B =7.05 K).

Experimental binary mixture adsorption isotherm of ZIF-11 and ZIF-12 are not available in the literature and it is the first study that provides the mixture isotherms of these materials. One approach to validate mixture adsorptions simulations is to apply IAST.

IAST is a useful thermodynamic method to predict multicomponent adsorption isotherms using thei single component adsorption data in many nanoporous materials except the ones which are energetically heterogeneous.[130] It was previously reported that multicomponent adsorption isotherms of many MOFs predicted using IAST are very close to the experimental data.[129] Thus, IAST was used to predict mixture adsorption isotherms and it was found that IAST predictions agree well with the results of GCMC simulations for CH_4/H_2, CO_2/CH_4 and CO_2/H_2 mixtures for both ZIF-11 and ZIF-12.

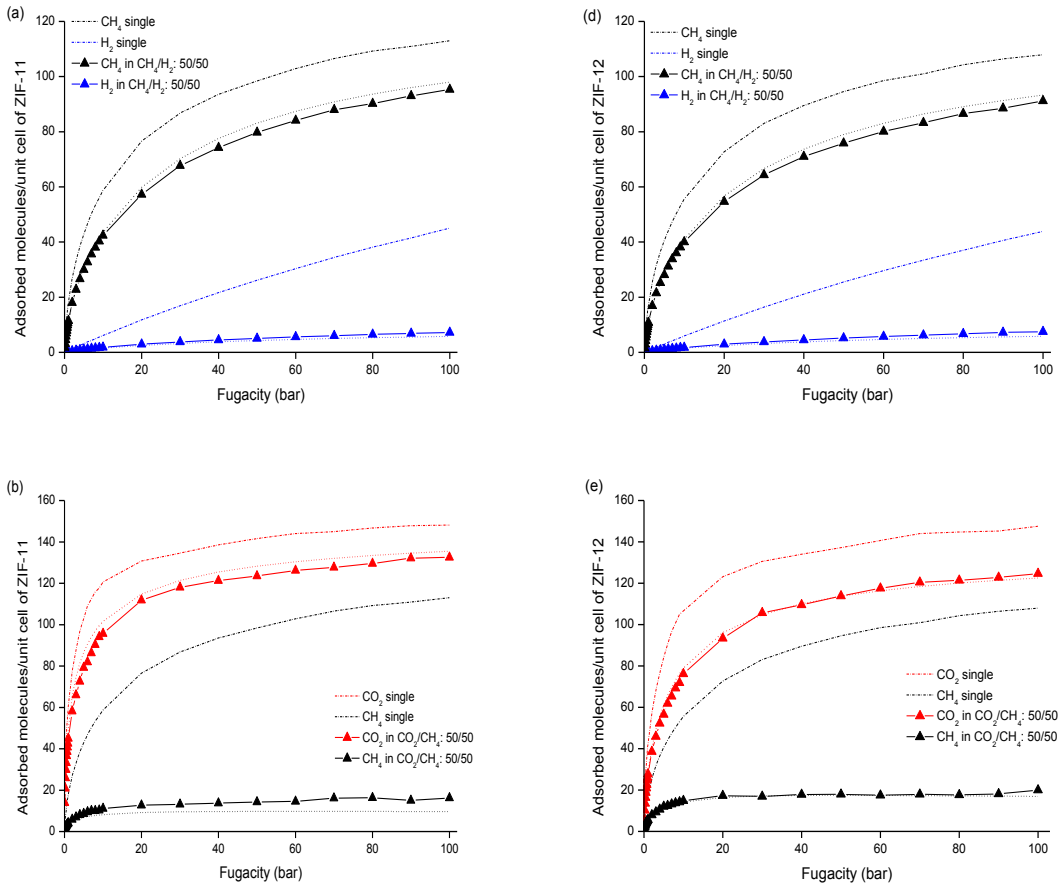

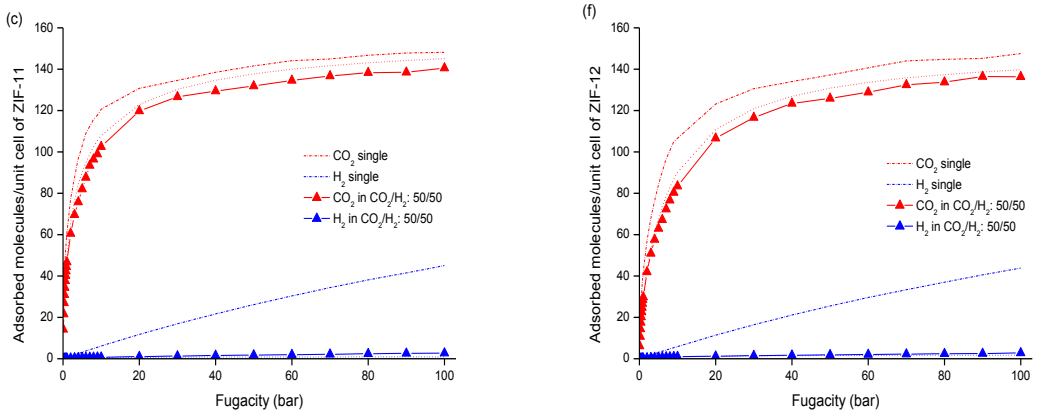

Figure 4.2: Equimolar mixture adsorption isotherms of (a) CH_4/H_2, (b) CO_2/CH_4 and (c) CO_2/H_2 of ZIF-11 and (d) CH_4/H_2, (e) CO_2/CH_4 and (f) CO_2/H_2 in ZIF-12 at 298 K. Black, blue and red lines and symbols represent CH_4, H_2 and CO_2, respectively. Dotted lines represent predictions of IAST.

Adsorption selectivity shows the ability of a material to separate different components in gas mixtures. Adsorption selectivities of ZIF-11 and ZIF-12 for CH_4/H_2, CO_2/CH_4 and CO_2/H_2 mixtures in different compositions are presented in Figure 4.3. Adsorption selectivities of ZIF-11 and ZIF-12 for CH_4/H_2 in mixtures containing 10% and 50% CH_4 in the bulk phase are similar. This indicates that metal ions do not play significant role in separation of CH_4 from H_2. However, metal ions affect single component adsorption because more CH_4 and H_2 are adsorbed in ZIF-11 than that in ZIF-12 as discussed previously. Adsorption selectivity for CH_4 over H_2 decreases with increasing pressure since entropic effects that promote adsorption of H_2 are dominant at higher pressures. Adsorption selectivity of ZIF-11 and ZIF-12 for CO_2/CH_4 is lower than CH_4/H_2 adsorption selectivities of these materials due to the competitive adsorption between CO_2 and CH_4 molecules in the pores. ZIF-11 has higher adsorption selectivity than ZIF-12 for both CO_2/CH_4:50/50 and 10/90 bulk mixtures. At 20 bar, adsorption selectivity for CO_2 is

8.8 in ZIF-11, whereas it is 5.4 in ZIF-12 in equimolar CO_2/CH_4 mixture. This difference in adsorption selectivities of two ZIFs can be explained by the energy parameters of Zn and Co atoms which are the only different atoms in structures of ZIF-11 and ZIF-12, respectively. The atomic partial charges of the atoms are also very similar (see Table A1). Thus, CO_2 is more favorably adsorbed in ZIF-11, which makes CO_2/CH_4 selectivity of ZIF-11 higher than that of ZIF-12. It is important to note that CO_2/CH_4 selectivities of ZIF-12 with 10% and 50% CO_2 in the bulk phase are similar because more CH_4 molecules are adsorbed in ZIF-12 for CO_2/CH_4:10/90 mixture. Adsorption selectivity of ZIF-11 and ZIF-12 for CO_2/H_2 are very large since CO_2 is the strongly adsorbed component whereas H_2 is the weakly adsorbed one. The discussion made for the comparison of CO_2/CH_4 selectivity in ZIF-11 and ZIF-12 is valid for the comparison of adsorption selectivities of ZIF-11 and ZIF-12 for CO_2/H_2. Adsorption selectivity of ZIF-11 for CO_2 over H_2 is considerably high (482 for CO_2/H_2:1/99 at 10 bar) and it can be attributed to both non-competitive adsorption of CO_2 and H_2 components and favorable interactions of CO_2 with the framework atoms.

Recently, Atci et al.[51] assessed adsorption selectivity of many ZIFs: ZIF-2, ZIF-3, ZIF-6, ZIF-10, ZIF-60, ZIF-65, ZIF-69, ZIF-79, ZIF-81 and ZIF-90 for CH_4/H_2 (10/90), CO_2/CH_4 (10/90) and CO_2/H_2 (1/99) mixtures using GCMC simulations at 298 K. As compared to these ZIFs, both ZIF-11 and ZIF-12 outperform ZIF-2, ZIF-3, ZIF-6, ZIF-10, ZIF-60, ZIF-65, ZIF-69 and ZIF-90 in adsorption-based separation of CH_4 from H_2 at the same conditions. There is no ZIF among the listed ones above having higher CO_2/CH_4 and CO_2/H_2 adsorption selectivity than ZIF-11. For example, the most promising ZIF in CO_2/H_2 separation was reported as ZIF-69 and CO_2/H_2 selectivity of ZIF-69 was calculated as 240 in Atci's study.[51] However, the selectivity of ZIF-11 under the same conditions is 431. CO_2 selectivity of ZIF-12 over CH_4 and H_2 were also compared with other ZIFs and it was found that ZIF-12 is a better adsorbent candidate than ZIF-65, ZIF-69, ZIF-81 and ZIF-90 (ZIF-69 and ZIF-81) for CO_2/CH_4 (CO_2/H_2) separations due to its higher adsorption

selectivity. The reason for exceptional selectivity of ZIF-11 and ZIF-12 can be attributed to high framework pore volume (13982 $Å^3$) and narrow pores (3.3 Å pore openings in diameter with 14.6 Å large cages).

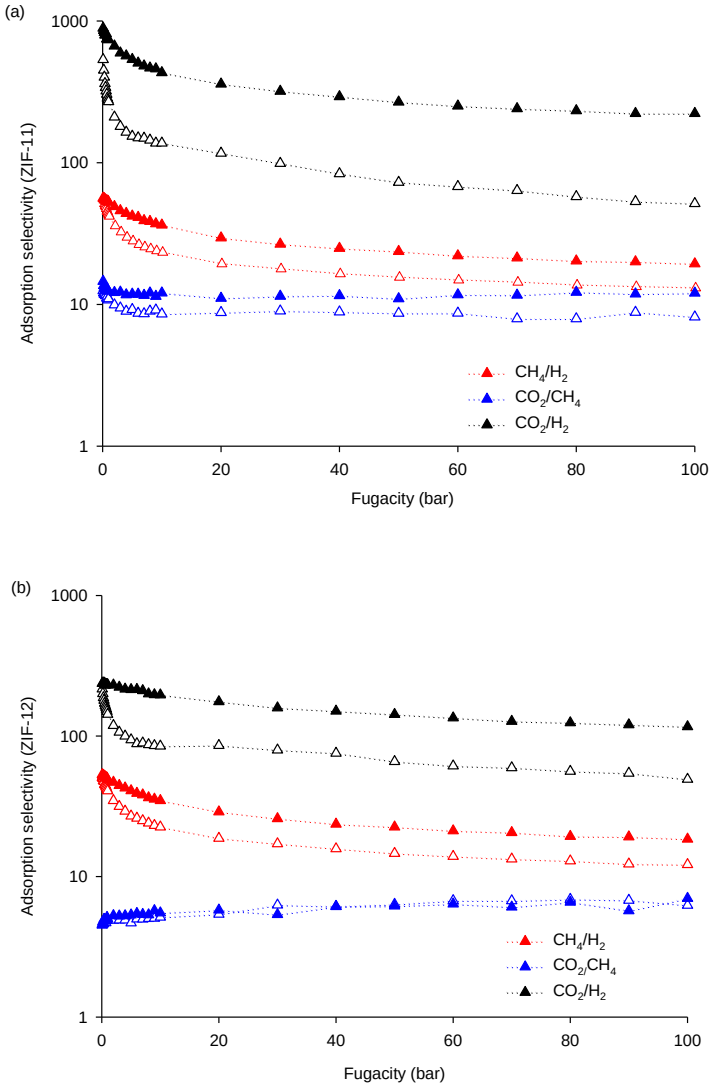

Figure 4.3: Adsorption selectivity of (a) ZIF-11 and (b) ZIF-12 for CH_4/H_2, CO_2/CH_4 and CO_2/H_2 mixtures at 298 K. Open (closed) symbols represent CH_4/H_2:50/50 (10/90), CO_2/CH_4:50/50 (10/90) and CO_2/H_2:50/50 (1/99) mixtures.

It is crucial to evaluate the gas separation potential of ZIF-11 and ZIF-12 among the widely studied MOFs and zeolites. Adsorption selectivity alone is not a sufficient criterion to decide the suitability of an adsorbent for a specific gas separation. Regeneration of the adsorbent is important for an economic adsorption-based separation. This depends on "working capacity" (or delta loading) which is the adsorbed amount that is remained after desorption process. In this study, working capacity and adsorption selectivity were used to compare ZIF-11 and ZIF-12 with MOF and zeolite adsorbents. To be consistent with the simulations, working capacity of CH_4 and CO_2 was evaluated at adsorption and desorption pressures of 10 and 1 bar, respectively. Figure 4.4 represents the working capacities and adsorption selectivities of materials for CH_4/H_2, CO_2/CH_4 and CO_2/H_2 separations. The most promising adsorbent candidates are expected to be located on top right hand corner of Figure 4.4. Figure 4.4 (a) shows that ZIF-11 and ZIF-12 have the highest adsorption selectivity for CH_4/H_2 mixture but mediocre working capacity for CH_4 compared to traditional MOF and zeolite adsorbents. The most promising adsorbents that outperform ZIF-11 and ZIF-12 are MgMOF-177 and ZnMOF-177. The result of high working capacities of these MOFs was previously explained by the fact that they have very high surface areas and high pore volumes.[139] Most of zeolites and MOFs (TSC, CuBTT, MOF-177, BeBTB and rho-ZMOF) exhibit low CH_4 selectivities (<10) although some of them have high working capacities. As compared to other ZIFs that were evaluated using simulations, ZIF-11 and ZIF-12 have the highest CH_4 selectivity (23.6 and 22.5, respectively) and delta loading (2.0 and 1.9, respectively) combination. Figure 4.4 (b) shows that MgMOF-177 and ZnMOF-177 exhibit higher CO_2/CH_4 adsorption selectivities than ZIF-11 and ZIF-12, respectively. In previous studies, high adsorption selectivities of the MOFs for CO_2 were ascribed to metal cation sites in the framework.[140] Adsorption selectivity of MgMOF-74 (ZIF-11) is higher compared to ZnMOF-74 (ZIF-12) since CO_2 molecules have more favorable interactions with the Mg (Zn) than Zn (Co). It is important

to note that NaX exhibits very high CO_2 selectivity due to the strong electrostatic interactions between CO_2 and non-framework cation (Na^+), but it has very low working capacity. ZIF-11 and ZIF-12 can be classified as adsorbents having mediocre CO_2 selectivity and mediocre working capacity and they can be good candidates for adsorption-based separation of CO_2/CH_4. The performance of ZIF, MOF and zeolite adsorbents for CO_2/H_2 separation is given in Figure 4.4 (c). ZIF-11 and ZIF-12 outperforms all other ZIFs recently studied [51] as well as most of MOFs and zeolites (MOR, NaX, MFI, DDR, ZIF-8 and CuBTC). Therefore, ZIF-11 and ZIF-12 are promising adsorbents for CH_4/H_2, CO_2/CH_4 and CO_2/H_2 mixture separation and they are needed to be examined in detail through experiments.

Effect of force field on adsorption selectivity and working capacity was also examined in this. Working capacities of ZIF-11 and ZIF-12 for CO_2 and CH_4 are always higher when UFF parameters are used since interaction parameters of UFF is higher than that of DREIDING. CH_4 selectivities of ZIF-11 and ZIF-12 are larger in UFF-based calculations. It is ascribed to more pronounced increase in CH_4 adsorption compared to H_2 adsorption when parameters are changed from DREIDING to UFF. Similar discussion is also valid for CO_2/H_2 separation. However, in CO_2/CH_4 separation, UFF and DREIDING-based adsorption selectivities for CO_2 over CH_4 are similar since both CO_2 and CH_4 have favorable interactions with framework atoms and the competition between these molecules is a lot more pronounced compared to the competition between CO_2-H_2 and CH_4-H_2.

4.2. Diffusion in ZIF-11 and ZIF-12

Membrane-based gas separation performance of materials is evaluated based on adsorption and diffusion characteristics of gas components. Figure 4.5 shows single component self-diffusivities of H_2, CO_2 and CH_4 computed from molecular dynamic simulations as a function of total loading. Light H_2 molecules diffuse faster than CO_2 and

CH_4. A general trend in self-diffusivities of gas components as a function of loading should be a decrease in the diffusivity of gases with increasing adsorbed loading due to steric

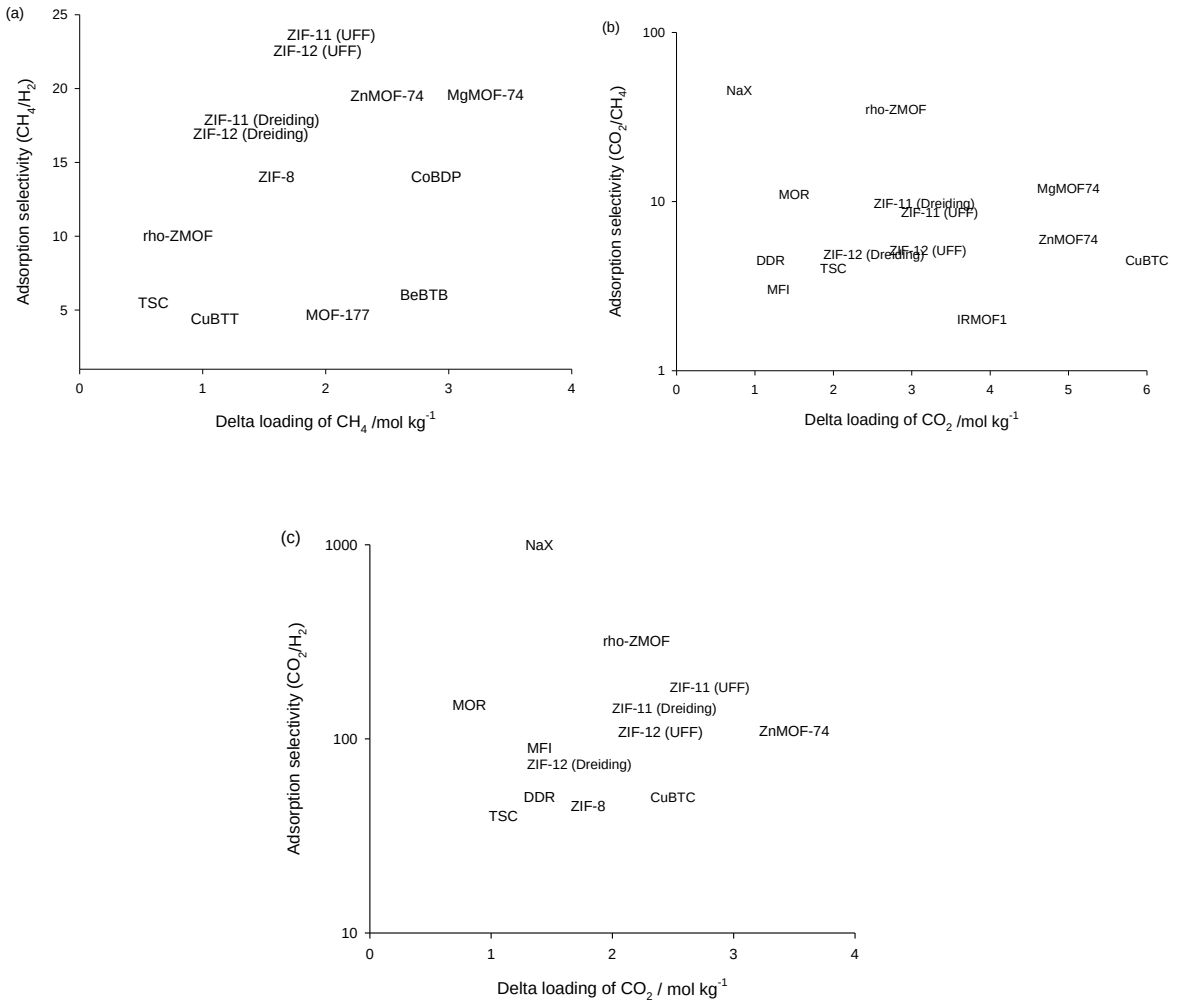

Figure 4.4: Comparison of adsorption selectivities and delta loadings of ZIF-11 and ZIF-12 (298 K) with other MOF and zeolite adsorbents [139] (300 K) for (a) CH_4/H_2, (b) CO_2/CH_4 and (c) CO_2/H_2 separations. The bulk composition of CH_4/H_2, CO_2/CH_4 and CO_2/H_2 mixtures are 50/50, 50/50 and 15/85 at 10 bar.

hindrance between diffusing molecules. However, this trend is not observed in diffusivities of small H_2 and CO_2 molecules which can be attributed to the large pore volume of ZIF-11 and ZIF-12 materials.

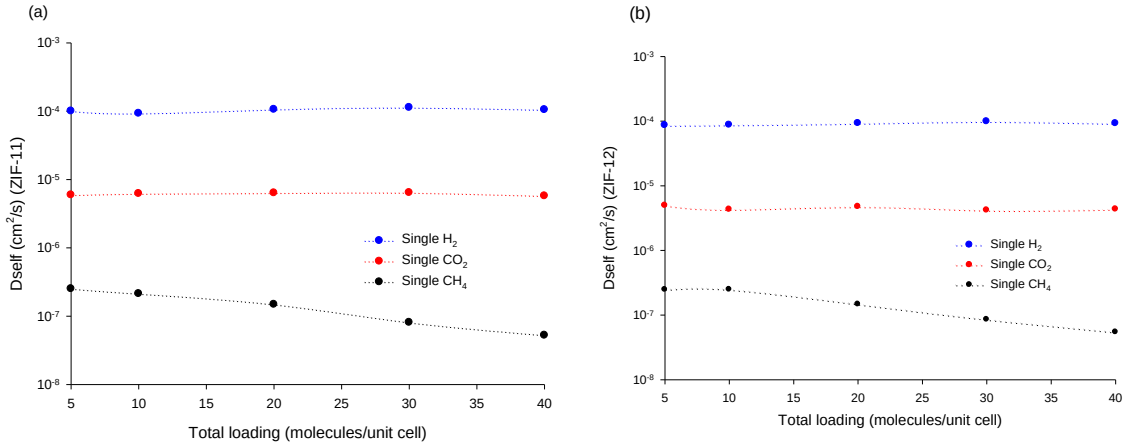

Figure 4.5: Single component self-diffusivities of H_2, CO_2 and CH_4 in (a) ZIF-11 and (b) ZIF-12 at 298 K.

It is important to examine diffusivities of gases in mixtures rather than as single components since mixture gas separation is desired in practical applications. Figure 4.6 shows single component and mixture self-diffusivities of H_2 and CO_2 in ZIF-11 and ZIF-12 at 298 K. Mixture self-diffusivities of H_2 (CO_2) were computed at the adsorbed loading concentrations for 50% and 90% H_2 (CO_2) in the bulk mixture. Self-diffusivities of H_2 (CO_2) in CO_2/H_2 mixture are smaller (larger) than the pure H_2 (CO_2) self-diffusivities. This can be explained by the momentum transfer between two competing different gas molecules that CO_2 (H_2) slows down (accelerates) faster (slower) diffusing H_2 (CO_2) in CO_2/H_2 mixture. Diffusivity of the slower (faster) component increases (decreases) as molar fraction of faster (slower) component increases in the bulk phase.

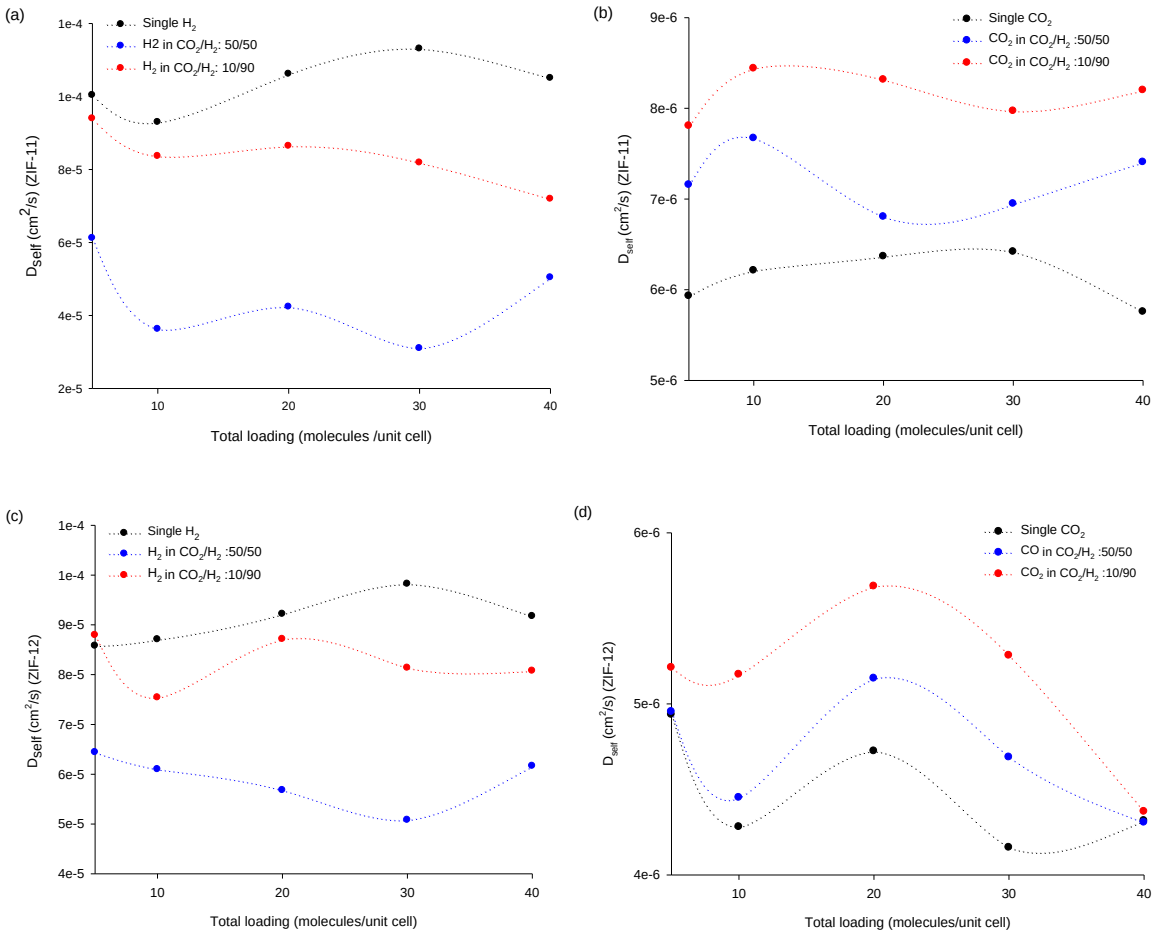

Figure 4.6: Single component and mixture self-diffusivities of H_2 and CO_2 in ZIF-11 (a, b) and ZIF-12 (c, d) at 298 K.

4.3. Membrane-Based Separation in ZIF-11 and ZIF-12

Adsorption selectivity, diffusion selectivity and permeation selectivity of ZIF-11 and ZIF-12 for CH_4/H_2 (10/90) mixture are shown in Figure 4.7. Adsorption selectivity favors CH_4 over H_2 since CH_4 molecules have more favorable interactions with the framework atoms of ZIF-11 and ZIF-12. Adsorption selectivities of CH_4 from H_2 in ZIF-11

and ZIF-12 are close to each other and decrease at high pressures due to the steric hindrance as discussed earlier (see Figure 4.7 (a)). For example, at 5 bar, CH_4 selectivity in ZIF-11 (ZIF-12) is 42 (40), whereas at 40 bar, it is 24 (24). ZIF-11 and ZIF-12 exhibit low diffusion selectivity for CH_4 since strongly adsorbed CH_4 molecules diffuse more slowly than the weakly adsorbed H_2 molecules. Diffusion selectivities of ZIF-11 and ZIF-12 are similar as in adsorption selectivity. The combined effect of adsorption and diffusion selectivities results in permeation (membrane) selectivities. Permeation selectivities of CH_4 over H_2 in ZIF-11 and ZIF-12 are predicted to be smaller (larger) than the adsorption (diffusion) selectivity for CH_4 since low diffusion selectivity decreases the effect of high adsorption selectivity on permeation selectivity. This case was also observed in previous studies on MOF and ZIF membranes.[50, 129] Permeation selectivity for CH_4 over H_2 in ZIF-11 and ZIF-12 are nearly the same since both adsorption and diffusion selectivities are similar in these materials. Compared to zeolite membranes, permeation selectivities of ZIF-11 and ZIF-12 for CH_4 are found to be higher. For example, permeation selectivity of LTA and CHA for CH_4 over H_2 was reported as 0.001 and 0.004, respectively.

Adsorption, diffusion and permeation selectivity of ZIF-11 and ZIF-12 for CO_2/CH_4 mixture are shown in Figure 4.7 (b). Adsorption selectivity favors CO_2 over CH_4 in both ZIF-11 and ZIF-12 due to electrostatic interactions between CO_2 and ZIF atoms which is absent for CH_4. The adsorption selectivity of ZIF-11 is higher than ZIF-12 as discussed previously. Similar to adsorption selectivity, diffusion selectivity favors CO_2 and it is found to be higher in ZIF-11. Permeation selectivity for CO_2/CH_4 mixture in ZIF-11 and ZIF-12 are found to be very high due to high adsorption and high diffusion selectivity for CO_2 over CH_4. This case is different than what is observed for CH_4/H_2 mixture since adsorption and diffusion do not compensate each other for CO_2/CH_4 mixture. This is desired because this type of gas mixture/ZIF systems leads to high permeation selectivity since both adsorption and diffusion favor the same component. For example, at 20 bar, permeation selectivity for

CO_2 is 665 in ZIF-11, whereas it is 255 in ZIF-12. This large difference between permeation selectivities of ZIF-11 and ZIF-12 arises from differences in adsorption and diffusion selectivities. For example, adsorption (diffusion) selectivity of ZIF-11 for CO_2 over CH_4 is 11 (60) whereas that of ZIF-12 is 6 (44). Membrane selectivities of ZIF-11 and ZIF-12 were compared to other ZIFs (ZIF-2, ZIF-3, ZIF-6, ZIF-10, ZIF-60, ZIF-65, ZIF-69, ZIF-79, ZIF-81, ZIF-90) which are also computed using molecular simulations.[51] Both ZIF-11 and ZIF-12 outperform all ZIFs. For example, ZIF-11 and ZIF-12 have higher permeation selectivity for CO_2 than ZIF-90 which exhibits the highest CO_2 selectivity (22) among the studied ZIFs.

Figure 4.7 (c) shows that adsorption selectivity of ZIF-11 for CO_2/H_2 mixture is higher than that of ZIF-12, similar to observations for CO_2/CH_4 mixture. Permeation selectivities of ZIF membranes are smaller than the adsorption selectivities for CO_2 over H_2 since diffusion favor H_2 over CO_2 in both ZIFs. The permeation selectivities of ZIFs are higher than several other ZIFs [51] and permeation-based selectivities of these ZIFs for CH_4/H_2, CO_2/CH_4 and CO_2/H_2 separations can be found in Table B1, Table B2 and Table B3, respectively.

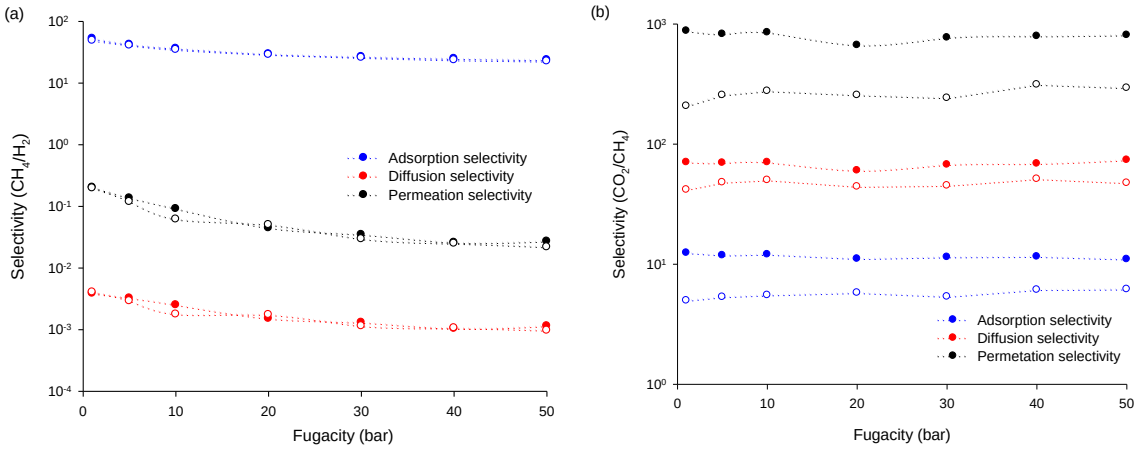

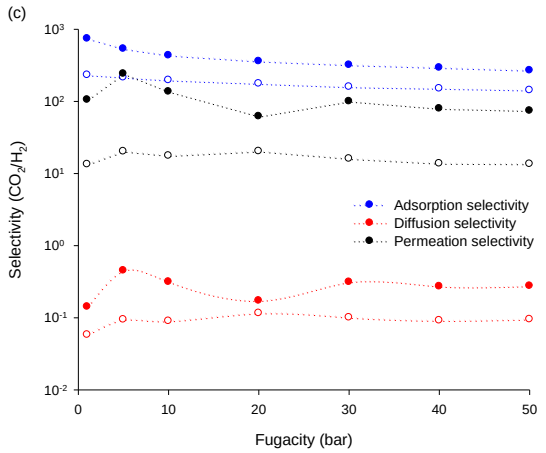

Figure 4.7: Adsorption selectivity, diffusion selectivity and permeation selectivity of ZIF-11 and -12 for (a) CH_4/H_2, (b) CO_2/H_2 and (c) CO_2/CH_4 mixtures at 298 K. Close (open) symbols represent ZIF-11 (ZIF-12). The bulk gas mixtures are CH_4/H_2:10/90, CO_2/H_2:1/99 and CO_2/CH_4:10/90.

Two important factors determining performance of a membrane are permeability and permeation selectivity. Both high permeability and high permeation selectivity are needed for an economic membrane-based gas separation process. Permeability determines the required membrane area and selectivity determines the purity of gas product. Permeability and permeation selectivity of ZIF-11 and ZIF-12 were compared to other MOFs and ZIFs in Figure 4.8. A promising membrane would be located at the top right hand corner of the diagram. Permeation selectivities for CH_4/H_2 mixture at 10 bar are given in Figure 4.8 (a). ZIF-11 and ZIF-12 are promising candidates for separation of H_2 from CH_4 because they exhibit very high H_2 permeability and permeation selectivity. ZIF-11 and ZIF-12 outperform zeolite and MOF membranes. Figure 4.8 (b) shows that permeation selectivities of ZIF-11 and ZIF-12 are significantly higher than that of other nanoporous materials due to their molecular sieving properties for CO_2/CH_4 separation. They have

better separation performance than widely studied DDR and CHA which also show high permeation selectivities toward CH_4 due to their narrow windows that control molecular transport inside the material's pores.[141, 142] Therefore, diffusion selectivity favors CO_2 over CH_4 as in ZIF-11 and ZIF-12. Although ZIF-11 and ZIF-12 have mediocre CO_2 selectivities, they have the best permeability-selectivity combination. Figure 4.8 (c) shows membrane performances of ZIFs for CO_2/H_2 separation. ZIF-11 and ZIF-12 have high CO_2 selectivities and permeabilities compared to many MOF and zeolite membranes since adsorption strongly favors CO_2 over H_2.

Effect of the force field on gas permeability and permeation selectivity of ZIF membranes was also investigated. Permeation selectivity for CH_4 over H_2 is higher when DREIDING force field parameters were used in the simulations (see Figure 4.8 (a)). When the DREIDING force field was used higher CH_4/H_2 selectivity was observed. This can be explained by examining the changes in adsorption and diffusion of gases when the force field was changed. Both CH_4 and H_2 adsorption decreased when DREIDING was used. Due to the weaker interactions between framework atoms and gases, the diffusivity of both gases increased. This increase is more pronounced for CH_4 compared to H_2. The increase in diffusivities of gases is more dominant compared to the decrease in adsorption. Therefore, permeation selectivity favors CH_4 more strongly when DREIDING was used compared to UFF. For CO_2/CH_4 separation (see Figure 4.8 (b)), in ZIF-11, diffusivities of components increase when parameters changed from UFF to DREIDING. Increase in CO_2 diffusivity is more pronounced than that in CH_4, thus diffusion selectivity and permeation selectivity favor CO_2 over CH_4 when DREIDING was used instead of UFF. On the other hand in ZIF-12, diffusivity of CH_4 molecules slightly increases whereas that of CO_2 molecules decreases when DREIDING parameters are used. This decrease in CO_2 diffusivity in ZIF-12 at some loadings was also shown in Figure 4.6 (d). Therefore, permeation selectivity of ZIF-12 for CO_2/CH_4 mixture with DREIDING-based simulations is lower than that of with

UFF-based simulations. Similar discussion is valid for permeation selectivity of ZIF-11 and ZIF-12 for CO_2 over H_2 (see Figure 4.8 (c)). Permeation selectivity of ZIF-12 increases when parameters were changed from UFF to DREIDING.

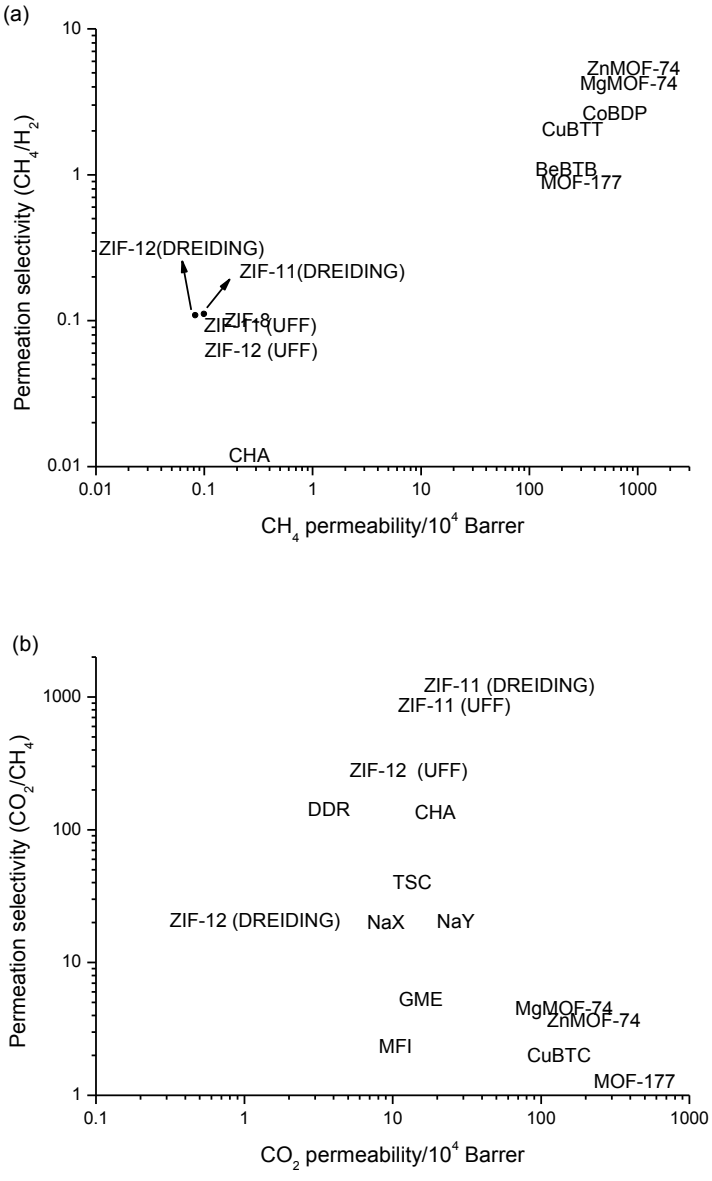

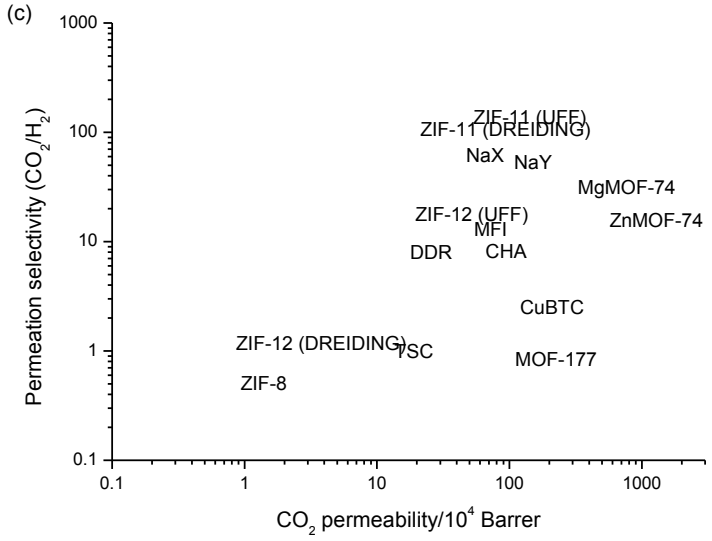

Figure 4.8: Comparison of ZIF membranes with other nanoporous membranes for (a) CH_4/H_2, (b) CO_2/CH_4 and (c) CO_2/H_2 mixture separations. The bulk gas mixtures are CH_4/H_2:10/90 (50/50), CO_2/CH_4:10/90 (50/50) and CO_2/H_2:1/99 (15/85) for ZIF-11 and ZIF-12 (membranes other than ZIF-11 and ZIF-12). Data for materials except ZIF-11 and ZIF-12 were taken from ref [139].

Chapter 5

ZIF-BASED MMMs for H_2/CH_4, H_2/CO_2 and CO_2/CH_4 SEPARATIONS

ZIFs are promising membrane materials as discussed in Chapter 4. However, fabrication of defect-free, thin layer ZIF membranes is challenging and costly. Using ZIFs as filler particles in polymer membranes combines easy fabrication and low cost of polymers with high gas separation performance of ZIFs. In this chapter, performances of 360 new ZIF-based MMMs for H_2/CH_4, H_2/CO_2 and CO_2/CH_4 separations were examined.

5.1. Validation of Theoretical Methods

Theoretical permeability predictions were compared with the available experimental data to validate the accuracy of the methodology. Experimental measurements of CO_2, CH_4, H_2 and N_2 permeability through ZIF-based MMMs were collected from literature. There is a large amount of gas permeability data (totally 56 data points) for ZIF-8 [79, 88-91] and ZIF-90 [80] -based MMMs, therefore molecular simulations were performed for ZIF-8 and ZIF-90 at the same temperature and pressure with the experiments. Gas permeabilities of pure ZIFs computed using molecular simulations and gas permeabilities of pure polymers taken from literature were implemented into the theoretical permeation models to predict permeabilities and selectivities of ZIF-based MMMs. Maxwell and modified Felske models were used to predict gas permeability in MMMs since Erucar and Keskin [143] had previously tested many theoretical permeation models and showed that Maxwell (modified Felske) model is

the most accurately predicting model among the models which take ideal (non-ideal) morphology into account. Percent average absolute relative error (AARE%) values were calculated to evaluate the deviation between the theoretical predictions and experimental measurements:

$$AARE\% = \frac{100}{N^*}\sum_{i=1}^{N}\left|\frac{P_i^{cal} - P_i^{exp}}{P_i^{exp}}\right| \quad (5.1)$$

Here, P_i^{cal}, P_i^{exp} and N* are permeability calculated by models, permeability measured by experiments and number of data points, respectively. The AARE% values were presented in Table 5.1. Permeability predictions of Maxwell model were found to be closer to the experimental data than permeability predictions of the modified Felske model. This was attributed to the large changes in experimental gas permeability data from one filler loading to another, which was captured better by the Maxwell model predictions. Therefore, gas selectivity and permeability of ZIF-based MMMs introduced in this chapter were computed using Maxwell model.

Table 5.1: AARE% values for gas permeability in ZIF-8 and ZIF-90-based MMMs.

ZIF[a]	Model	H_2	CO_2	N_2	CH_4
ZIF-8	Maxwell	5.21	17.04	5.28	0.79
	modified Felske	56.83	36.62	43.69	44.14
ZIF-90	Maxwell	-	14.57	-	10.22
	modified Felske	-	39.28	-	22.54

[a]The polymers used in ZIF-8 (ZIF-90)-based MMMs are Matrimid, Ultem and PPEES (Matrimid, Ultem and 6FDA-DAM).

Figure 5.2 represents comparison of theoretical permeability results with the experimental data for ZIF-8-based MMMs. Experimental H_2, CO_2, CH_4 and N_2 permeability data were taken from the study of Song et al.,[90] Ordonez et al.,[79] Diaz et al.[88] and Dai et al.[91] in which ZIF-8/polymer MMMs were synthesized. Matrimid, PPEES and Ultem were used as polymers in these membranes. Experimental data of mixed gas permeability in ZIF-8-based MMMs was taken from the study of Basu et al.[89] Figure 5.2 shows that theoretical results match well with the experiments for 48 data points.

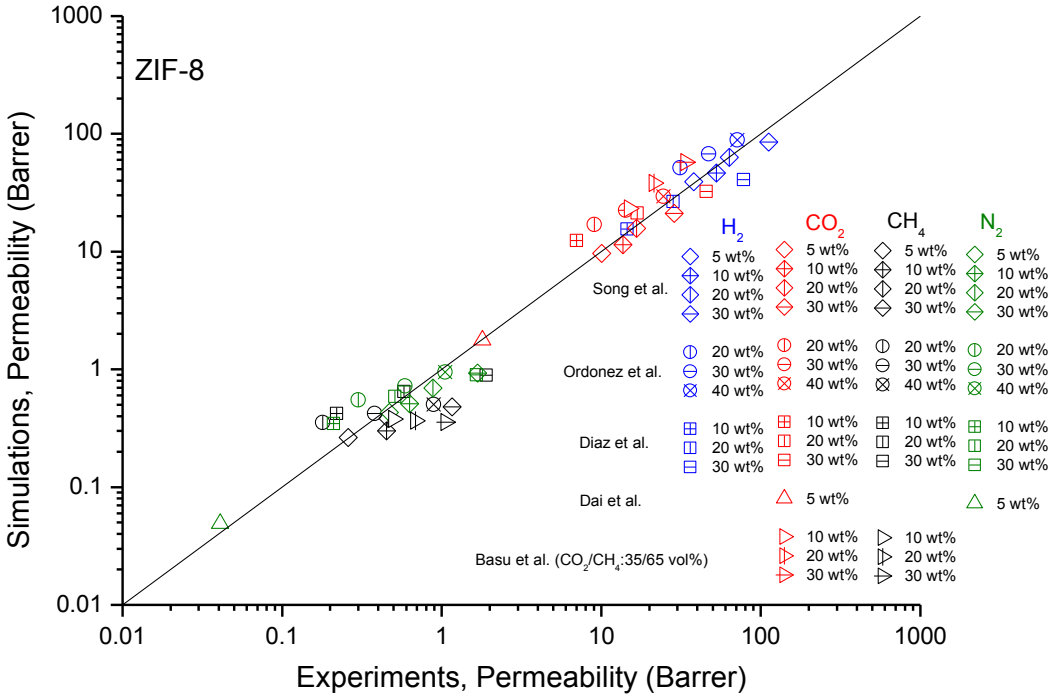

Figure 5.1: Comparison of predicted gas permeability data with experiments for ZIF-8-based MMMs.[79, 88-91]

Permeabilities of ZIF-90-based MMMs were also computed to further check the validity of the theory and they were compared with the measured CO_2 permeabilities reported by Bae et al.[80] It was found that calculations agree well with the experiments for 8 data points as shown in Figure 5.2. Therefore, this theoretical approach is appropriate to make predictions for permeability and selectivity of the new ZIF/polymer MMMs for H_2/CH_4, H_2/CO_2 and CO_2/CH_4.separations.

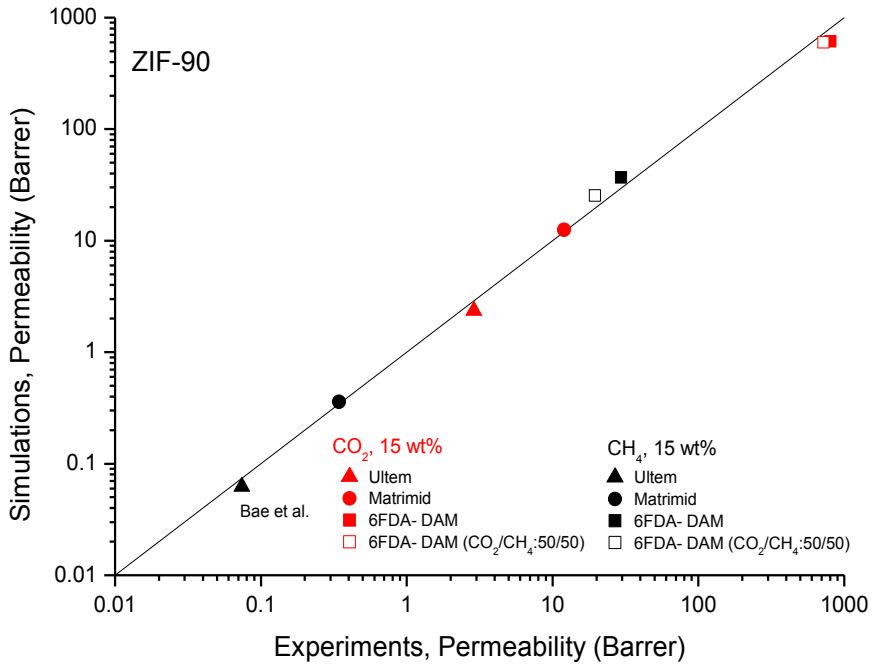

Figure 5.2: Comparison of predicted gas permeability data with experiments for ZIF-90-based MMMs.[80]

5.2. Performance of Pure ZIF and Polymer Membranes

Permeability and ideal selectivity of ZIFs were shown in Figure 5.3 together with the Robeson's upper bound to get the first information about the gas separation

performances of ZIF and polymer membranes in H_2/CH_4, H_2/CO_2 and CO_2/CH_4 separations. Gas permeability data of pure polymers were taken from the study of Robeson et al.,[24] whereas gas permeability data of pure ZIFs were calculated using molecular simulations as described in Chapter 3. Calculated pure gas permeabilities and ideal selectivities of all ZIFs are given in Table C5. Figure 5.3 (a) shows predicted H_2 permeabilities and H_2/CH_4 selectivities of ZIFs with experimental data of polymers. All ZIFs, except ZIF-2, ZIF-79 and ZIF-81, exceed the upper bound. ZIF-11, ZIF-12, ZIF-65 and ZIF-90 exhibit both high permeability (10^4-10^5 Barrers) and high selectivity (>10) which indicates that these ZIFs are promising candidates that can carry polymers above the upper bound. ZIF-3, ZIF-6, ZIF-10 and ZIF-60 have high H_2 permeability (>10^5 Barrers) but low H_2/CH_4 selectivity (0.3-0.6). They are still good candidates because these ZIFs can enhance permeability of pure polymers (such as polyimides, Hyflon, Matrimid, PPEES) which have low permeability (<100 Barrers) but high selectivity (>10). Figure 5.3 (b) represents permeability and ideal selectivity of pure polymers and ZIFs for H_2/CO_2 separation. All ZIFs have exceptionally high H_2 permeability but a few of them (ZIF-65, ZIF-81 and ZIF-90) exhibit high selectivity. Most of the pure polymers used for H_2/CO_2 suffer from low H_2 permeability. Thus, ZIFs can carry polymers, such as polyester, polyaniline, polyimide and Matrimid above the upper bound by improving their permeability. Similar to H_2/CH_4 separation, the aim of incorporating ZIF fillers into polymers in H_2/CO_2 separation is to enhance gas permeability of polymers by introducing nanoporous ZIFs. Figure 5.3 (c) shows that ZIF-11 and ZIF-12 are promising fillers for CO_2/CH_4 separations and they are above the upper bound due to higher permeabilities (>10^4 Barrers) and higher selectivities (>100) compared to pure polymers. ZIF-65 and ZIF-90 are also close to the upper bound. Although they have similar selectivities to pure polymers, they show at least one order of magnitude larger CO_2 permeabilities than

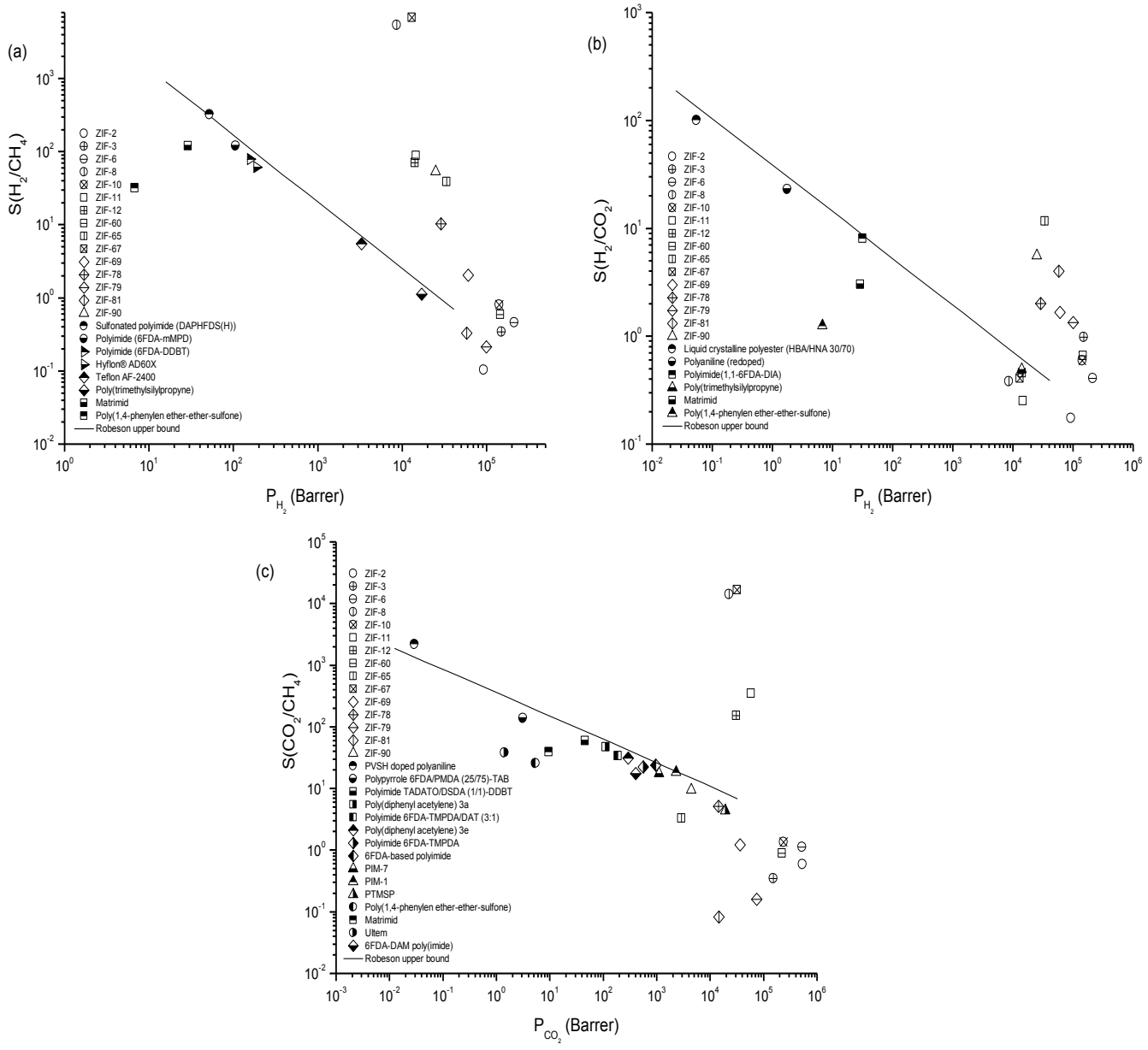

Figure 5.3: Selectivities and permeabilities of the pure ZIFs and polymers for (a) H_2/CH_4, (b) H_2/CO_2 and (c) CO_2/CH_4 separations.

polymers. Incorporation of ZIF-65 and ZIF-90 into polymers can enhance permeability of polymers without decreasing their selectivity A general observation from Figure 5.3 is that ZIFs have generally high permeabilities compared to pure polymers. Thus, permeability of many ZIF/polymer combinations is expected to be higher than that of pure polymers.

5.3. Predicting Gas Separation Performance of New ZIF-Based MMMs

Figure 5.4 shows H_2 permeability and selectivity of ZIF-69 and ZIF-90-based MMMs for H_2/CH_4 separation. Filled (open) symbols represent performances of pure polymers (ZIFs) and stars represent predictions of Maxwell model for the performances of MMMs in which volume fraction of ZIFs increases from 0.1 to 0.4. The polymers are generally characterized by low H_2 permeability but high H_2 selectivity. Therefore, highly H_2 permeable ZIFs, ZIF-69 and ZIF-90, which exhibit different H_2 selectivities, were chosen to observe the separation performance of MMMs. Figure 5.4 (a) represents separation performance of MMMs in which nonselective ZIF-69 (H_2/CH_4 selectivity of 2.05) was incorporated as filler particles. A small volume fraction of ZIF-69 was able to easily carry the polymers above the upper bound by improving their permeability without changing their selectivity. Similarly, Figure 5.4 (b) shows that H_2 selective ZIF-90 (H_2/CH_4 selectivity of 53.65) enhances the permeability of the polymers without changing the selectivity of most polymers (polyimide and Hyflon). Figure 5.4 also indicates that MMMs' permeabilities do not change significantly when a more selective ZIF is chosen as filler particles. For example, ZIF-69 increases permeability of Hyflon from 187 to 326 Barrers when used at a volume fraction of 0.2. Similarly, Hyflon's permeability will change from 187 to 323 Barrers if ZIF-90 is used.

The identity of the ZIFs becomes important for the polymers which are close to the lower corner of the upper bound. For example, if ZIF-69 is incorporated in Teflon, permeability of Teflon will change from 3300 to 6698 Barrers whereas its selectivity

remains constant at ~5.5 (at a volume fraction of 0.3). On the other hand, if ZIF-90 is used to make MMM, both permeability and selectivity of polymer will increase from 3300 to

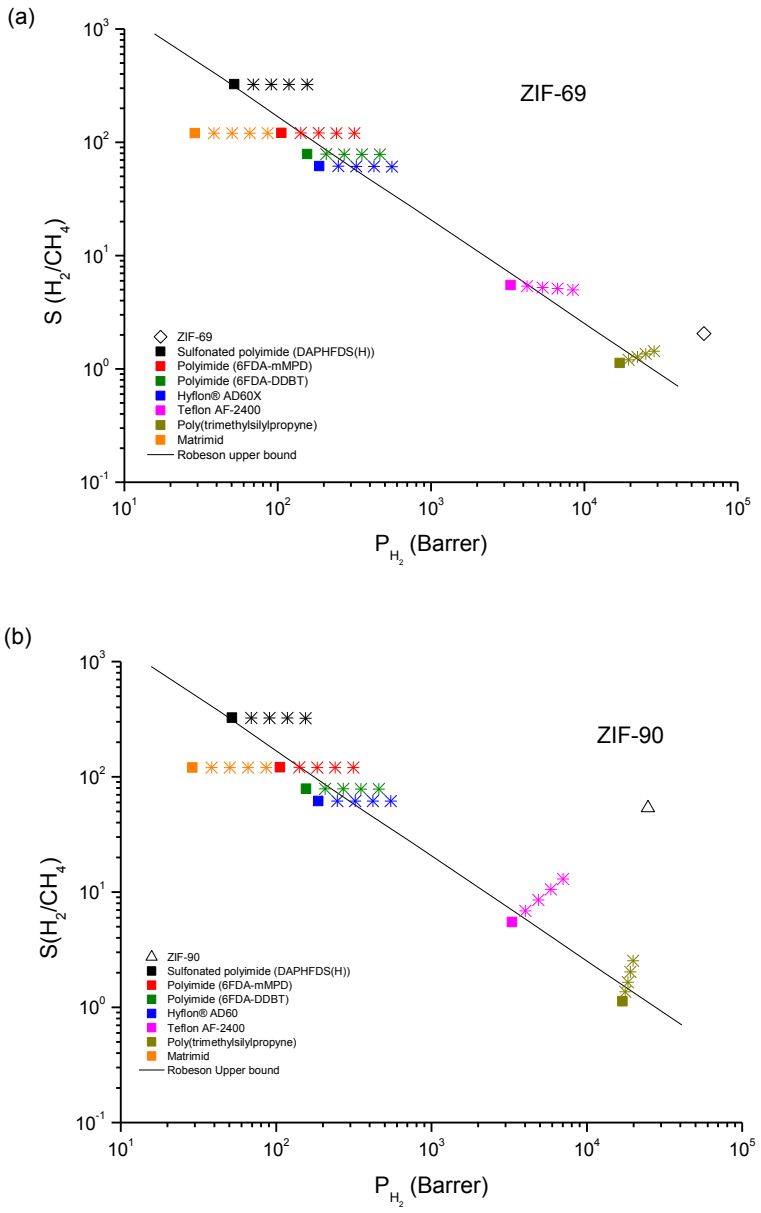

Figure 5.4: Performance of a) ZIF-69 and b) ZIF-90-based MMMs for H_2/CH_4 separation.

5857 Barrers and 5.5 to 10.5, respectively. This example emphasizes that choosing a highly selective and permeable ZIF as filler particles is not enough, matching it with the correct polymer is very important to obtain MMMs with high gas separation performance. The gas separation performance of other ZIF/polymer MMMs for H_2/CH_4 separation is given in Figure D1.

Figure 5.5 represents H_2 permeability and H_2/CO_2 selectivity of ZIF-79 and ZIF-65-based MMMs. Similar plots for all other ZIF-based MMMs are given in Figure D2. ZIFs are promising fillers for H_2/CO_2 separations since they are able to carry all polymers, except Matrimid, above the upper bound. Despite its low permeability (28.88) and selectivity (3.03), Matrimid is the mostly studied polymer in MMMs due to its excellent mechanical properties, high glass transition temperature, good adhesion with fillers and low cost. Finding a filler particle to improve separation properties of Matrimid above the upper bound has special importance. A filler particle with H_2/CO_2 selectivity of 50 and H_2 permeability of 100 Barrers is required to carry Matrimid above the upper bound for H_2/CO_2 separation. Although ZIF-65 is the best filler candidate among all ZIF candidates considered in this work for H_2/CO_2 separation, it is not able to carry Matrimid above the upper bound. ZIF-65 shows exceptionally high performance when it is incorporated in PTMSP (see Figure 5.5 (a)) since it increases H_2 permeability and selectivity of PTMSP from 13900 to 20056 Barrers and 0.495 to 1.27, respectively. Figure 5.5 (b) shows gas separation performance of MMMs containing ZIF-79 as fillers. Pure ZIF-79 has lower permeability and selectivity than ZIF-65 but it still improves separation performance of polymers. As the volume fraction of ZIF-79 particles increases from 0 to 0.4 in polyimide (1,1-6FDA-DIA), H_2 permeability increases from 31 up to 94 Barrers.

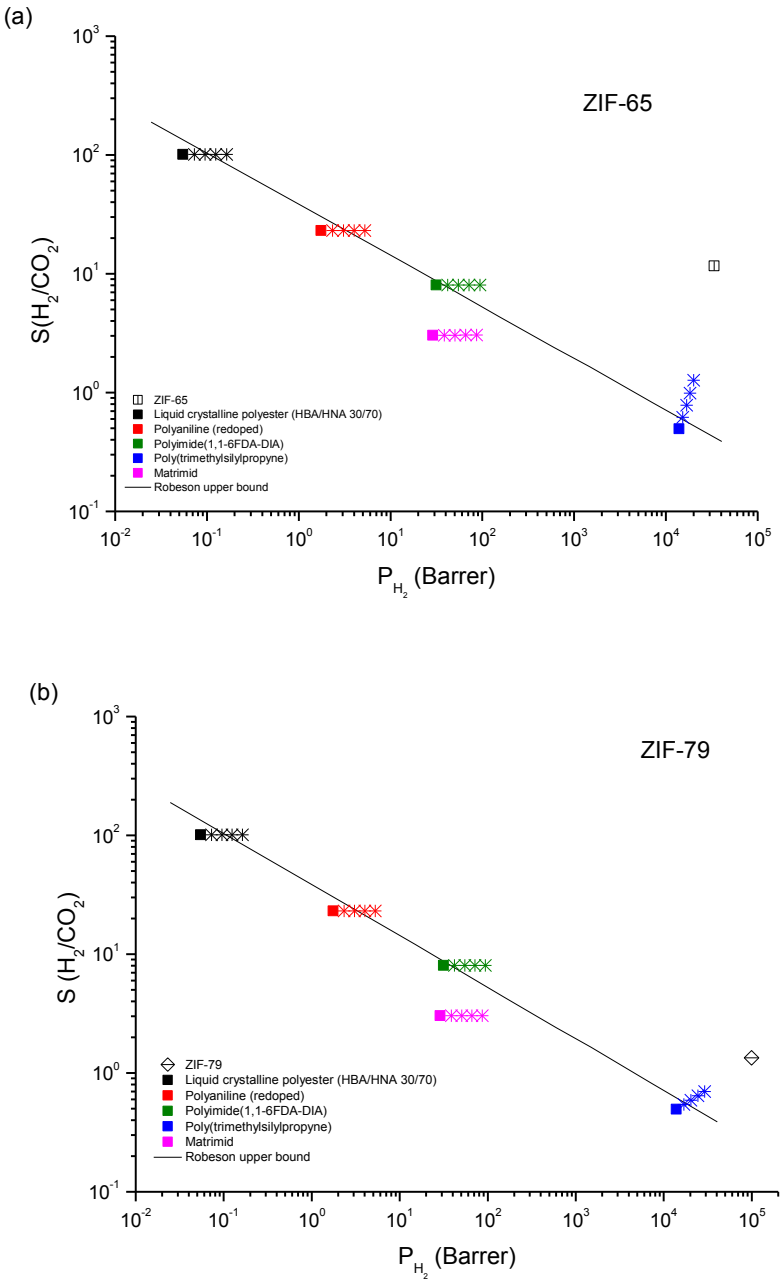

Figure 5.5: Performance of a) ZIF-65 and b) ZIF-79-based MMMs for H_2/CO_2 separation.

Figure 5.6 illustrates CO_2 permeability and selectivity of MMMs composed of weakly selective (ZIF-10) and highly selective (ZIF-11) filler particles. Gas separation performance of other ZIF/polymer MMMs for CO_2/CH_4 separation can be found in Figure D3. Incorporation of ZIF-10 into polymers increases permeability of all polymers but selectivity generally remains unchanged as represented in Figure 5.6 (a). The only exceptional case is PTMSP. PTMSP is the polymer with the lowest selectivity and its selectivity is the most seriously affected one from the addition of weakly selective ZIF-10. Selectivity of PTMSP decreased from 4.42 to 3.81 because CO_2 selectivity of PTMSP is slightly larger than that of ZIF-10 (1.32). Increase in CO_2 permeability without a significant change in CO_2 selectivity is enough to carry some ZIF-10/polymer MMMs above the upper bound, such as ZIF-10/TADATO-DSDA and ZIF-10/poly (diphenyl acetylene)-3a MMMs. Figure 5.6 (b) shows effects of incorporation a highly selective and highly permeable ZIF into polymer on CO_2 permeability and selectivity. All MMMs are more CO_2 permeable compared to pure polymers due to very high permeability of ZIF-11 ($\sim 6\times10^4$ Barrers) and most of them have higher selectivity than pure polymers. Both CO_2 permeability and CO_2 selectivity of polyimide, 6FDA-TMPDA, PIM-7, PIM-1 and PTMSP are significantly enhanced with the addition of ZIF-11. These polymers can exceed the Robeson's upper bound if the volume fraction of ZIF-11 is around 0.2. For example, the CO_2 permeability and selectivity of PIM-1 membrane increase from 2300 to 3792 Barrers and 18.4 to 28.7, respectively when ZIF-11 at a volume fraction of 0.2 is incorporated into PIM-1.

Performances of 360 new ZIF-based MMMs for separation of H_2/CH_4, H_2/CO_2 and CO_2/CH_4 were predicted using molecular simulations and permeation models. Some ZIF/polymer combinations were identified as highly promising MMMs for specific gas separations. Reliable approaches are needed to save time and effort for the performance predictions of a huge number of MMMs before doing extensive calculations. At this point,

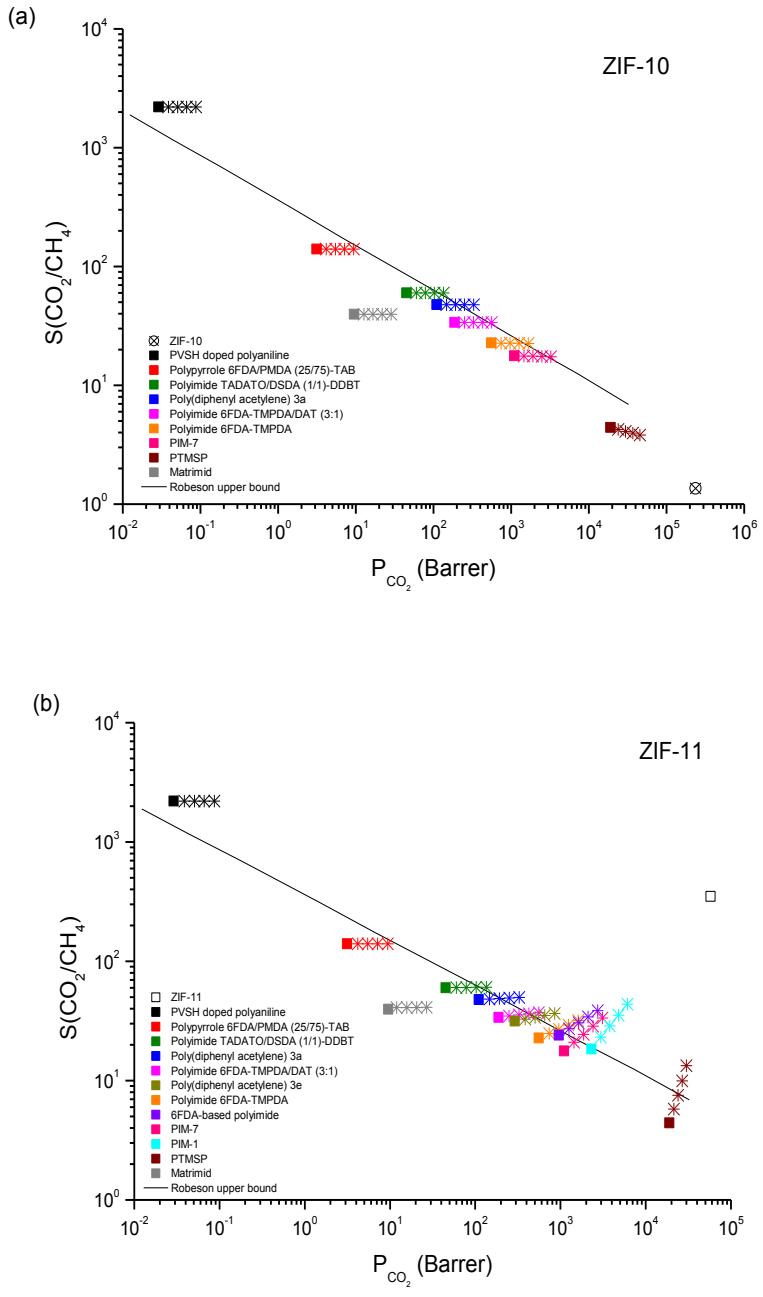

Figure 5.6: Performance of a) ZIF-10 and b) ZIF-11-based MMMs for CO_2/CH_4 separation.

relating molecular level properties and gas separation performance of MMMs will be very useful. It was observed that promising MMMs are the ones composed of filler particles that are highly selective. For example, ZIF-11 and ZIF-12 were shown to enhance selectivity of polymers for CO_2/CH_4 separation since they exhibit high CO_2 selectivities (>100) compared to pure polymers. Results of molecular simulations showed that these high selectivities arise from the large differences in diffusion rates of gas components. Equilibrium molecular dynamics (EMD) simulations were used to calculate corrected diffusivities of CO_2 and CH_4 in ZIF-11 and ZIF-12. The results indicated that corrected diffusivity of larger CH_4 molecules is much slower ($6\text{-}8\times10^{-8}$ cm^2/s) than that of smaller CO_2 molecules ($5\text{-}7\times10^{-6}$ cm^2/s) due to the narrow pores of these ZIFs. The large difference between corrected diffusivities is responsible for the discrepancy in gas permeability which directly affects selectivity. Similarly, ZIF-90 carries more polymers above upper bound than other ZIFs for H_2/CH_4 separations because it has the highest H_2 selectivity (54) among all ZIFs. This is again due to the differences in diffusion rates of gases. The diffusion of CH_4 molecules (3×10^{-7} cm^2/s) is slow while small H_2 molecules (2×10^{-4} cm^2/s) diffuse a lot faster. Therefore, ZIFs are expected to exhibit high selectivity when diffusivity ratio of the components is large. Figure 5.7 represents the correlation between the ideal selectivity of ZIFs and the ratio of corrected diffusivities of gases in ZIFs calculated from molecular simulations. This correlation underlines the fact that a ZIF having large diffusion selectivity for a gas pair can be a useful material as filler particles in polymer membranes and EMD simulations are enough to estimate the gas separation performance of ZIF-based MMMs.

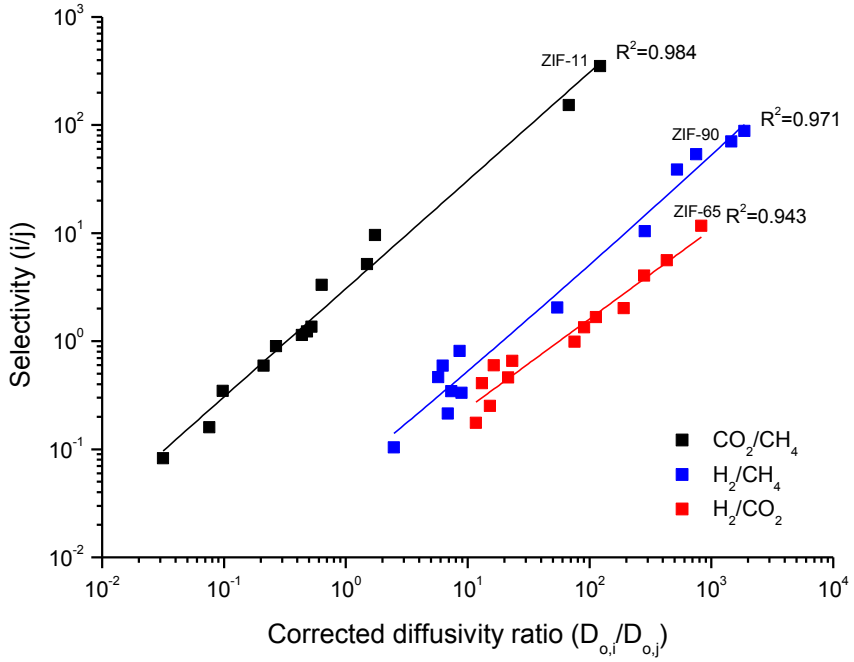

Figure 5.7: Relation between ideal selectivity of ZIFs and the ratio of corrected diffusivity of gases in ZIFs. Data for ZIF-67 and ZIF-8 were not included since corrected diffusivity of CH_4 is smaller than 10^{-8} cm^2/s which is the limit of the molecular dynamics simulations to accurately quantify diffusion.

Chapter 6

MOLECULAR MODELING of MMMs for CO_2/N_2 SEPARATION

6.1. Validation of Theoretical Models with Experimental Data

Accurate prediction of gas permeabilities in MMMs requires implementation of filler and polymer permeabilities into appropriate theoretical models. Three different permeation models were tested for prediction of gas permeability of experimentally fabricated ZIF and MOF-based MMMs for CO_2/N_2 separation. These models are Maxwell, extended Maxwell and modified Maxwell model. Extended Maxwell and modified Maxwell models were developed based on Maxwell model and they account for filler interactions and non-ideal morphology. Comparative analysis on the accuracy of these related models was done and limitations of the models based on filler loading were studied. The accuracy of these models was determined by calculating AARE% values which are given in Table 6.1. Cumulative AARE% results (Table 6.1 (a)) include permeability predictions of MMMs containing fillers from 3 wt% up to 40 wt% loading. Loading based AARE% values (Table 6.1(b)) were calculated for: (1) MMMs with 3-10 wt% filler loadings, (2) MMMs with 15-20 wt% filler loadings (3) MMMs with 30-40 wt% filler loadings. Cumulative results showed that modified Maxwell model is the best predicting permeation model since AARE% values of this model are significantly lower than others. Loading based results showed that there is not a significant difference between the predictions of Maxwell and modified Maxwell model up to the filler loading of 20 wt%.

However, predictions of modified Maxwell model is significantly more accurate than that of Maxwell model at higher filler loadings (≥30 wt%). Therefore, modified Maxwell model was used to estimate the gas permeability and selectivity of new MOF-based MMMs when the filler loading is larger than 20 wt%.

Table 6.1: AARE% values for gas permeability in CuBTC, IRMOF-1, ZIF-8 and ZIF-90-based MMMs (a) cumulative results (b) loading based results.

(a)

	CO_2	**N_2**
Maxwell	54.88	29.68
Extended Maxwell	59.93	33.07
Modified Maxwell	18.57	1.30

(b)

	MOF loading (wt%)*	**CO_2**	**N_2**
Maxwell	≤10	75.84	34.85
	≤20	16.59	18.37
	≥30	34.17	15.61
Extended Maxwell	≤10	77.94	36.54
	≤20	31.99	32.00
	≥30	43.31	68.85
Modified Maxwell	≤10	52.97	16.80
	≤20	13.91	12.47
	≥30	10.13	13.69

*≤10 includes 3, 5, 6, 10 wt%
≤20 includes 15 and 20 wt%
≥30 includes 30 and 40 wt%

Figure 6.1 compares permeability predictions of theoretical models with experimentally measured permeability data of MOF and ZIF-based MMMs. Theoretical permeability estimations of pure CO_2 and N_2 permeability were compared with 58 experimental data points in total, half of which were for CO_2 and the other half for N_2. 26 experimental data points which account for the measurements of permeability of pure CO_2 and N_2 in CuBTC/PDMS (5-40 wt%), CuBTC/PSF (16 wt%) and CuBTC/PI (3-6 wt%) were compared with the predictions of the theoretical models at the same conditions with the experiments. Predictions represented the experimental results reasonably well except the predictions for CuBTC/PI MMMs. Theoretical predictions slightly overestimated the results of the experimental measurements. Hu et al.[86] stated that their experimentally measured gas permeabilities are lower than expected. They explained that imperfect morphology of synthesized MMMs, such as blockage of CuBTC pores by polymer and polymer chain rigidification limited the penetration of CO_2 and N_2 molecules. These two factors led to lower CO_2 and N_2 permeability in CuBTC/PI MMMs. Similarly, gas separation performance of ZIF-8-based MMMs was evaluated and compared with 22 experimental data points. These data points include the measurements of pure CO_2 and N_2 permeabilities in ZIF-8/Matrimid (5-40 wt%), ZIF-8/Ultem (5 wt%) and ZIF-8/PPEES (10-30 wt%). In contrast to the previous discussions made for CuBTC/PI MMMs, theoretical predictions for ZIF-8/Matrimid and ZIF-8/PPEES MMMs slightly underestimated the results of experimental gas permeability measurements. This can be attributed to the increase in polymer free volume with inclusion of ZIF-8 into polymer matrix. Experiments also reported that molecules having larger kinetic diameter than the effective aperture size of ZIF-8 are still adsorbed in ZIF-8 because of the aperture flexibility.[144] As can be seen from Figure 6.1, the remaining CO_2 and N_2 permeability predictions in IRMOF-1 and ZIF-90-based MMMs agree well with the experimental permeability measurements.

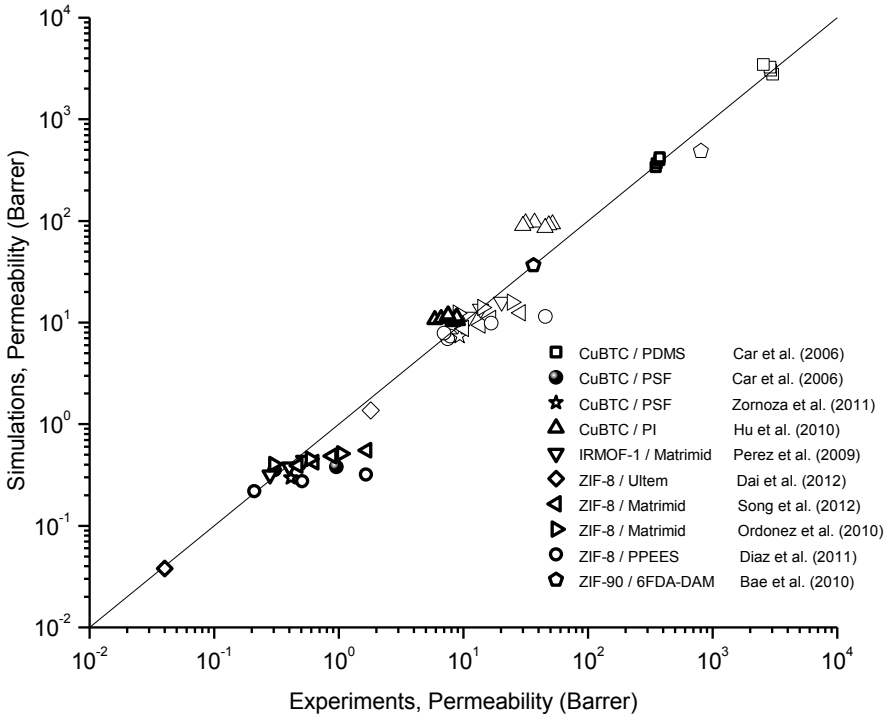

Figure 6.1: Comparison of experimental data and theoretical predictions for gas permeability in MOF and ZIF-based MMMs. Bold (light) symbols represent CO_2 (N_2) permeabilities of MMMs.

6.2. Effect of Filler Framework Flexibility on CO_2/N_2 Separation Performance of MMMs

Permeability predictions that have been represented so far were done based on the assumption that MOFs have rigid frameworks. It is important to investigate the effect of framework flexibility on gas permeability which depends on adsorption and diffusion of gases. Effect of framework flexibility on adsorption and diffusion was examined in recent

studies. It was shown that it is usually a good approximation to assume rigid framework in adsorption simulations except for the materials which are known to exhibit a structural phase transition upon adsorption.[145, 146] However, accounting for framework flexibility was proven to be crucial to obtain reliable gas diffusion properties in ZIF-8 in recent simulation studies.[110, 147-149] These studies demonstrated that flexibility has no significant effect on the diffusion of small molecules in large pores, but it can lead to diffusion coefficients to increase orders of magnitude in case of diffusion of large molecules in small pores. Haldoupis et al.[149] recently included framework flexibility in diffusion simulations and examined diffusion of H_2, He, Ar, CH_4 and Xe in ZIF-8. It was reported that CH_4 (Xe) diffusivity in flexible ZIF-8 is 5 (13) order of magnitude larger than the diffusivity of the molecules in rigid ZIF-8. Framework flexibility was shown to be unimportant for diffusion of molecules (H_2, He and Ar) whose kinetic diameters are smaller than the pore limiting diameter of ZIF-8. In a similar study, Hertag et al.[147] showed that self-diffusion coefficients of CH_4 computed for flexible ZIF-8 lattice are significantly higher than those for rigid structure.

Effect of inclusion of framework flexibility on permeability and selectivity of gases in MOF-based MMMs was analyzed in this part of the thesis. It was assumed that framework flexibility has no effect on adsorption of gases in ZIFs and MOFs, thus preexisting adsorption data was used in new permeability and selectivity calculations. Based on aforementioned studies, diffusion rates of gases are modified. Table 6.2 shows the predicted CO_2 permeabilities and CO_2/N_2 selectivities of pure MOFs and MOF-based MMMs together with the available experimental data. Three different cases were considered:

Case-1: The results of diffusion simulations performed using rigid framework were directly used in gas permeability and selectivity predictions of ZIF-8, ZIF-90, IRMOF-1

and CuBTC-based MMMs. As can be seen from Figure 6.1 and Table 6.2 these predictions agree well with the experimental measurements.

Case 2: In this scenario, it was assumed that diffusion of N_2 (large molecule) increases whereas that of CO_2 (small molecule) does not change when framework flexibility is taken into account. This case was created based on the findings of Haldoupis et al.[149] N_2 diffusivity obtained from simulations based on rigid lattice assumption was increased two orders of magnitude whereas CO_2 diffusivity was kept constant. It was found that N_2 permeability in pure MOFs increased two orders of magnitude, thus CO_2 selectivity decreased proportionally. On the other hand, MMM calculations indicated that CO_2 permeability and selectivity of MMMs are nearly constant. For example, CO_2/N_2 selectivity of ZIF-8/Matrimid MMM decreases from 22.5 to 22.4. This example demonstrates that flexibility can significantly change the gas separation performance of pure ZIFs and MOFs but it does not seriously affect the performance of MOF and ZIF-based MMMs.

Case 3: In this case, diffusivity of both CO_2 and N_2 were assumed to be faster due to the flexibility of the structure, but increase is more pronounced for the larger molecule (N_2). N_2 diffusivity obtained from simulations based on rigid lattice assumption was increased two orders of magnitude while CO_2 diffusivity was increased one order of magnitude. Slight enhancements in CO_2 permeability and selectivity were observed as presented in Table 6.2. The results of this case are still very similar to the results of case-1 where all calculations were performed based on rigid framework assumption. One may think that large changes in N_2 diffusivity may affect the performance of MOF-based MMMs. To examine this point, the diffusivity N_2 in ZIF-8 was increased 10 orders of magnitude while that of CO_2 was constant. In this case, very small, 0.4 %, decrease in CO_2 selectivity in ZIF-8/Matrimid was observed. (N_2 permeability in MMMs containing rigid frameworks (case-1) and flexible frameworks (case-2 and case-3) were compared in Figure D4)

Considering the similarity of selectivity and permeability predictions in rigid and flexible MOF containing MMMs and the large computational demand of flexible framework simulations, it is reasonable to screen MMMs using permeability predictions of rigid fillers to select the most promising MMM for the desired separation. More detailed calculations including flexibility can be performed once a MOF-based MMM is identified to exhibit very promising gas separation properties.

Table 6.2: Effect of framework flexibility on the CO_2 permeability (P) and CO_2/N_2 selectivity (S) predictions for pure MOFs and MOF-based MMMs. All MMM calculations were carried out using modified Maxwell model.

	Case-1		**Case-2**		**Case-3**			
	P	**S**	**P**	**S**	**P**	**S**		
CuBTC	392028	3.24	392028	0.03	3920280	0.32		
IRMOF-1	233216	1.84	233216	0.02	2332160	0.18		
ZIF-8	20720	292.68	20720	2.93	207200	29.27	**Experiments**	
ZIF-90	4367	2.29	4367	0.02	43670	0.23	**P**	**S**
CuBTC/PDMS	3028.50	8.23	3028.50	8.22	3037.94	8.25	2924.44	8.22
IRMOF-1/Matrimid	13.67	36.00	13.67	36.00	13.67	36.00	13.80	34.50
ZIF-8/Matrimid	10.91	22.50	10.91	22.41	10.91	22.42	16.63	18.90
ZIF-90/6FDA-DAM	485.24	13.23	485.24	13.23	510.24	13.91	804.53	22.00

Case-1: Rigid framework simulations were used to calculate diffusivities, $D_{N2rigid}$ and $D_{CO2rigid}$.

Case-2: $D_{N2}=D_{N2rigid}*100$

Case 3: $D_{N2}=D_{N2rigid}*100$ and $D_{CO2}=D_{CO2rigid}*10$

a, b and c represent the type of the polymers used in the MMM fabrication, PDMS, Matrimid and 6FDA-DAM, respectively.

All MMM permeability values were calculated at 20 wt% filler loading except ZIF-90 which is at 15 wt% loading.

Comparison of the results from these three scenarios suggests that the diffusivity of gases in MOFs has a significant effect on the performance of pure MOF membranes but the performance of MOF-based MMMs are mainly driven by the polymer, not the filler MOF

particles. This can be attributed to the nature of the permeation models which are strongly dominated by the gas permeability of the polymers rather than gas permeability of the fillers. In order to examine this phenomenon, Maxwell model was analyzed in detail. If the permeability of the filler is extremely larger than permeability of the pure polymer $(\lambda_{dm} \geq 100)$, then the first terms in both numerator and denominator of the Maxwell model can be omitted and Maxwell equation can be rewritten in the following form:

$$P_r = \frac{P}{P_m} = \frac{(1+2\phi)\lambda_{dm}}{(1-\phi)\lambda_{dm}} \tag{6.1}$$

Figure 6.2 illustrates the relation between relative permeability, $P_r = P/P_m$, (the ratio of MOF-based MMM's permeability to polymer's permeability) and $\lambda_{dm} = P_d/P_m$ (the ratio of MOF's permeability to polymer's permeability) as a function of filler loading. It can be concluded that permeability of MMM is nearly constant if the permeability of the filler is at least two orders of magnitude larger than the permeability of the pure polymer. For example, the permeability of MMM is equal to $1.33P_m$ for a filler volume fraction of 0.1 when λ_{dm} is larger than 100. Theoretical permeation models suggest that using a MOF filler that has gas permeability 100 times larger than the permeability of the polymer and using a MOF filler that has gas permeability 10000 times larger than the permeability of polymer will result in MMMs that have exactly same permeability properties if the filler volume fraction is same.

6.3. Predicting CO_2/N_2 Separation Performance of New MMMs

CO_2 permeability and CO_2/N_2 selectivity of MMMs containing BACMOH-10, BAHGUN, FOHQUO, JASNEX, MABJOP, MABJUV-01, MIHHOA, MIHHUG, MMIF, UFUNAK, UFUMUD-01, UGEPEB, YOPMAS, VEJZOA (ZIF-11), VEJZUG (ZIF-12) and GITTOT (ZIF-67) were predicted. These MOFs were specifically selected since they

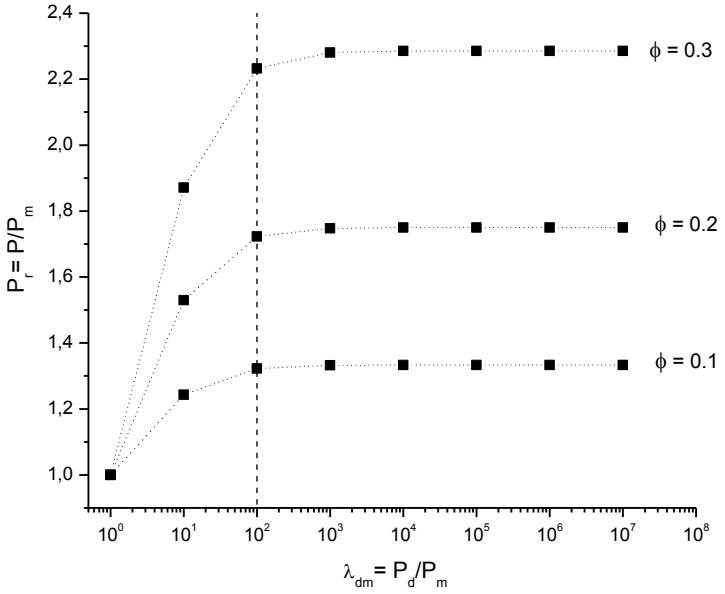

Figure 6.2: Effect of λ_{dm} on permeability of MMMs (P) as a function of filler volume.

have been reported as promising materials among many candidates. JASNEX, UFUNAK, UFUMUD-01 and YOPMAS were chosen because they were recently reported in the top 10 MOFs list that have the highest CO_2/N_2 membrane selectivities among 30000 MOF candidates.[150] UGEPEB, FOHQUO and BACMOH-10 were included since they were previously identified as promising candidates for CO_2 capture applications, UGEPEB and FOHQUO were specifically studied due to their high thermal stability of these materials after solvent removal.[151] BAHGUN, MABJOP, MABJUV-01, MIHHOA, MIHHUG, MMIF-based MMMs are reported to exhibit good CO_2/CH_4 separation performance.[143] Similarly, ZIF-11, ZIF-12 and ZIF-67 were selected since these materials have high CO_2/CH_4 selectivity.[51] Modified Maxwell model was used to estimate CO_2 and N_2 permeability in MMMs since the volume fraction of fillers increases up to 0.4. Figure 6.3

shows CO_2 permeability and selectivity of MMIF, UFUNAK, VEJZOA and MABJUV01-based MMMs. Figure 6.3 (a) illustrates the CO_2 separation performance predictions of MMMs made from a highly selective filler particle, MMIF. MMIF has the highest CO_2/ N_2 selectivity (~10^5) but the lowest CO_2 permeability (~10^3 Barrers) among all MOFs. CO_2 permeability of MMIF is higher than the permeability of poly[bis(2-(2-methoxyethoxy)ethoxy) phosphazene] and PIM-7 polymers, thus both CO_2 permeability and selectivity in poly[bis(2-(2-methoxyethoxy)ethoxy) phosphazene]/MMIF and PIM-7/MMIF membranes increase with MMIF loading. For all other polymers, the selectivity increase is obtained at the expense of decreasing permeability when MMIF is used as fillers. CO_2 permeability of MMMs decreases significantly due to the addition of a filler which is less CO_2 permeable than the polymers. Incorporation of MMIF at a volume fraction of 0.2 can carry all polymers above the upper bound except poly(trimethylgermylpropyne) and PTMSP. Therefore, high CO_2 selectivity over N_2 is not enough to carry polymeric membranes above the upper bound; permeability of filler particle has also great importance. Figure 6.3 (b) shows CO_2 permeability and selectivity of MMMs when a filler particle, UFUNAK, having both high CO_2 permeability (9×10^5 Barrers) and CO_2/N_2 selectivity (981) is added into polymers. Not only the CO_2 permeability but also the CO_2 selectivity of all polymers is significantly enhanced by the addition of UFUNAK into polymer matrix. This increase is more pronounced for UFUNAK/poly(trimethylgermyl propyne) and UFUNAK/PTMSP membranes since these polymers are located at the lower corner of the upper bound. UFUNAK can carry all polymers except PIM-7 above the upper bound for CO_2/N_2 separation. This demonstrates that fillers exhibiting both high selectivity and permeability are required to enhance the performance of membranes. PIM-7 is very far from the upper bound compared to other polymers and a filler volume fraction of 0.4 is not enough to bring PIM-7 close to the upper bound. Figure 6.3 (c) shows the performance predictions for MMMs having VEJZOA as

filler particles. VEJZOA exhibits mediocre CO_2 permeability (6×10^4 Barrers) and high CO_2/N_2 selectivity (132). Similar to the discussions of UFUNAK, VEJZOA increases CO_2 permeability and CO_2/N_2 selectivity of polymers. For example, CO_2 permeability of PIM-1 increases from 2300 to 2883 Barrers when the volume fraction of VEJZOA is equal to 0.2 and VEJZOA/PIM-1 MMM can exceed the upper bound at this filler loading. Figure 6.3 (d) shows CO_2 permeability and CO_2/N_2 selectivity of MABJUV01-based MMMs. MABJUV01 represents a filler particle with very high CO_2 permeability ($\sim10^5$) but low CO_2/N_2 selectivity (5). CO_2 permeability of all polymers increases when MABJUV01 are incorporated into polymers but CO_2/N_2 selectivity of polymers does not change significantly. PTMSP and poly(trimethylgermylpropyne) can be excluded from previous discussion since slight decrease in CO_2/N_2 selectivity of PTMSP/MABJUV01 and poly(trimethylgermylpropyne)/MABJUV01 membranes was observed. For example, CO_2 selectivity of PTMSP decreases from 10.7 to 9.6 Barrers when MABJUV01 is incorporated at a volume fraction of 0.4 but CO_2 permeability of the polymer increases from 29000 to 39000 Barrers. MOFs having high permeability and low selectivity such as MABJUV-01 will be useful to enhance the separation performance of polymers which have low permeability but high selectivity.

CO_2 permeability and CO_2/N_2 selectivity of other MOF-based MMMs are presented in Figure D5. CO_2/N_2 separation performance of MOF and ZIF fillers given in Table C6 can be classified as:

1- Fillers having *high CO_2 permeability and high CO_2/N_2 selectivity*: VEJZUG, GITTOT and UGEPEB. This group of fillers is promising candidates since they are able to carry all polymers above the upper bound. The discussions for UFUNAK-based MMMs are valid for MMMs including these MOFs.

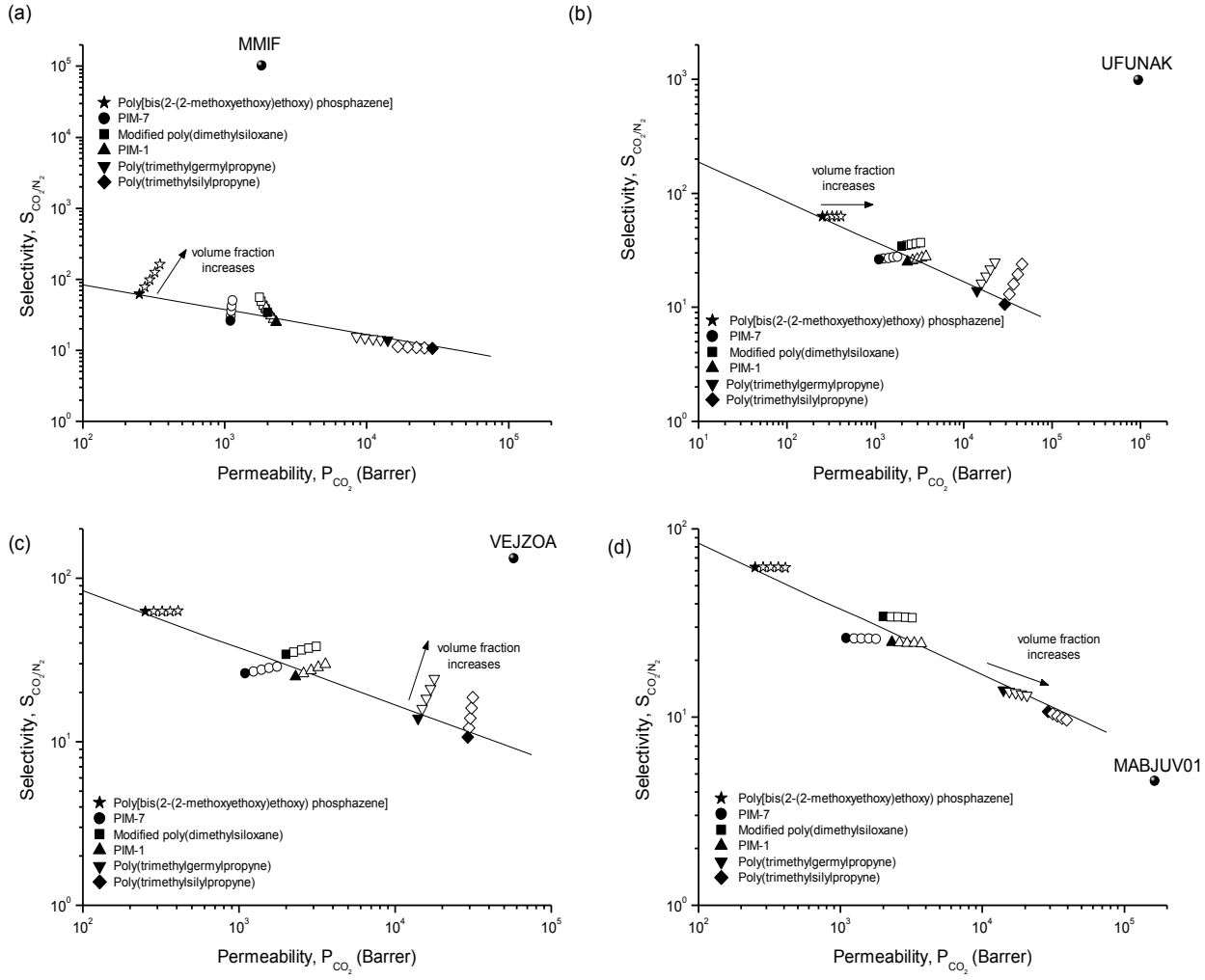

Figure 6.3: Predicted performances of a) MMIF b) UFUNAK c) VEJZOA and d) MABJUV01-based MMMs for CO_2/N_2 separation. The closed symbols represent the performance of pure polymers. The open symbols represent the performance of MOF-based MMMs where the volume fraction of the fillers increases from 0.1 to 0.4.

2- Fillers having *high CO_2 permeability but low CO_2/N_2 selectivity*: UFUMUD-01, MABJOP, BAHGUN and FOHQUO. MMMs containing these fillers show similar trends as MABJUV-01-based MMMs.
3- Fillers having *low CO_2 permeability and mediocre CO_2/N_2 selectivity*: YOPMAS and JASNEX. Incorporation of these fillers into polymers decreases CO_2 permeability of polymers without making any significant change in their selectivity. For example, CO_2 permeability of modified poly(dimethylsiloxane) decreases from 2000 Barrers to 1279 Barrers when YOPMAS is added into the polymer at a volume fraction of 0.3.
4- Fillers having *low CO_2 permeability and low CO_2/N_2 selectivity*: MIHHOA, MIHHUG and BACMOH-10. These fillers are not useful in CO_2/N_2 separations because dramatic decrease in CO_2 permeability and CO_2/N_2 selectivity is observed if the particles are added into polymers.

Some of the MOFs examined in this work were selected due to their high CO_2/CH_4 selectivity. As can be seen from Figure 6.4, a promising MOF for CO_2/CH_4 separation is not necessarily a good candidate for CO_2/N_2 separation. For example, FOHQUO has both high CO_2 permeability and CO_2/CH_4 selectivity, thus it carries polymers above the upper bound when used as filler particles in several polymers.[143] However, incorporation of FOHQUO into polymers decreases CO_2/N_2 selectivity of polymers as presented in Figure D5(i). BAHGUN, FOHQUO, MIHHOA and MIHHUG also have high CO_2/CH_4 selectivity but low CO_2/N_2 selectivity. This can be attributed to the low CH_4 permeability of these MOFs due to the slow diffusion of CH_4 molecules compared to smaller N_2 molecules. Selectivity of MOFs is strongly related with the ratio of gas diffusivities as shown in Figure D6 and Figure 5.7. No relation was found between the MOFs' selectivity and the ratio of adsorption amounts of gases in MOFs as represented in Figure D6. The correlation between

the MOFs' selectivity and diffusion ratio of gases in MOFs presents a practical approach for gaining insight about the performance of MOFs as fillers before doing MMM calculations.

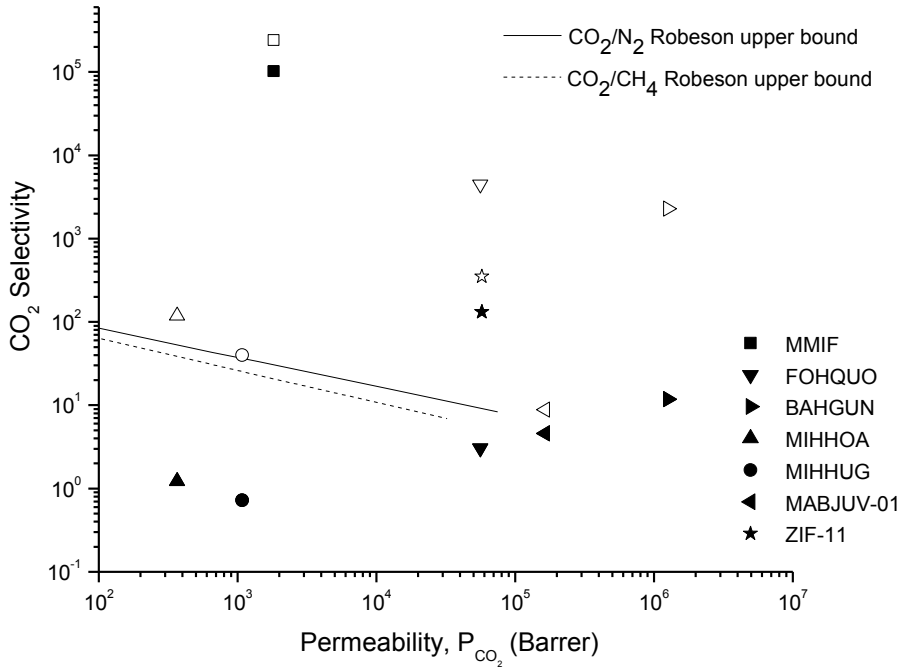

Figure 6.4: CO_2/CH_4 and CO_2/N_2 separation performance of pure MOFs with corresponding Robeson upper bound. Open and closed symbols in represent CO_2/CH_4 and CO_2/N_2 performances, respectively.

6.4. Strategies for Matching Polymers and Fillers for MMMs

Strategies to selecting appropriate polymers and fillers in MMM applications are presented in this part of the thesis. First approach is to create hypothetical fillers that represent different scenarios and then find real MOFs for realizing the scenarios. This approach previses separation performances of real MOFs before doing extensive

calculations if permeability and selectivity of hypothetical MOFs are close to that of real fillers. Figure 6.5 shows the performance of MMMs composed of hypothetical fillers and PDMS. PDMS was chosen since it is a commercial polymer and widely used for fabrication of MOF-based MMMs in experiments. PDMS has mediocre permeability and low selectivity with a CO_2 permeability of 2503 Barrers and CO_2/N_2 selectivity of 8.2. Three different scenarios were considered to follow the changes in CO_2/N_2 separation performance of hypothetical MOF/PDMS membranes:

1- Incorporation of fillers which *enhance CO_2 selectivity of PDMS without changing its permeability* by using a highly selective MOF as fillers.
2- Incorporation of fillers which *enhance both CO_2 selectivity and CO_2 permeability of PDMS* by using a MOF with high CO_2 selectivity and permeability.
3- Incorporation of fillers which *enhance CO_2 permeability of PDMS without changing its selectivity* by adding a MOF with high CO_2 permeability.

As can be seen from Figure 6.5, these hypothetical MOFs are MOF1 (scenario 1), MOF2 (scenario 2), MOF3 (scenario 2) and MOF4 (scenario 3). Maxwell model was used for permeability predictions. Open symbols represent the predicted performances of MMMs having hypothetical MOFs as fillers. The way CO_2 permeability and CO_2/N_2 selectivity changes with addition of hypothetical MOF1 into PDMS presents the first scenario. Hypothetical MOF1 exhibits higher CO_2/N_2 selectivity but lower CO_2 permeability than pure PDMS. Results show that pairing PDMS with MOF1 increases PDMS's selectivity without changing its permeability. However, MOF1 cannot carry PDMS above the upper bound. MMIF can be a representative hypothetical MOF1 among real MOFs that were considered. Hypothetical MOF2 and MOF3 have higher CO_2

permeability and CO_2/N_2 selectivity than PDMS. CO_2 selectivity change in hypothetical MOF2/PDMS membranes is more pronounced than that in hypothetical MOF3/PDMS MMMs since selectivity of pure hypothetical MOF2 is higher than that of hypothetical MOF3. VEJZUG (also known as ZIF-12) and VEJZOA (also known as ZIF-11) are examples of hypothetical MOF2 and hypothetical MOF3 fillers, respectively. It is important to note that MOF2-based PDMS membranes can exceed the upper bound if the volume fraction of the MOF fillers is around 0.3. Finally, hypothetical MOF4 have higher CO_2 permeability but lower CO_2/N_2 selectivity than pure PDMS. Enhancement in CO_2 permeability without any change in selectivity was observed when hypothetical MOF4 added to pure PDMS. MABJOP can be considered as hypothetical MOF4 type filler. Figure 6.5 underlines the fact that it is possible to improve the separation performance of polymers that are away from the upper bound, such as PDMS, by selecting appropriate MOF fillers.

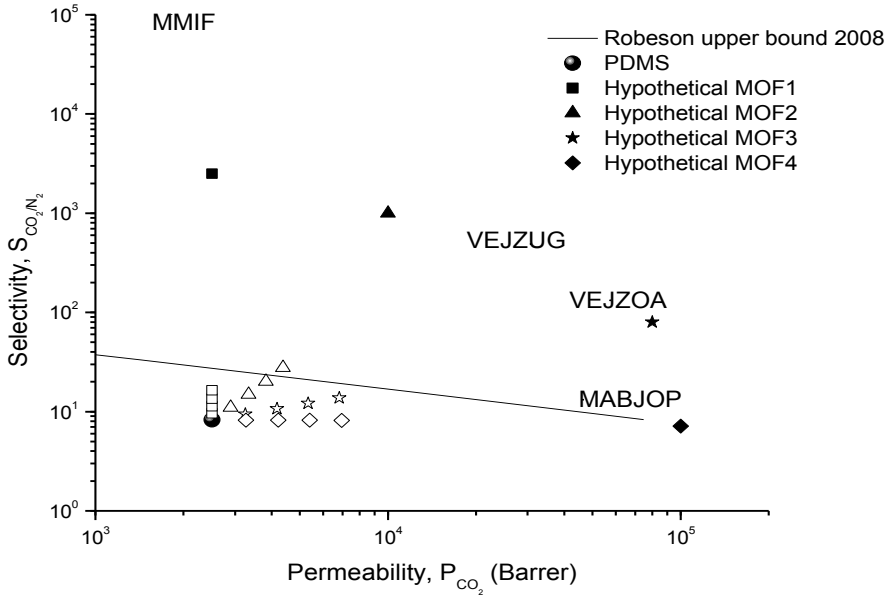

Figure 6.5: Predictions of Maxwell model for the performance of hypothetical MOF-based PDMS membranes.

Second approach is based on determination of facilitation ratio for selection of right polymer. The performance enhancements of different polymers were tested using UFUNAK as filler particles. The polymers are the ones lying on the Robeson upper bound for CO_2/N_2 separation. Facilitation ratio can be described as the change in gas permeability of a MMM with respect to pure polymer. It is a useful method to investigate the effect of filler loading on gas transport properties of MMMs. Figure 6.6 shows facilitation ratio of UFUNAK-based MMMs as a function of UFUNAK loading. The solid (dashed) lines show the effect of filler loading on CO_2 (N_2) permeability of MMMs and the numbers on the figure show the slopes of the corresponding lines. As can be seen from Figure 6.6, the facilitation ratio calculated for CO_2 increases linearly with increasing UFUNAK loading in all MMMs. It was found that enhancement in the CO_2 gas permeation of UFUNAK-based MMMs, except the ones composed of poly(trimethylgermylpropyne) and PTMSP polymers, is nearly the same with a slope of 0.0156. Facilitation ratios computed for N_2 permeability are smaller than the facilitation ratios computed for CO_2, which suggests that all MMMs are more selective for CO_2. Facilitation ratios of poly(trimethygermylpropyne)/UFUNAK and modified PTMSP/UFUNAK membranes decreased as a function of UFUNAK loading. The decrease can be attributed to N_2 permeability in UFUNAK which is lower than that of the polymers, thus incorporation of more filler particles restricts the permeability of N_2 in these MMMs. Figure 6.6 can be used to get insight about the comparative performance of MMMs when a specific filler particle is incorporated into different polymers. For example, CO_2 facilitation ratio of poly[bis(2-(2-methoxyethoxy)ethoxy) phosphazene] MMMs with an UFUNAK volume fraction of 0.3 was calculated as 0.45, whereas it was 0.41 for UFUNAK/PTMSP MMMs. This result shows that UFUNAK performs better in poly[bis(2-(2-methoxyethoxy)ethoxy) phosphazene] polymer than PTMSP-based membranes for CO_2/N_2 separation.

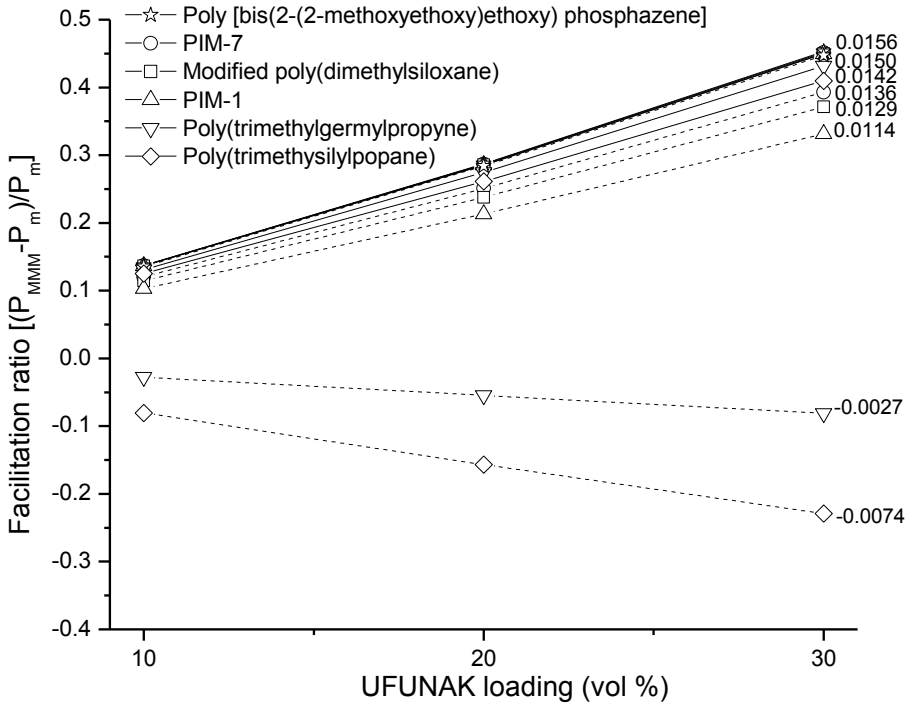

Figure 6.6: Facilitation ratio of UFUNAK-based MMMs. The solid (dashed) lines show facilitation ratio of MMMs calculated for CO_2 (N_2) permeability.

The approaches that have been mentioned so far present the ways for selection of appropriate filler for a specific polymer and appropriate polymer for a specific filler to obtain high performance filler/polymer combinations. Determination of process conditions is as crucial as matching appropriate filler and polymers together. Effect of temperature on CO_2 permeability and CO_2/N_2 selectivity of MMMs was investigated. Since the permeation models combine individual permeability of filler and polymer, effects of temperature on filler and polymer permeability were examined separately and new permeabilities were

included in the permeation model. Keskin et al.[152] previously reported that the performance of pure MOFs are not significantly affected from the temperature. Figure 6.7 represents the effect of temperature on permeability and selectivity of pure polymers and MMMs. The polymers are PEO, 6FDA-IPDA, HQDPA-DBA and CLP. They were specifically chosen since permeability and selectivity data of polymers at different temperatures are reported from the experiments which were performed to study the effect of temperature on CO_2/N_2 separation performance of polymers.[153] As can be seen from Figure 6.7, CO_2 permeability of pure polymers increases at the expense of CO_2/N_2 selectivity when temperature increases. This can be explained by solubility and diffusivity trends of gases in polymers: The diffusivity of CO_2 increases with temperature, but its solubility decreases.[154, 155] CO_2 permeability increases as a result of diffusivity increase which is more pronounced than solubility decrease. On the other hand, diffusivity of N_2 increases with temperature while its solubility is nearly constant. The decrease in CO_2/N_2 selectivity is due to larger increase in N_2 permeability than CO_2 permeability. PEO and CLP polymers have larger CO_2 permeability and CO_2/N_2 selectivity than other polymers and they are more significantly affected from temperature change due to favorable interactions of with CO_2. PEO has polar ether linkages and has affinity for CO_2 due to the dipole-quadrupole interactions. Similarly, PEO containing and cross-linked polymer films (CLP) prepared from poly (ethylene glycol) dimethacrylate (DM) and poly (ethylene glycol) methyl ether methacrylate (MM) has polar groups. UFUNAK was used as filler particles in MMM calculations since it significantly improves CO_2 permeability and CO_2/N_2 selectivity of pure polymers and its volume fraction was set to 0.2. Figure 6.7 shows that the same permeability and selectivity trend as pure polymer membranes is valid for UFUNAK-based MMMs. Enhancement in CO_2 permeability with temperature is more pronounced in UFUNAK/PEO and UFUNAK/CLP membranes than the permeability enhancement in other MMMs. For example, if HQDPA-DBA is used as polymer, MMM's

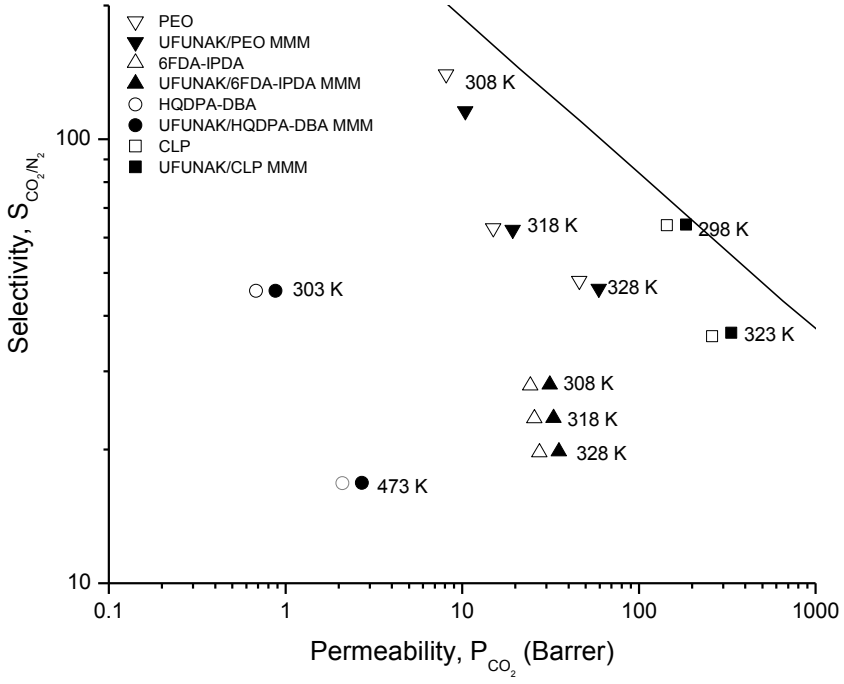

Figure 6.7: Effect of temperature on CO_2 permeability and CO_2/N_2 selectivity of UFUNAK-based MMMs.

CO_2 permeability (selectivity) which is 0.88 Barrers (46) at 303 K increases (decreases) to 2.6 Barrers (17) when temperature is increased by 170 K. On the other hand, CO_2 permeability (selectivity) of UFUNAK/CLP MMM increases (decreases) from 185 (64) to 334 Barrers (37) when temperature increases from 298 K to 323 K. Although temperature increase in UFUNAK/CLP MMM is relatively very small (25 K) compared to that in UFUNAK/HQDPA-DBA MMMs (170 K), permeability increase in UFUNAK/CLP is very significant. Decrease in CO_2/N_2 selectivity of UFUNAK/CLP MMM (27) is very close to that of UFUNAK/HQPDA-DBA MMM (29) when temperature is increased. This example

demonstrates that temperature has a significant effect on the permeability of some polymers and since polymer's permeability is dominant in MMM performance as discussed earlier, the choice of filler/polymer combination and operating temperature is crucial in MMM-based gas separation operations.

6.5. MMMs Containing Two Different Types of Fillers

Most experimental studies have concentrated on MMMs consisting of one type of filler and one type of polymer. On the other hand, recent attention is focused on MMMs containing two different types of fillers embedded in one type of polymer [96, 97] to decrease agglomeration and increase permeability and selectivity. Although it is not possible to visualize the physical scene (e.g. behavior of polymer and fillers when combined together) of MMM or include interactions between the filler particles, it is possible to make estimations of permeability and selectivity of filler1/filler2/polymer MMMs.

In this part of the thesis, atomically detailed simulations and an empirical model (equation (3.31)) were used to predict gas permeability of a MMM composed of a zeolite, a MOF and polymer for the first time in literature. Equation (3.31) gives the formulation that was used to compute gas permeability of MMMs. P_1 and P_2 are the gas permeability of S1C/PSF and MOF/PSF, respectively. The MOF was either ZIF-8 or CuBTC. Permeability of pure MOF was calculated using atomically detailed simulations as described in Chapter 3, permeability of MOF/PSF was computed using Maxwell model and permeability of S1C/PSF was taken from literature.[96] Permeabilities of MOF/PSF and S1C/PSF were combined in equation (3.31) to predict permeabilities of ZIF-8/S1C/PSF and CuBTC/S1C/PSF membranes. These predictions were then compared with the experimental data.[96] Figure 6.8 demonstrates that CO_2 permeability predictions for MOF/PFS (ZIF-8/PSF and CuBTC/PSF) and MOF/zeolite/PSF (ZIF-8/S1C/PSF and CuBTC/S1C/PSF) membranes agree well with the experimental data.

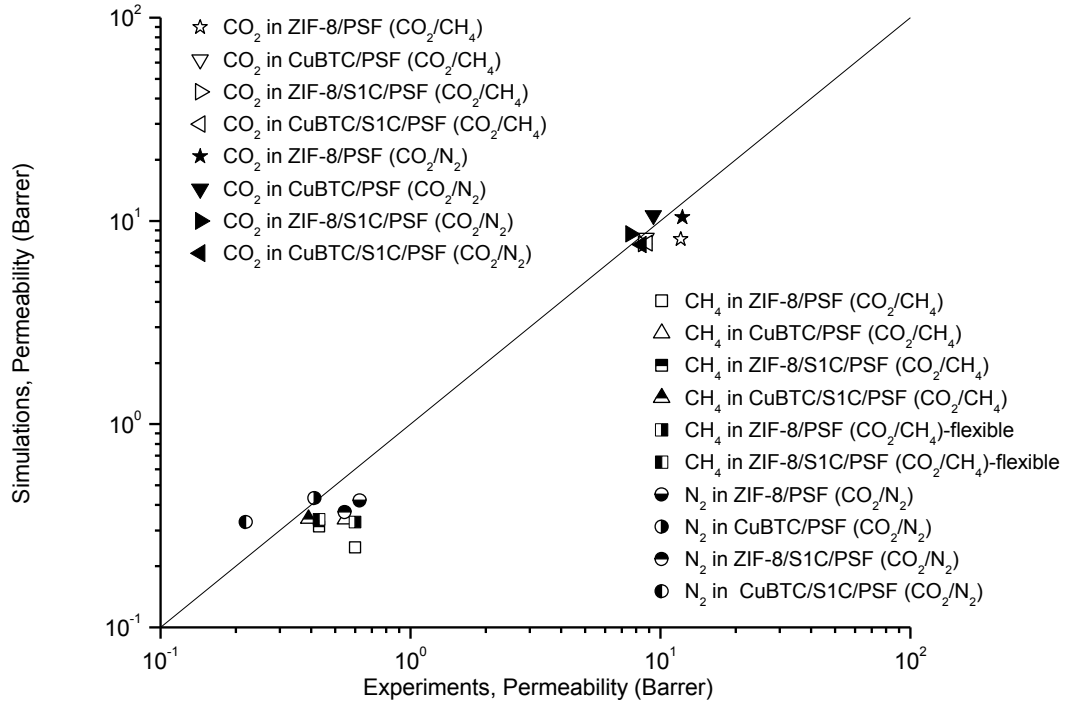

Figure 6.8: Comparison of experimental data and theoretical predictions for MOF/zeolite-polymer MMMs. CO_2/N_2 and CO_2/CH_4 mixtures are equimolar and all the fillers are at the same total loading of 16 wt%.

Theoretical predictions for CH_4 permeability of membranes containing ZIF-8 are remarkably smaller than measured CH_4 permeability. This can be attributed to diffusion of large CH_4 molecules through smaller but flexible ZIF-8 pores as explained in section 6.2. Therefore, CH_4 permeability in ZIF-8/PSF membrane was recalculated using CH_4 diffusivity data in flexible ZIF-8 which was reported by Haldoupis et al.[149] As can be seen from Figure 6.8, recalculated CH_4 permeabilities are in a better agreement with the experimental data. It was previously discussed that permeability of MOF-based MMMs are

mainly driven by the polymer and the flexibility of the filler particles does not have importance if the permeability ratio, P_d/P_m, is greater than 100. The CH_4 permeability was calculated as 0.69 Barrers in rigid ZIF-8 and was measured as 0.19 Barrers in PSF. Since permeability ratio (3.7) is significantly smaller than 100, permeability of MOF-based MMMs is affected from the flexibility of filler particles. However, this effect is still negligible. The methodology that described in this part can be used to make predictions for MMMs composed of two different types of fillers as dispersed phase and a polymer as continuous phase.

Chapter 7

CONCLUSIONS and OUTLOOK

This thesis first introduces two ZIFs, ZIF-11 and ZIF-12, which are not experimentally studied in detail in the literature. Atomically detailed simulations were performed to determine adsorption-based and membrane-based gas separation performances of ZIF-11 and ZIF-12. ZIF-11 and ZIF-12 were found to be very promising membrane and adsorbent materials for separation of CO_2 from CH_4 and H_2 compared to other nanoporous materials, such as zeolites and other ZIFs. Effect of central metal ion which is the only difference between these materials was found to be significant in separation of mixtures containing CO_2.

Exceptionally high membrane performance of ZIFs aroused interest in testing these materials as filler particles in polymers. Molecular simulations were used to assess the gas separation performance of a series of ZIF-based MMMs for CO_2/CH_4, H_2/CH_4 and H_2/CO_2 separations. Predicted gas selectivity and permeability of MMMs were compared with the available experimental data of MMMs in which ZIF-8 and ZIF-90 were used as filler particles. After showing the good agreement between the predictions of theoretical methods and experimental data, the selectivity and permeability of 360 new MMMs composed of 15 different ZIFs and 24 different polymers were investigated. Results of calculations showed that there are several promising ZIF/polymer pairs whose gas permeability and selectivity greatly exceed those of pure polymers. ZIF-11, ZIF-90 and ZIF-65 were found to be promising filler candidates for CO_2/CH_4, H_2/CH_4 and H_2/CO_2 separations, respectively. The

ZIFs in which the molecular diffusivities of gas molecules show large differences are the ones exhibiting high selectivity for a particular species and these ZIFs are the best filler candidates to enhance the selectivity of the polymers

Because CO_2/N_2 separation hold great promise in industry, sixteen different MOFs (BACMOH-10, BAHGUN, FOHQUO, JASNEX, MABJOP, MABJUV-01, MIHHOA, MIHHUG, MMIF, UFUNAK, UFUMUD-01, UGEPEB, YOPMAS, VEJZOA (ZIF-11), VEJZUG (ZIF-12) and GITTOT (ZIF-67)) were studied as filler particles in MMMs for CO_2/N_2 separation. Results indicated that UFUNAK is the best filler candidate since it carries all the polymers above the upper bound by increasing CO_2 permeability and CO_2/N_2 selectivity when incorporated into the polymers. Gas permeability and selectivity of MMMs composed of two different types of fillers (MOF/zeolite) were predicted and compared with the experimental data. Predictions agreed well with the experimental measurements. Therefore, the new methodology introduced in this thesis can be used to assess the gas separation performances of new MOF/zeolite/polymer MMMs. Effect of MOF flexibility on the permeability and selectivity properties of MOF-based MMMs was investigated and it was found that it is acceptable to make performance predictions of MMMs using rigid filler framework if $P_d >> P_m$ and $\phi \leq 0.3$. This outcome was supported by analyzing mathematical permeation models which are mostly dependent on gas permeability of polymers rather than that of fillers. It was also shown that operating temperature of membrane is also crucial in MMM applications.

The theoretical approach used to predict the performance of MMMs in gas separations makes several assumptions and these assumptions should be clearly discussed to allow judgments to be made about the potential impact of these assumptions in real world performance of materials. Moreover, future experimental and theoretical studies that will be helpful to accelerate the design and development of new MOFs and MOF-based MMMs should be clearly stated.

- In this thesis, perfect and defect-free MOF-based MMMs were assumed in all calculations. In practical applications, defects and pinholes can be formed during fabrication of the membranes. It is encouraging to know that experiments so far reported that there is a good adhesion between MOFs and polymers in MMMs.
- All pure MOFs structures that were assessed as adsorbents and membranes were assumed to be rigid. The results of calculations in this study can differ from the results of the studies considering framework flexibility since diffusion of large molecules in smaller pores is possible due to reversible change in flexible framework when guest molecules are introduced. Therefore, the permeabilities presented in this study could be lower if the MOFs have pores showing molecular sieving mechanism. To include the flexibility in simulations, computationally demanding flexible force fields are needed. Once a MOF is identified to be flexible in experiments, more detailed calculations can be performed to support experimental results.
- All permeability and selectivity predictions of MOF-based MMMs were performed based on the assumption that MMMs have rigid MOF fillers. This assumption was validated to reproduce the experimental permeability data.
- Pore size, shape, loading, orientation and distribution of the MOF particles in the polymers affect the performance of MOF-based MMMs in gas separations. Computational studies can be used to screen the materials to identify the materials with desired characteristics, whereas the loading, orientation and distribution of MOFs in polymers are more likely to be explored by experiments or fully atomic simulations on the MOF/polymer interfaces.
- The calculations in this thesis do not make any predictions about the long term stability of MOFs and MOF/polymer MMMs. A MOF or MOF/polymer MMM that

shows high separation performance can be useless in practical applications if it does not have a good stability. This issue is more likely to be addressed by experiments.

BIBLIOGRAPHY

[1] J.T. Houghton, Global Warming: The Complete Briefing, Cambridge University Press, 2004.
[2] H. Yang, Z. Xu, M. Fan, R. Gupta, R.B. Slimane, A.E. Bland, I. Wright, Progress in carbon dioxide separation and capture: A review, J. Environ. Sci. 20 (2008) 14-27.
[3] N.W. Ockwig, T.M. Nenoff, Membranes for Hydrogen Separation, Chem. Rev. 107 (2007) 4078-4110.
[4] D. Aaron, C. Tsouris, Separation of CO_2 from Flue Gas: A Review, Sep. Sci. Technol. 40 (2005) 321-348.
[5] P. Bernardo, E. Drioli, G. Golemme, Membrane Gas Separation: A Review/State of the Art, Ind. Eng. Chem. Res. 48 (2009) 4638-4663.
[6] A. Meisen, X. Shuai, Research and development issues in CO_2 capture, Energy Convers. Manage. 38, Supplement (1997) S37-S42.
[7] S.M. Auerbach, K.A. Carrado, P.K. Dutta, Handbook of Zeolite Science and Technology, Taylor & Francis, 2003.
[8] A. Phan, C.J. Doonan, F.J. Uribe-Romo, C.B. Knobler, M. O'Keeffe, O.M. Yaghi, Synthesis, Structure, and Carbon Dioxide Capture Properties of Zeolitic Imidazolate Frameworks, Acc. Chem. Res. 43 (2009) 58-67.
[9] K.S. Park, Z. Ni, A.P. Côté, J.Y. Choi, R. Huang, F.J. Uribe-Romo, H.K. Chae, M. O'Keeffe, O.M. Yaghi, Exceptional chemical and thermal stability of zeolitic imidazolate frameworks, PNAS 103 (2006) 10186-10191.
[10] K.T. Chue, J.N. Kim, Y.J. Yoo, S.H. Cho, R.T. Yang, Comparison of Activated Carbon and Zeolite 13X for CO_2 Recovery from Flue Gas by Pressure Swing Adsorption, Ind. Eng. Chem. Res. 34 (1995) 591-598.
[11] D. Ko, R. Siriwardane, L.T. Biegler, Optimization of a Pressure-Swing Adsorption Process Using Zeolite 13X for CO_2 Sequestration, Ind. Eng. Chem. Res. 42 (2002) 339-348.
[12] M.T. Ho, G.W. Allinson, D.E. Wiley, Reducing the Cost of CO_2 Capture from Flue Gases Using Pressure Swing Adsorption, Ind. Eng. Chem. Res. 47 (2008) 4883-4890.
[13] E.S. Kikkinides, R.T. Yang, S.H. Cho, Concentration and recovery of carbon dioxide from flue gas by pressure swing adsorption, Ind. Eng. Chem. Res. 32 (1993) 2714-2720.

[14] S. Sircar, T.C. Golden, Purification of Hydrogen by Pressure Swing Adsorption, Sep. Sci. Technol. 35 (2000) 667-687.
[15] P. Cen, R.T. Yang, Bulk gas separation by pressure swing adsorption, Ind. Eng. Chem. Fundam. 25 (1986) 758-767.
[16] J. Yang, C.-H. Lee, J.-W. Chang, Separation of Hydrogen Mixtures by a Two-Bed Pressure Swing Adsorption Process Using Zeolite 5A, Ind. Eng. Chem. Res. 36 (1997) 2789-2798.
[17] S. Cavenati, C.A. Grande, A.E. Rodrigues, Separation of mixtures by layered pressure swing adsorption for upgrade of natural gas, Chem. Eng. Sci. 61 (2006) 3893-3906.
[18] P.W.F. Riemer, I.C. Webster, W.G. Ormerod, H. Audus, Results and full fuel cycle study plans from the IEA greenhouse gas research and development programme, Fuel 73 (1994) 1151-1158.
[19] M. Knudsen, The law of the molecular flow and viscosity of gases moving through tubes, Ann. Phys 28 (1909) 75.
[20] P. Pandey, R.S. Chauhan, Membranes for gas separation, Prog. Polym. Sci. 26 (2001) 853-893.
[21] J.D. Seader, E.J. Henley, D.K. Roper, Separation Process Principles, Wiley, 2010.
[22] Y. Yampolskii, Polymeric Gas Separation Membranes, Macromolecules 45 (2012) 3298-3311.
[23] L.M. Robeson, Correlation of separation factor versus permeability for polymeric membranes, J. Membr. Sci. 62 (1991) 165-185.
[24] L.M. Robeson, The upper bound revisited, J. Membr. Sci. 320 (2008) 390-400.
[25] J. Caro, Are MOF membranes better in gas separation than those made of zeolites?, Current Opinion in Chemical Engineering 1 (2011) 77-83.
[26] O. Shekhah, J. Liu, R.A. Fischer, C. Woll, MOF thin films: existing and future applications, Chem. Soc. Rev. 40 (2011) 1081-1106.
[27] T. Johnson, S. Thomas, Nitrogen/oxygen permeability of natural rubber, epoxidised natural rubber and natural rubber/epoxidised natural rubber blends, Polymer 40 (1999) 3223-3228.
[28] A. Nabe, E. Staude, G. Belfort, Surface modification of polysulfone ultrafiltration membranes and fouling by BSA solutions, J. Membr. Sci. 133 (1997) 57-72.
[29] L. Shao, B.T. Low, T.-S. Chung, A.R. Greenberg, Polymeric membranes for the hydrogen economy: Contemporary approaches and prospects for the future, J. Membr. Sci. 327 (2009) 18-31.
[30] M.W. Ackley, S.U. Rege, H. Saxena, Application of natural zeolites in the purification and separation of gases, Microporous and Mesoporous Mater. 61 (2003) 25-42.
[31] M.E. Davis, R.F. Lobo, Zeolite and molecular sieve synthesis, Chem. Mater. 4 (1992) 756-768.

[32] R. Banerjee, H. Furukawa, D. Britt, C. Knobler, M. O'Keeffe, O.M. Yaghi, Control of Pore Size and Functionality in Isoreticular Zeolitic Imidazolate Frameworks and their Carbon Dioxide Selective Capture Properties, JACS 131 (2009) 3875-3877.
[33] B. Wang, A.P. Cote, H. Furukawa, M. O/'Keeffe, O.M. Yaghi, Colossal cages in zeolitic imidazolate frameworks as selective carbon dioxide reservoirs, Nature 453 (2008) 207-211.
[34] R. Banerjee, A. Phan, B. Wang, C. Knobler, H. Furukawa, M. O'Keeffe, O.M. Yaghi, High-Throughput Synthesis of Zeolitic Imidazolate Frameworks and Application to CO_2 Capture, Science 319 (2008) 939-943.
[35] J.-R. Li, J. Sculley, H.-C. Zhou, Metal–Organic Frameworks for Separations, Chem. Rev. 112 (2011) 869-932.
[36] H. Huang, W. Zhang, D. Liu, B. Liu, G. Chen, C. Zhong, Effect of temperature on gas adsorption and separation in ZIF-8: A combined experimental and molecular simulation study, Chem. Eng. Sci. 66 (2011) 6297-6305.
[37] S. Sircar, T.C. Golden, M.B. Rao, Activated carbon for gas separation and storage, Carbon 34 (1996) 1-12.
[38] H.-c. Guo, F. Shi, Z.-f. Ma, X.-q. Liu, Molecular Simulation for Adsorption and Separation of CH_4/H_2 in Zeolitic Imidazolate Frameworks, J. Phys. Chem. C 114 (2010) 12158-12165.
[39] S.S. Han, S.-H. Choi, W.A. Goddard, Zeolitic Imidazolate Frameworks as H2 Adsorbents: Ab Initio Based Grand Canonical Monte Carlo Simulation, J. Phys. Chem. C 114 (2010) 12039-12047.
[40] E.-Y. Chen, Y.-C. Liu, T.-Y. Sun, Q. Wang, L.-J. Liang, Effects of substituent groups and central metal ion on hydrogen adsorption in zeolitic imidazolate frameworks, Chem. Eng. Sci. 97 (2013) 60-66.
[41] Y.-S. Li, F.-Y. Liang, H. Bux, A. Feldhoff, W.-S. Yang, J. Caro, Molecular Sieve Membrane: Supported Metal–Organic Framework with High Hydrogen Selectivity, Angew. Chem. Int. Ed. 49 (2010) 548-551.
[42] H. Bux, F. Liang, Y. Li, J. Cravillon, M. Wiebcke, J.r. Caro, Zeolitic Imidazolate Framework Membrane with Molecular Sieving Properties by Microwave-Assisted Solvothermal Synthesis, JACS 131 (2009) 16000-16001.
[43] H. Guo, G. Zhu, I.J. Hewitt, S. Qiu, "Twin Copper Source" Growth of Metal−Organic Framework Membrane: $Cu_3(BTC)_2$ with High Permeability and Selectivity for Recycling H2, JACS 131 (2009) 1646-1647.
[44] A. Huang, H. Bux, F. Steinbach, J. Caro, Molecular-Sieve Membrane with Hydrogen Permselectivity: ZIF-22 in LTA Topology Prepared with 3-Aminopropyltriethoxysilane as Covalent Linker, Angew. Chem. Int. Ed. 49 (2010) 4958-4961.

[45] X. Dong, K. Huang, S. Liu, R. Ren, W. Jin, Y.S. Lin, Synthesis of zeolitic imidazolate framework-78 molecular-sieve membrane: defect formation and elimination, J. Mater. Chem. 22 (2012) 19222-19227.
[46] A. Huang, W. Dou, J. Caro, Steam-Stable Zeolitic Imidazolate Framework ZIF-90 Membrane with Hydrogen Selectivity through Covalent Functionalization, JACS 132 (2010) 15562-15564.
[47] A. Huang, J. Caro, Covalent Post-Functionalization of Zeolitic Imidazolate Framework ZIF-90 Membrane for Enhanced Hydrogen Selectivity, Angew. Chem. Int. Ed. 50 (2011) 4979-4982.
[48] Y. Liu, E. Hu, E.A. Khan, Z. Lai, Synthesis and characterization of ZIF-69 membranes and separation for CO_2/CO mixture, J. Membr. Sci. 353 (2010) 36-40.
[49] Y. Liu, G. Zeng, Y. Pan, Z. Lai, Synthesis of highly c-oriented ZIF-69 membranes by secondary growth and their gas permeation properties, J. Membr. Sci. 379 (2011) 46-51.
[50] S. Keskin, Atomistic Simulations for Adsorption, Diffusion, and Separation of Gas Mixtures in Zeolite Imidazolate Frameworks, J. Phys. Chem. C 115 (2011) 800-807.
[51] E. Atci, S. Keskin, Understanding the Potential of Zeolite Imidazolate Framework Membranes in Gas Separations Using Atomically Detailed Calculations, J. Phys. Chem. C 116 (2012) 15525-15537.
[52] T.C. Merkel, B.D. Freeman, R.J. Spontak, Z. He, I. Pinnau, P. Meakin, A.J. Hill, Ultrapermeable, Reverse-Selective Nanocomposite Membranes, Science 296 (2002) 519-522.
[53] D.Q. Vu, W.J. Koros, S.J. Miller, Mixed matrix membranes using carbon molecular sieves: II. Modeling permeation behavior, J. Membr. Sci. 211 (2003) 335-348.
[54] D.Q. Vu, W.J. Koros, S.J. Miller, Mixed matrix membranes using carbon molecular sieves: I. Preparation and experimental results, J. Membr. Sci. 211 (2003) 311-334.
[55] D.Q. Vu, W.J. Koros, S.J. Miller, Effect of condensable impurity in CO_2/CH_4 gas feeds on performance of mixed matrix membranes using carbon molecular sieves, J. Membr. Sci. 221 (2003) 233-239.
[56] C.M. Zimmerman, A. Singh, W.J. Koros, Tailoring mixed matrix composite membranes for gas separations, J. Membr. Sci. 137 (1997) 145-154.
[57] M. Anson, J. Marchese, E. Garis, N. Ochoa, C. Pagliero, ABS copolymer-activated carbon mixed matrix membranes for CO_2/CH_4 separation, J. Membr. Sci. 243 (2004) 19-28.
[58] H.J.C. te Hennepe, W.B.F. Boswerger, D. Bargeman, M.H.V. Mulder, C.A. Smolders, Zeolite-filled silicone rubber membranes Experimental determination of concentration profiles, J. Membr. Sci. 89 (1994) 185-196.
[59] C. Bartels-Caspers, E. Tusel-Langer, R.N. Lichtenthaler, Sorption isotherms of alcohols in zeolite-filled silicone rubber and in PVA-composite membranes, J. Membr. Sci. 70 (1992) 75-83.

[60] E. Okumus, T. Gurkan, L. Yilmaz, Development of a Mixed-Matrix Membrane for Pervaporation, Sep. Sci. Technol. 29 (1994) 2451-2473.
[61] I.F.J. Vankelecom, C. Dotremont, M. Morobé, J.B. Uytterhoeven, C. Vandecasteele, Zeolite-Filled PDMS Membranes. 1. Sorption of Halogenated Hydrocarbons, J. Phys. Chem. B 101 (1997) 2154-2159.
[62] M. Jia, K.-V. Peinemann, R.-D. Behling, Molecular sieving effect of the zeolite-filled silicone rubber membranes in gas permeation, J. Membr. Sci. 57 (1991) 289-292.
[63] T.W. Pechar, M. Tsapatsis, E. Marand, R. Davis, Preparation and characterization of a glassy fluorinated polyimide zeolite-mixed matrix membrane, Desalination 146 (2002) 3-9.
[64] D. Sen, H. Kalipcilar, L. Yilmaz, Development of zeolite filled polycarbonate mixed matrix gas separation membranes, Desalination 200 (2006) 222-224.
[65] S. Kim, T.W. Pechar, E. Marand, Poly(imide siloxane) and carbon nanotube mixed matrix membranes for gas separation, Desalination 192 (2006) 330-339.
[66] T.T. Moore, R. Mahajan, D.Q. Vu, W.J. Koros, Hybrid membrane materials comprising organic polymers with rigid dispersed phases, AIChE Journal 50 (2004) 311-321.
[67] R. Mahajan, R. Burns, M. Schaeffer, W.J. Koros, Challenges in forming successful mixed matrix membranes with rigid polymeric materials, J. Appl. Polym. Sci. 86 (2002) 881-890.
[68] S. Husain, W.J. Koros, Mixed matrix hollow fiber membranes made with modified HSSZ-13 zeolite in polyetherimide polymer matrix for gas separation, J. Membr. Sci. 288 (2007) 195-207.
[69] Shu, S. Husain, W.J. Koros, A General Strategy for Adhesion Enhancement in Polymeric Composites by Formation of Nanostructured Particle Surfaces, J. Phys. Chem. C 111 (2006) 652-657.
[70] M.A. Aroon, A.F. Ismail, T. Matsuura, M.M. Montazer-Rahmati, Performance studies of mixed matrix membranes for gas separation: A review, Sep. Purif. Technol. 75 (2010) 229-242.
[71] H. Vinh-Thang, S. Kaliaguine, Predictive Models for Mixed-Matrix Membrane Performance: A Review, Chem. Rev. (2013).
[72] Y. Li, T.-S. Chung, C. Cao, S. Kulprathipanja, The effects of polymer chain rigidification, zeolite pore size and pore blockage on polyethersulfone (PES)-zeolite A mixed matrix membranes, J. Membr. Sci. 260 (2005) 45-55.
[73] Y. Li, H.-M. Guan, T.-S. Chung, S. Kulprathipanja, Effects of novel silane modification of zeolite surface on polymer chain rigidification and partial pore blockage in polyethersulfone (PES)-zeolite A mixed matrix membranes, J. Membr. Sci. 275 (2006) 17-28.
[74] T.T. Moore, W.J. Koros, Non-ideal effects in organic–inorganic materials for gas separation membranes, J. Mol. Struct. 739 (2005) 87-98.

[75] R. Mahajan, W.J. Koros, Mixed matrix membrane materials with glassy polymers. Part 1, Polym. Eng. Sci. 42 (2002) 1420-1431.
[76] R. Mahajan, W.J. Koros, Mixed matrix membrane materials with glassy polymers. Part 2, Polym. Eng. Sci. 42 (2002) 1432-1441.
[77] T.-S. Chung, L.Y. Jiang, Y. Li, S. Kulprathipanja, Mixed matrix membranes (MMMs) comprising organic polymers with dispersed inorganic fillers for gas separation, Prog. Polym. Sci. 32 (2007) 483-507.
[78] R. Mahajan, W.J. Koros, Factors Controlling Successful Formation of Mixed-Matrix Gas Separation Materials, Ind. Eng. Chem. Res. 39 (2000) 2692-2696.
[79] M.J.C. Ordoñez, K.J. Balkus Jr, J.P. Ferraris, I.H. Musselman, Molecular sieving realized with ZIF-8/Matrimid mixed-matrix membranes, J. Membr. Sci. 361 (2010) 28-37.
[80] T.-H. Bae, J.S. Lee, W. Qiu, W.J. Koros, C.W. Jones, S. Nair, A High-Performance Gas-Separation Membrane Containing Submicrometer-Sized Metal–Organic Framework Crystals, Angew. Chem. Int. Ed. 49 (2010) 9863-9866.
[81] E.V. Perez, K.J. Balkus Jr, J.P. Ferraris, I.H. Musselman, Mixed-matrix membranes containing MOF-5 for gas separations, J. Membr. Sci. 328 (2009) 165-173.
[82] H.B. Tanh Jeazet, C. Staudt, C. Janiak, Metal-organic frameworks in mixed-matrix membranes for gas separation, Dalton Trans. 41 (2012) 14003-14027.
[83] H. Yehia, T.J. Pisklak, J.P. Ferraris, K.J. Balkus, I.H. Musselman, Methane facilitated transport using copper (II) biphenyl dicarboxylate-triethylenediamine/poly (3-acetoxyethylthiophene) mixed matrix membranes, Polymer Preprints 45 (2004).
[84] F.G. Kerry, Industrial Gas Handbook: Gas Separation And Purification, CRC Press, 2007.
[85] Anja Car, Chrtomir Stropnik, K.-V. Peinemann, Hybrid membrane materials with different metal–organic frameworks (MOFs) for gas separation, Desalination 200 (2006) 424-426.
[86] J. Hu, H. Cai, H. Ren, Y. Wei, Z. Xu, H. Liu, Y. Hu, Mixed-Matrix Membrane Hollow Fibers of $Cu_3(BTC)_2$ MOF and Polyimide for Gas Separation and Adsorption, Ind. Eng. Chem. Res. 49 (2010) 12605-12612.
[87] R. Adams, C. Carson, J. Ward, R. Tannenbaum, W. Koros, Metal organic framework mixed matrix membranes for gas separations, Microporous Mesoporous Mater. 131 (2010) 13-20.
[88] K. Díaz, M. López-González, L.F. del Castillo, E. Riande, Effect of zeolitic imidazolate frameworks on the gas transport performance of ZIF8-poly(1,4-phenylene ether-ether-sulfone) hybrid membranes, J. Membr. Sci. 383 (2011) 206-213.
[89] S. Basu, A. Cano-Odena, I.F.J. Vankelecom, MOF-containing mixed-matrix membranes for CO_2/CH_4 and CO_2/N_2 binary gas mixture separations, Sep. Purif. Technol. 81 (2011) 31-40.

[90] Q. Song, S.K. Nataraj, M.V. Roussenova, J.C. Tan, D.J. Hughes, W. Li, P. Bourgoin, M.A. Alam, A.K. Cheetham, S.A. Al-Muhtaseb, E. Sivaniah, Zeolitic imidazolate framework (ZIF-8) based polymer nanocomposite membranes for gas separation, Energy Environ. Sci. 5 (2012) 8359-8369.
[91] Y. Dai, J.R. Johnson, O. Karvan, D.S. Sholl, W.J. Koros, Ultem/ZIF-8 mixed matrix hollow fiber membranes for CO_2/N_2 separations, J. Membr. Sci. 401–402 (2012) 76-82.
[92] T. Yang, Y. Xiao, T.-S. Chung, Poly-/metal-benzimidazole nano-composite membranes for hydrogen purification, Energy Environ. Sci. 4 (2011) 4171-4180.
[93] T. Li, Y. Pan, K.-V. Peinemann, Z. Lai, Carbon dioxide selective mixed matrix composite membrane containing ZIF-7 nano-fillers, J. Membr. Sci. 425–426 (2013) 235-242.
[94] B. Seoane, J.M. Zamaro, C. Tellez, J. Coronas, Insight into the crystal synthesis, activation and application of ZIF-20, RSC Advances 1 (2011) 917-922.
[95] G. Yilmaz, S. Keskin, Predicting the Performance of Zeolite Imidazolate Framework/Polymer Mixed Matrix Membranes for CO_2, CH_4, and H_2 Separations Using Molecular Simulations, Ind. Eng. Chem. Res. 51 (2012) 14218-14228.
[96] B. Zornoza, B. Seoane, J.M. Zamaro, C. Téllez, J. Coronas, Combination of MOFs and Zeolites for Mixed-Matrix Membranes, ChemPhysChem 12 (2011) 2781-2785.
[97] A. Galve, D. Sieffert, C. Staudt, M. Ferrando, C. Güell, C. Téllez, J. Coronas, Combination of ordered mesoporous silica MCM-41 and layered titanosilicate JDF-L1 fillers for 6FDA-based copolyimide mixed matrix membranes, J. Membr. Sci. 431 (2013) 163-170.
[98] M.R. Kamal, I.A. Jinnah, L.A. Utracki, Permeability of oxygen and water vapor through polyethylene/polyamide films, Polym. Eng. Sci. 24 (1984) 1337-1347.
[99] J. Barbier, A Study of Permeability to Gases. Mixtures of Natural Rubber and Other Elastomers, Rubber Chem. Technol. 28 (1955) 814-820.
[100] D.S. Lee, W.K. Kang, J.H. An, S.C. Kim, Gas transport in polyurethane-polystyrene interpenetrating polymer network membranes. II. Effect of crosslinked state and annealing, J. Membr. Sci. 75 (1992) 15-27.
[101] S.L. Doo, S.J. Dae, H.K. Tae, C.K. Sung, Gas transport in polyurethane-polystyrene interpenetrating polymer network membranes. I. Effect of synthesis temperature and molecular structure variation, J. Membr. Sci. 60 (1987) 233-252.
[102] M.R. Coleman, R. Kohn, W.J. Koros, Gas-separation applications of miscible blends of isomeric polyimides, J. Appl. Polym. Sci. 50 (1993) 1059-1064.
[103] G.C. Kapantaidakis, S.P. Kaldis, X.S. Dabou, G.P. Sakellaropoulos, Gas permeation through PSF-PI miscible blend membranes, J. Membr. Sci. 110 (1996) 239-247.
[104] A.F. Ismail, R.A. Rahim, W.A.W.A. Rahman, Characterization of polyethersulfone/Matrimid 5218 miscible blend mixed matrix membranes for O_2/N_2 gas separation, Sep. Purif. Technol. 63 (2008) 200-206.

[105] S. Basu, A. Cano-Odena, I.F.J. Vankelecom, Asymmetric Matrimid/[$Cu_3(BTC)_2$] mixed-matrix membranes for gas separations, J. Membr. Sci. 362 (2010) 478-487.
[106] F. Dorosti, M.R. Omidkhah, M.Z. Pedram, F. Moghadam, Fabrication and characterization of polysulfone/polyimide–zeolite mixed matrix membrane for gas separation, Chem. Eng. J. 171 (2011) 1469-1476.
[107] S. Rafiq, Z. Man, A. Maulud, N. Muhammad, S. Maitra, Separation of CO_2 from CH4 using polysulfone/polyimide silica nanocomposite membranes, Sep. Purif. Technol. 90 (2012) 162-172.
[108] E.L. First, C.A. Floudas, MOFomics: Computational pore characterization of metal–organic frameworks, Microporous and Mesoporous Mater. 165 (2013) 32-39.
[109] D. Wu, C. Wang, B. Liu, D. Liu, Q. Yang, C. Zhong, Large-scale computational screening of metal-organic frameworks for CH_4/H_2 separation, AIChE Journal 58 (2012) 2078-2084.
[110] A. Battisti, S. Taioli, G. Garberoglio, Zeolitic imidazolate frameworks for separation of binary mixtures of CO_2, CH_4, N_2 and H_2: A computer simulation investigation, Microporous Mesoporous Mater. 143 (2011) 46-53.
[111] E.-Y. Chen, Y.-C. Liu, M. Zhou, L. Zhang, Q. Wang, Effects of structure on hydrogen adsorption in zeolitic imidazolate frameworks, Chem. Eng. Sci. 71 (2012) 178-184.
[112] V. Buch, Path integral simulations of mixed para-D[sub 2] and ortho-D[sub 2] clusters: The orientational effects, J. Chem. Phys. 100 (1994) 7610-7629.
[113] Q. Yang, C. Zhong, Molecular Simulation of Adsorption and Diffusion of Hydrogen in Metal−Organic Frameworks, J. Phys. Chem. B 109 (2005) 11862-11864.
[114] F. Darkrim, D. Levesque, Monte Carlo simulations of hydrogen adsorption in single-walled carbon nanotubes, J. Chem. Phys. 109 (1998) 4981-4984.
[115] M.G. Martin, J.I. Siepmann, Transferable Potentials for Phase Equilibria. 1. United-Atom Description of n-Alkanes, J. Phys. Chem. B 102 (1998) 2569-2577.
[116] J.J. Potoff, J.I. Siepmann, Vapor–liquid equilibria of mixtures containing alkanes, carbon dioxide, and nitrogen, AIChE Journal 47 (2001) 1676-1682.
[117] K. Makrodimitris, G.K. Papadopoulos, D.N. Theodorou, Prediction of Permeation Properties of CO_2 and N_2 through Silicalite via Molecular Simulations, J. Phys. Chem. B 105 (2001) 777-788.
[118] F. Allen, The Cambridge Structural Database: a quarter of a million crystal structures and rising, Acta Crystallographica Section B 58 (2002) 380-388.
[119] T. Sagara, J. Klassen, E. Ganz, Computational study of hydrogen binding by metal-organic framework-5, J. Chem. Phys. 121 (2004) 12543-12547.
[120] G. Garberoglio, Computer Simulation of the Adsorption of Light Gases in Covalent Organic Frameworks, Langmuir 23 (2007) 12154-12158.

[121] D. Liu, C. Zheng, Q. Yang, C. Zhong, Understanding the Adsorption and Diffusion of Carbon Dioxide in Zeolitic Imidazolate Frameworks: A Molecular Simulation Study, J. Phys. Chem. C 113 (2009) 5004-5009.
[122] B. Liu, Q. Yang, C. Xue, C. Zhong, B. Smit, Molecular simulation of hydrogen diffusion in interpenetrated metal-organic frameworks, PCCP 10 (2008) 3244-3249.
[123] S.L. Mayo, B.D. Olafson, W.A. Goddard, DREIDING: a generic force field for molecular simulations, J. Phys. Chem. 94 (1990) 8897-8909.
[124] Q. Xu, C. Zhong, A General Approach for Estimating Framework Charges in Metal−Organic Frameworks, J. Phys. Chem. C 114 (2010) 5035-5042.
[125] T. Watanabe, T.A. Manz, D.S. Sholl, Accurate Treatment of Electrostatics during Molecular Adsorption in Nanoporous Crystals without Assigning Point Charges to Framework Atoms, J. Phys. Chem. C 115 (2011) 4824-4836.
[126] D. Frenkel, B. Smit, Understanding Molecular Simulation: From Algorithms to Applications, Elsevier Science, 2001.
[127] P. Hünenberger, Thermostat Algorithms for Molecular Dynamics Simulations, in: C. Holm, K. Kremer (Eds.) Advanced Computer Simulation, Springer Berlin Heidelberg, 2005, pp. 105-149.
[128] D.S. Sholl, Understanding Macroscopic Diffusion of Adsorbed Molecules in Crystalline Nanoporous Materials via Atomistic Simulations, Acc. Chem. Res. 39 (2006) 403-411.
[129] S. Keskin, D.S. Sholl, Efficient Methods for Screening of Metal Organic Framework Membranes for Gas Separations Using Atomically Detailed Models, Langmuir 25 (2009) 11786-11795.
[130] M. Murthi, R.Q. Snurr, Effects of Molecular Siting and Adsorbent Heterogeneity on the Ideality of Adsorption Equilibria, Langmuir 20 (2004) 2489-2497.
[131] R.E. Kesting, A.K. Fritzsche, Polymeric gas separation membranes, Wiley, 1993.
[132] R. Krishna, J.M. van Baten, In silico screening of zeolite membranes for CO_2 capture, J. Membr. Sci. 360 (2010) 323-333.
[133] R.H.B. Bouma, A. Checchetti, G. Chidichimo, E. Drioli, Permeation through a heterogeneous membrane: the effect of the dispersed phase, J. Membr. Sci. 128 (1997) 141-149.
[134] J.C. Maxwell, A Treatise on Electricity and Magnetism, Clarendon Press, 1873.
[135] Y.C. Chiew, E.D. Glandt, The effect of structure on the conductivity of a dispersion, J. Colloid Interface Sci. 94 (1983) 90-104.
[136] A.S. Michaels, H.J. Bixler, Flow of gases through polyethylene, J. Polym. Sci. 50 (1961) 413-439.
[137] B. Shimekit, H. Mukhtar, T. Murugesan, Prediction of the relative permeability of gases in mixed matrix membranes, J. Membr. Sci. 373 (2011) 152-159.

[138] B. Assfour, S. Leoni, S. Yurchenko, G. Seifert, Hydrogen storage in zeolite imidazolate frameworks. A multiscale theoretical investigation, Int. J. Hydrogen Energy 36 (2011) 6005-6013.
[139] R. Krishna, J.M. van Baten, In silico screening of metal-organic frameworks in separation applications, Phys.Chem. Chem. Phys. 13 (2011) 10593-10616.
[140] D. Britt, H. Furukawa, B. Wang, T.G. Glover, O.M. Yaghi, Highly efficient separation of carbon dioxide by a metal-organic framework replete with open metal sites, PNAS 106 (2009) 20637-20640.
[141] S.E. Jee, D.S. Sholl, Carbon Dioxide and Methane Transport in DDR Zeolite: Insights from Molecular Simulations into Carbon Dioxide Separations in Small Pore Zeolites, JACS 131 (2009) 7896-7904.
[142] S. Li, J.L. Falconer, R.D. Noble, R. Krishna, Interpreting Unary, Binary, and Ternary Mixture Permeation Across a SAPO-34 Membrane with Loading-Dependent Maxwell−Stefan Diffusivities, J. Phys. Chem. C 111 (2007) 5075-5082.
[143] I. Erucar, S. Keskin, Screening Metal–Organic Framework-Based Mixed-Matrix Membranes for CO_2/CH_4 Separations, Ind. Eng. Chem. Res. 50 (2011) 12606-12616.
[144] C. Zhang, R.P. Lively, K. Zhang, J.R. Johnson, O. Karvan, W.J. Koros, Unexpected Molecular Sieving Properties of Zeolitic Imidazolate Framework-8, J. Phys. Chem. Lett. 3 (2012) 2130-2134.
[145] F. Salles, D.I. Kolokolov, H. Jobic, G. Maurin, P.L. Llewellyn, T. Devic, C. Serre, G.r. Ferey, Adsorption and Diffusion of H_2 in the MOF Type Systems MIL-47(V) and MIL-53(Cr): A Combination of Microcalorimetry and QENS Experiments with Molecular Simulations, J. Phys. Chem. C 113 (2009) 7802-7812.
[146] F. Salles, A. Ghoufi, G. Maurin, R.G. Bell, C. Mellot-Draznieks, G. Férey, Molecular Dynamics Simulations of Breathing MOFs: Structural Transformations of MIL-53(Cr) upon Thermal Activation and CO_2 Adsorption, Angew. Chem. Int. Ed. 47 (2008) 8487-8491.
[147] L. Hertäg, H. Bux, J. Caro, C. Chmelik, T. Remsungnen, M. Knauth, S. Fritzsche, Diffusion of CH_4 and H_2 in ZIF-8, J. Membr. Sci. 377 (2011) 36-41.
[148] H. Bux, C. Chmelik, J.M. van Baten, R. Krishna, J. Caro, Novel MOF-Membrane for Molecular Sieving Predicted by IR-Diffusion Studies and Molecular Modeling, Adv. Mater. 22 (2010) 4741-4743.
[149] E. Haldoupis, T. Watanabe, S. Nair, D.S. Sholl, Quantifying Large Effects of Framework Flexibility on Diffusion in MOFs: CH_4 and CO_2 in ZIF-8, Chemphyschem 15 (2012) 3449-3452.
[150] T. Watanabe, D.S. Sholl, Accelerating Applications of Metal–Organic Frameworks for Gas Adsorption and Separation by Computational Screening of Materials, Langmuir 28 (2012) 14114-14128.

[151] E. Haldoupis, S. Nair, D.S. Sholl, Finding MOFs for Highly Selective CO_2/N_2 Adsorption Using Materials Screening Based on Efficient Assignment of Atomic Point Charges, J. Am. Chem. Soc. 134 (2012) 4313-4323.
[152] S. Keskin, D.S. Sholl, Selecting metal organic frameworks as enabling materials in mixed matrix membranes for high efficiency natural gas purification, Energy Environ. Sci. 3 (2010) 343-351.
[153] C.E. Powell, G.G. Qiao, Polymeric CO_2/N_2 gas separation membranes for the capture of carbon dioxide from power plant flue gases, J. Membr. Sci. 279 (2006) 1-49.
[154] H. Lin, B.D. Freeman, Gas solubility, diffusivity and permeability in poly(ethylene oxide), J. Membr. Sci. 239 (2004) 105-117.
[155] Y. Hirayama, Y. Kase, N. Tanihara, Y. Sumiyama, Y. Kusuki, K. Haraya, Permeation properties to CO_2 and N_2 of poly(ethylene oxide)-containing and crosslinked polymer films, J. Membr. Sci. 160 (1999) 87-99.

APPENDIX

Appendix-A: Atomic representations and charges of ZIF-11 and ZIF-12

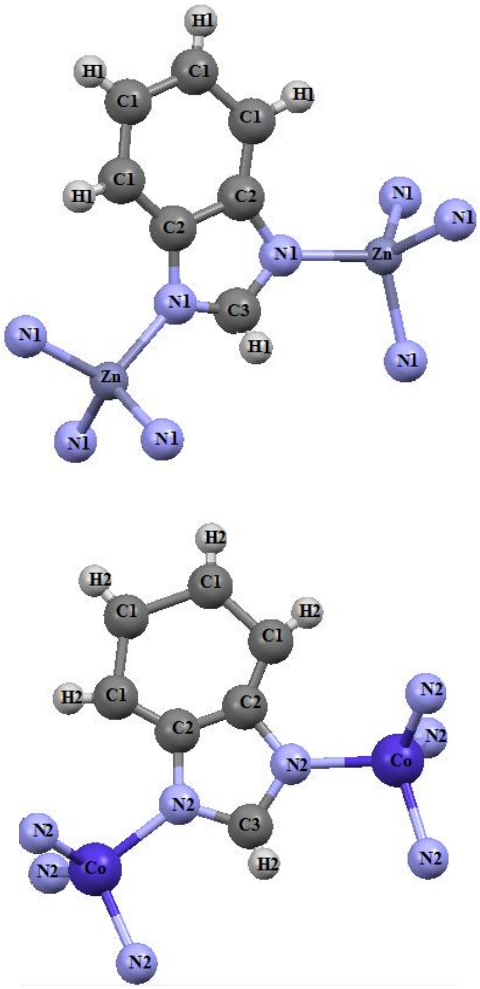

Figure A1: Atomic representations of ZIF-11 (top) and ZIF-12 (bottom)

Table A1: Partial charges of ZIF-11 and ZIF-12 structures

Atoms	q (e)
C1	-0.139
C2	0.222
C3	0.209
N1	-0.350
N2	-0.440
Zn	0.787
Co	0.700
H1	0.044
H2	0.091

Appendix-B: Adsorption-based, diffusion-based and permeation-based selectivities of ZIFs

Table B1: Adsorption-based, diffusion-based and permeation-based selectivities of ZIFs at 10 bar and 298 K for CH_4/H_2:10/90.

ZIFs	S_{ads} (CH_4/H_2)	S_{diff} (CH_4/H_2)	S_{perm} (CH_4/H_2)
ZIF-11 (UFF)	36.30	0.003	0.09
ZIF-12 (UFF)	34.71	0.002	0.06
ZIF-2	33.01	0.32	10.62
ZIF-3	29.06	0.10	3.00
ZIF-6	13.69	0.16	2.19
ZIF-10	11.05	0.15	1.65
ZIF-60	10.93	0.16	1.73
ZIF-65	14.37	0.002	0.03
ZIF-69	39.23	0.06	2.41
ZIF-79	52.17	0.18	9.39
ZIF-81	40.09	0.17	6.77
ZIF-90	15.16	0.001	0.02

Data for ZIFs, except ZIF-11 and ZIF-12, were taken from ref.[51]

Table B2: Adsorption-based, diffusion-based and permeation-based selectivities of ZIFs at 10 bar and 298 K for CO_2/CH_4:10/90.

ZIFs	S_{ads} (CO_2/CH_4)	S_{diff} (CO_2/CH_4)	S_{perm} (CO_2/CH_4)
ZIF-11 (UFF)	12.05	70.48	849.05
ZIF-12 (UFF)	5.51	346.97	1913.32
ZIF-2	5.22	0.31	1.63
ZIF-3	4.73	0.52	2.46
ZIF-6	2.87	0.34	0.98
ZIF-10	2.86	0.50	1.44
ZIF-60	3.32	0.41	1.36
ZIF-65	7.67	0.59	4.56
ZIF-69	6.64	0.41	2.71
ZIF-79	4.62	0.14	0.65
ZIF-81	6.73	0.07	0.47
ZIF-90	9.53	2.34	22.29

Data for ZIFs, except ZIF-11 and ZIF-12, were taken from ref.[51]

Table B3: Adsorption-based, diffusion-based and permeation-based selectivities of ZIFs at 10 bar and 298 K for CO_2/H_2:1/99.

ZIFs	S_{ads} (CO_2/H_2)	S_{diff} (CO_2/H_2)	S_{perm} (CO_2/H_2)
ZIF-11 (UFF)	431.91	0.32	136.08
ZIF-12 (UFF)	196.10	0.10	19.19
ZIF-2	160.87	0.09	13.70
ZIF-3	176.43	0.02	3.75
ZIF-6	34.68	0.05	1.67
ZIF-10	27.55	0.06	1.70
ZIF-60	31.21	0.07	2.14
ZIF-65	102.08	0.001	0.12
ZIF-69	240.07	0.02	4.09
ZIF-79	195.94	0.02	3.92
ZIF-81	235.91	0.01	2.41
ZIF-90	137.44	0.002	0.32

Data for ZIFs, except ZIF-11 and ZIF-12, were taken from ref.[51]

Appendix-C: Permeability and selectivity of polymers, ZIFs and MOFs

Table C1: Permeability and selectivity of pure polymers for CO_2/CH_4 separation.

Polymer	P(CO_2)	S (CO_2/CH_4)
PVSH doped polyaniline	0.029	2200
Polypyrrole 6FDA/PMDA (25/75)-TAB	3.13	140
Polyimide TADATO/DSDA (1/1)-DDBT	45	60
Poly(diphenyl acetylene) 3a	110	47.8
Polyimide 6FDA-TMPDA/DAT (3:1)	187.6	33.9
Poly(diphenyl acetylene) 3e	290	31.5
Polyimide 6FDA-TMPDA	555.7	22.7
6FDA-based polyimide	958	24
PIM-7	1100	17.7
PIM-1	2300	18.4
PTMSP	19000	4.42
PPEES	5.36	25.52
Matrimid	9.52	39.67
Ultem	1.4	37.94
6FDA-DAM	401.36	17.46

Permeability unit is Barrers. Data for all polymers were taken from Robeson et al.[24] except Matrimid,[79] Ultem,[79] 6FDA-DAM poly(imide) [80] and PPEES.[88]

Table C2: Permeability and selectivity of pure polymers for H_2/CH_4 separation.

Polymer	$P(H_2)$	$S\ (H_2/CH_4)$
Sulfonated polyimide (DAPHFDS(H))	52	325
Polyimide (6FDA-mMPD)	106	121
Polyimide (6FDA-DDBT)	156	78.8
Hyflon® AD60X	187	61.7
Teflon AF-2400	3300	5.5
Poly(trimethylsilylpropyne)	17000	1.13
Matrimid	28.88	120.33
PPEES	6.74	32.1

Permeability unit is Barrers. Data for all polymers were taken from Robeson et al.[24] except Matrimid,[79] Ultem,[79] 6FDA-DAM poly(imide) [80] and PPEES.[88]

Table C3: Permeability and selectivity of pure polymers for H_2/CO_2 separation.

Polymer	$P(H_2)$	$S\ (H_2/CO_2)$
Liquid crystalline polyester (HBA/HNA 30/70)	0.05	100.9
Polyaniline (redoped)	1.75	23.1
Polyimide(1,1-6FDA-DIA)	31.4	8.05
Poly(trimethylsilylpropyne)	13900	0.495
Matrimid	28.88	3.03
PPEES	6.74	1.26

Permeability unit is Barrers. Data for all polymers were taken from Robeson et al. [24] except Matrimid,[79] Ultem,[79] 6FDA-DAM poly(imide) [80] and PPEES.[88]

Table C4: Permeability and selectivity of pure polymers for CO_2/N_2 separation.

Polymer	$P(CO_2)$	S (CO_2/N_2)
Poly(bis(2-(2-methoxyethoxy)ethoxy) phosphazene)	250	62.5
PIM-7	1100	26.2
Modified poly (dimethylsiloxane)	2000	34.2
PIM-1	2300	25
Poly(trimethylgermylpropyne)	14000	14
Poly(trimethylsilylpropyne)	29000	10.7
PSF	5.9	24.7
	6.4	19.5
PDMS	2503	8.2
PPEES	5.36	35.7
	9.52	30.7
Matrimid	8.07	22.4
	9.0	36.0
Ultem	1.10	36.0
6FDA-DAM	401.36	14.0
PEO	8.1	140.0
6FDA-IPDA	24.3	27.9
HQDPA-DBA	0.683	45.5
CLP	144.0	64.0

Permeability unit is Barrer. Data for all polymers were taken from Robeson et al.[24] except PSF,[85, 96] PDMS,[85] PPEES,[88] Matrimid,[79, 81, 90] Ultem,[91] 6FDA-DAM,[80] PEO,[153] 6FDA-IPDA,[153] HQDPA-DBA [153] and CLP [153].

Table C5: Permeability, selectivity and corrected diffusivity of gases in ZIFs for CO_2/CH_4, H_2/CH_4 and H_2/CO_2 separations at 2 bar and 298 K.

	P (CO_2)	**P (CH_4) (Barrers)**	**P (H_2)**	**D_o-CO_2**	**D_o-CH_4 (cm^2/s)**	**D_o-H_2**	**S(CO_2/CH_4)**	**S(H_2/CH_4)**	**S(H_2/CO_2)**
ZIF-2	526447	885988	92056	5.3E-05	2.5E-04	6.2E-04	0.59	0.10	0.18
ZIF-3	151138	434894	149140	1.5E-05	1.5E-04	1.1E-03	0.35	0.34	0.99
ZIF-6	522057	459004	213322	1.2E-04	2.8E-04	1.6E-03	1.14	0.47	0.41
ZIF-10	236319	174018	141259	7.0E-05	1.3E-04	1.2E-03	1.36	0.81	0.60
ZIF-11	57558	164	14474	7.2E-06	5.9E-08	1.1E-04	351.00	88.00	0.25
ZIF-12	30768	201	14144	5.1E-06	7.6E-08	1.1E-04	153.00	70.41	0.46
ZIF-60	219833	244010	144742	5.2E-05	1.9E-04	1.2E-03	0.90	0.59	0.66
ZIF-65	2892	870	33667	4.0E-07	6.2E-07	3.3E-04	3.33	39.00	12.00
ZIF-67	31718	1.88	12978	4.8E-06	8.5E-10	1.1E-04	-	-	0.41
ZIF-69	36082	29340	60179	4.8E-06	9.9E-06	5.4E-04	1.23	2.05	1.67
ZIF-78	14300	2780	28847	1.4E-06	9.7E-07	2.8E-04	5.00	10.00	2.02
ZIF-79	74034	463924	99324	9.2E-06	1.2E-04	8.4E-04	0.16	0.21	1.34
ZIF-81	14390	174267	58011	1.9E-06	6.0E-05	5.4E-04	0.08	0.33	4.00
ZIF-90	4429	461	24755	5.4E-07	3.1E-07	2.3E-04	10.00	54.00	6.00

For ZIF-67, gas selectivity for systems including CH_4 are not tabulated because the corrected diffusivity of CH_4 in this material was too slow ($<10^{-8}$ cm^2/s) to be measured by EMD simulations.

Table C6: CO_2 permeability and CO_2/N_2 selectivity of pure MOFs and ZIFs at 2 bar and 298 K.

Material	P(CO_2)	S (CO_2/N_2)
BACMOH-10	1.28	0.0006
BAHGUN	1261701	11.77
FOHQUO	56173	3.03
JASNEX	0.37	1165780
MABJOP	46429	13.14
MABJUV-01	164493	4.57
MIHHOA	366	1.23
MIHHUG	1078	0.72
MMIF	1822	102180
UFUNAK	951308	981
UFUMUD-01	61271	10.74
UGEPEB	88611	317
YOPMAS	2.46	1015
VEJZOA (ZIF-11)	57558	132
VEJZUG (ZIF-12)	30768	487
GITTOT (ZIF-67)	31718	252

Appendix-D: Performance of MOF and ZIF-based MMMs for H_2/CH_4, H_2/CO_2, CO_2/CH_4 and CO_2/N_2 separations

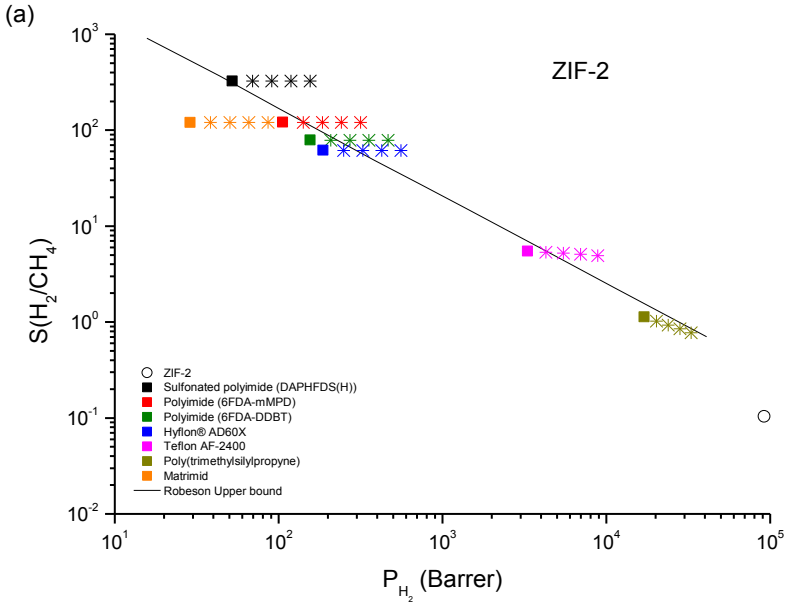

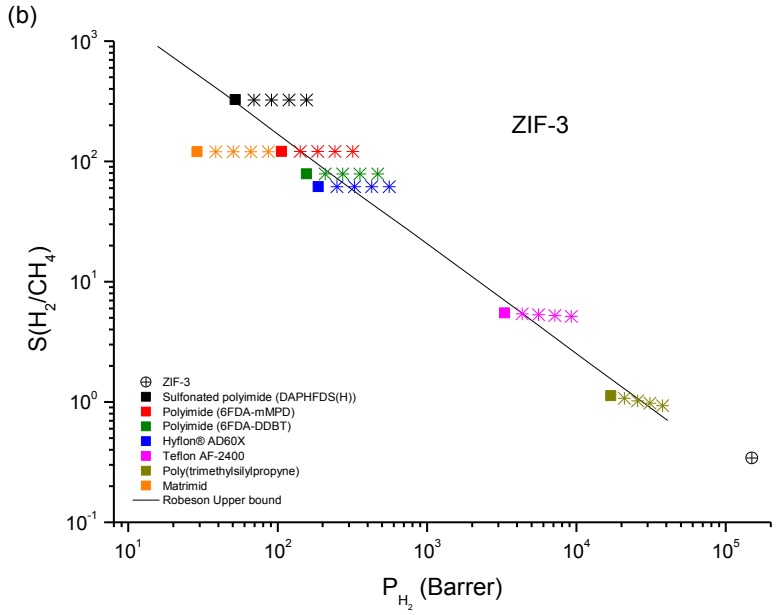

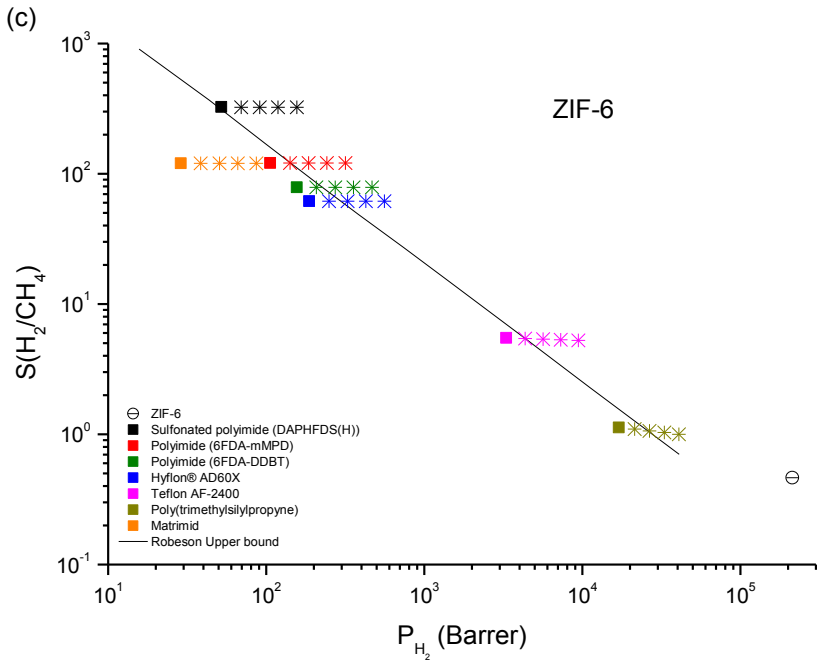
(c)
ZIF-6
ZIF-6
Sulfonated polyimide (DAPHFDS(H))
Polyimide (6FDA-mMPD)
Polyimide (6FDA-DDBT)
Hyflon® AD60X
Teflon AF-2400
Poly(trimethylsilylpropyne)
Matrimid
Robeson Upper bound
S(H2/CH4)
PH2 (Barrer)

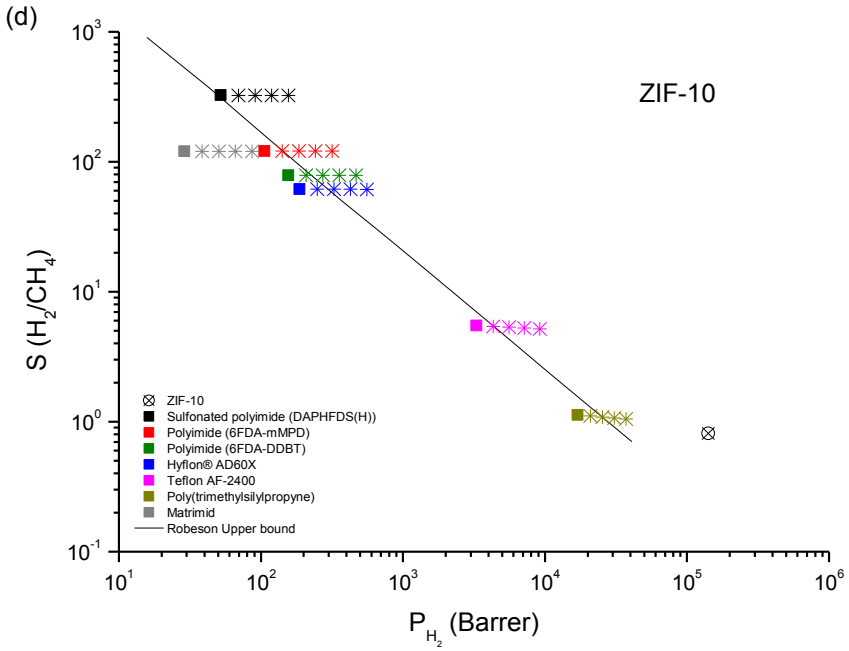
(d)
ZIF-10
ZIF-10
Sulfonated polyimide (DAPHFDS(H))
Polyimide (6FDA-mMPD)
Polyimide (6FDA-DDBT)
Hyflon® AD60X
Teflon AF-2400
Poly(trimethylsilylpropyne)
Matrimid
Robeson Upper bound
S (H2/CH4)
PH2 (Barrer)

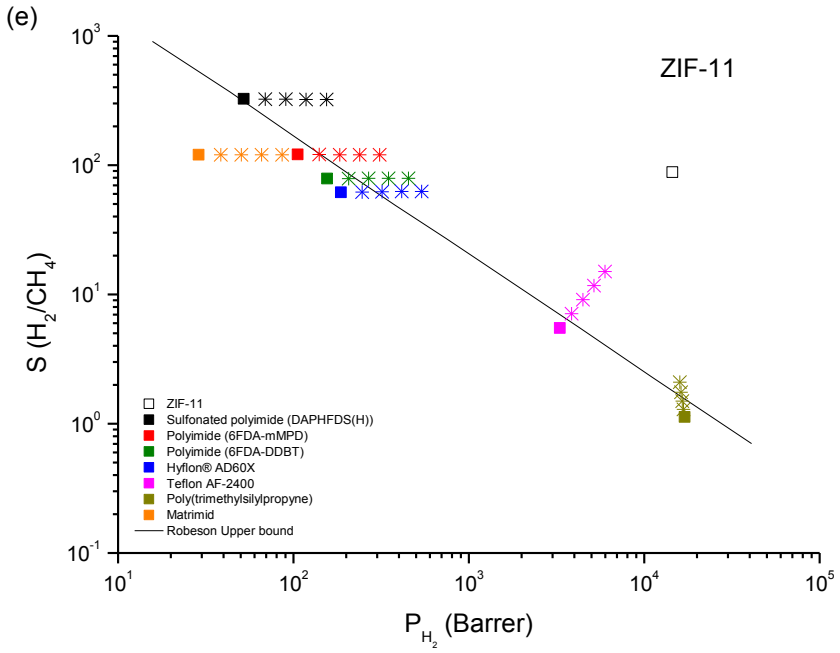
(e)
ZIF-11
S (H2/CH4)
P H2 (Barrer)
ZIF-11
Sulfonated polyimide (DAPHFDS(H))
Polyimide (6FDA-mMPD)
Polyimide (6FDA-DDBT)
Hyflon® AD60X
Teflon AF-2400
Poly(trimethylsilylpropyne)
Matrimid
Robeson Upper bound

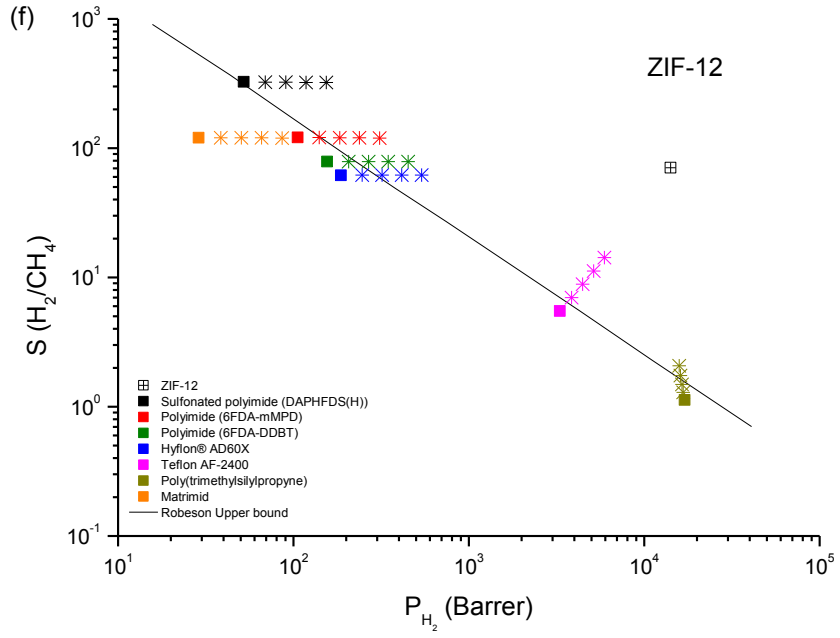
(f)
ZIF-12
S (H2/CH4)
P H2 (Barrer)
ZIF-12
Sulfonated polyimide (DAPHFDS(H))
Polyimide (6FDA-mMPD)
Polyimide (6FDA-DDBT)
Hyflon® AD60X
Teflon AF-2400
Poly(trimethylsilylpropyne)
Matrimid
Robeson Upper bound

(g)

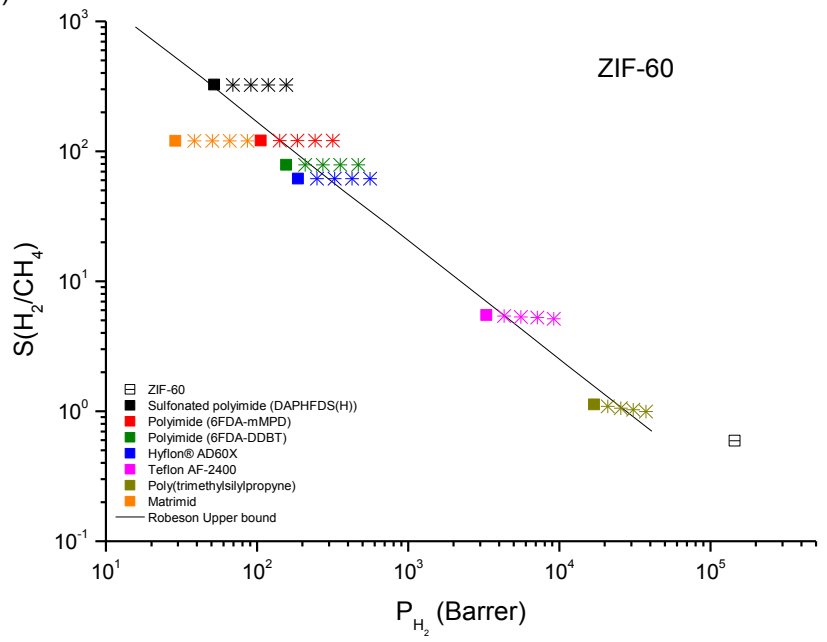
ZIF-60
S(H2/CH4)
PH2 (Barrer)
ZIF-60
Sulfonated polyimide (DAPHFDS(H))
Polyimide (6FDA-mMPD)
Polyimide (6FDA-DDBT)
Hyflon® AD60X
Teflon AF-2400
Poly(trimethylsilylpropyne)
Matrimid
Robeson Upper bound

(h)

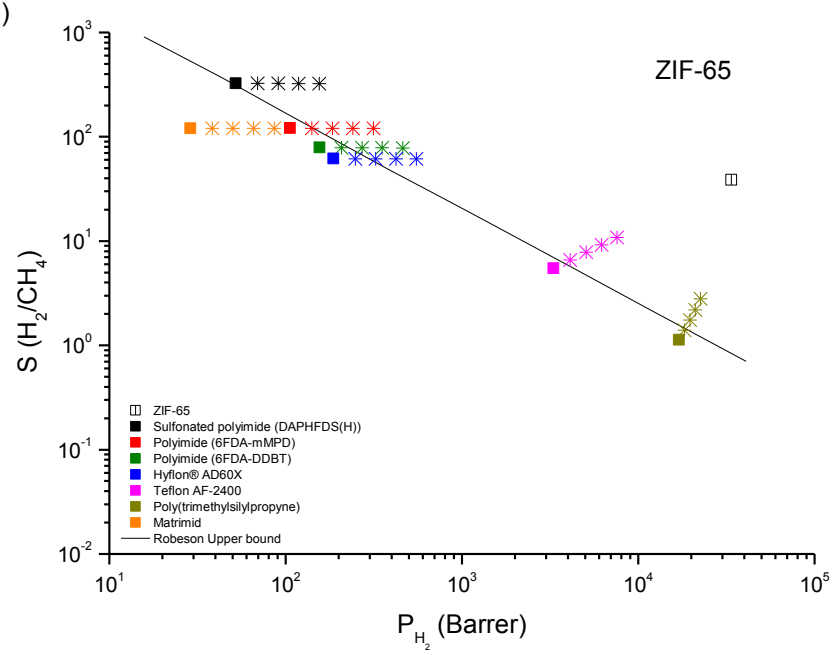
ZIF-65
S (H2/CH4)
PH2 (Barrer)
ZIF-65
Sulfonated polyimide (DAPHFDS(H))
Polyimide (6FDA-mMPD)
Polyimide (6FDA-DDBT)
Hyflon® AD60X
Teflon AF-2400
Poly(trimethylsilylpropyne)
Matrimid
Robeson Upper bound

(i)

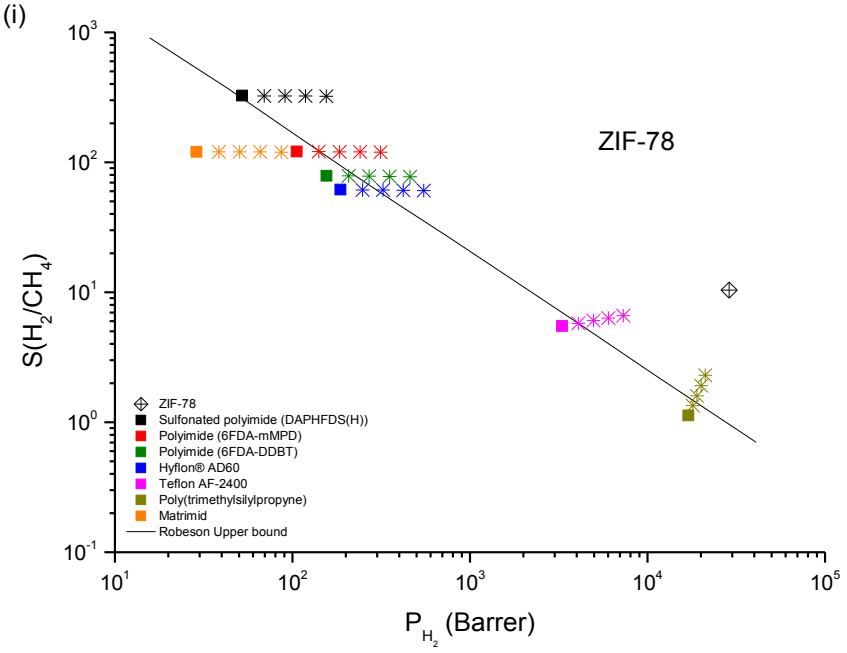
ZIF-78
S(H2/CH4)
PH2 (Barrer)
ZIF-78
Sulfonated polyimide (DAPHFDS(H))
Polyimide (6FDA-mMPD)
Polyimide (6FDA-DDBT)
Hyflon® AD60
Teflon AF-2400
Poly(trimethylsilylpropyne)
Matrimid
Robeson Upper bound

(j)

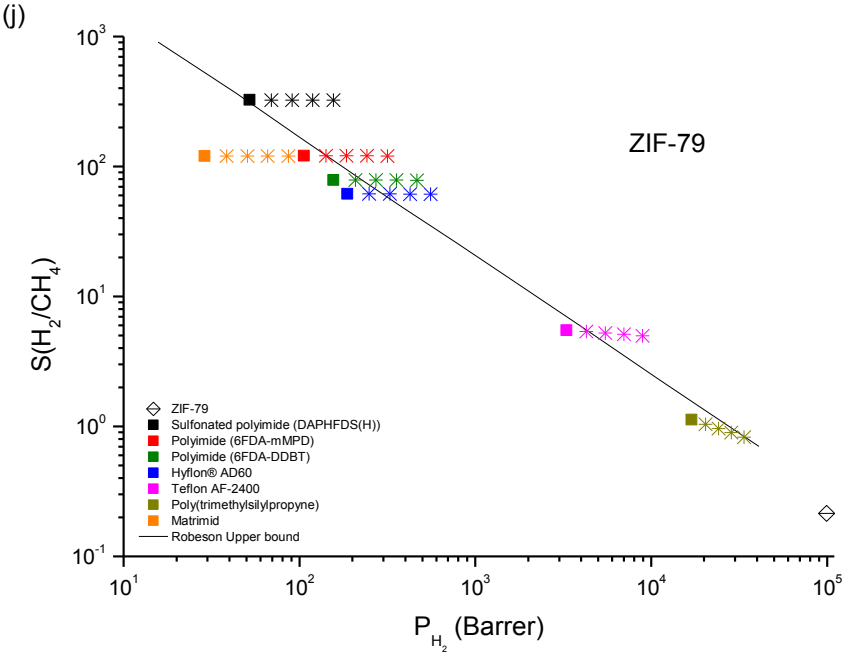
ZIF-79
S(H2/CH4)
PH2 (Barrer)
ZIF-79
Sulfonated polyimide (DAPHFDS(H))
Polyimide (6FDA-mMPD)
Polyimide (6FDA-DDBT)
Hyflon® AD60
Teflon AF-2400
Poly(trimethylsilylpropyne)
Matrimid
Robeson Upper bound

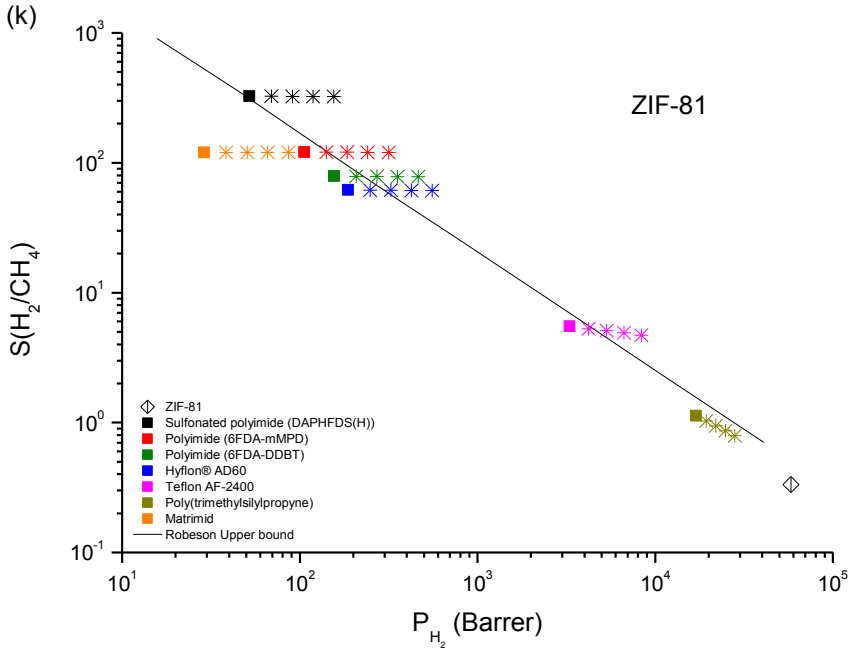

Figure D1: Performance of ZIF-based MMMs for H_2/CH_4 separation. Squares represent the performance of pure polymers and stars represent the performance of MMMs where the volume fraction of the fillers increases from 0.1 to 0.4.

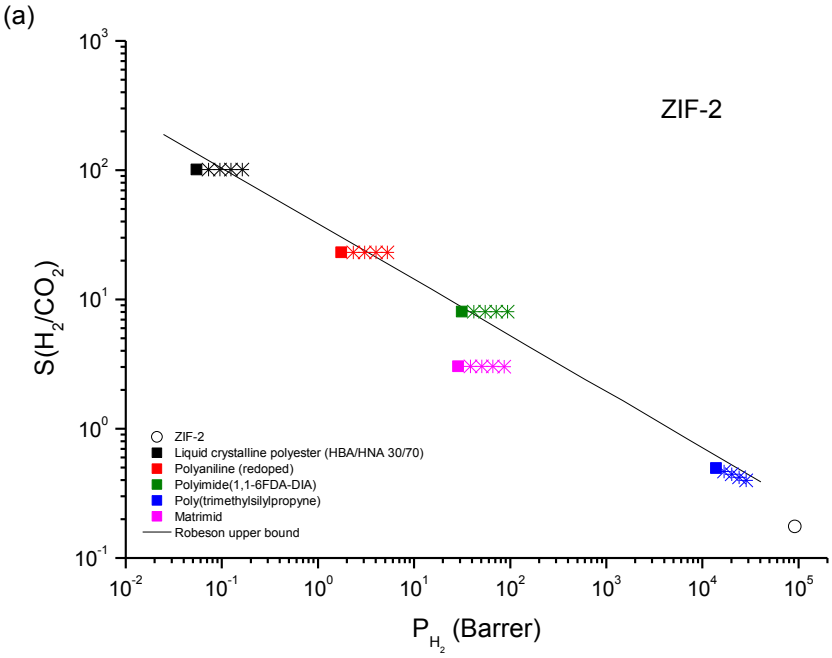
(a)
ZIF-2
S(H2/CO2)
P H2 (Barrer)
ZIF-2
Liquid crystalline polyester (HBA/HNA 30/70)
Polyaniline (redoped)
Polyimide(1,1-6FDA-DIA)
Poly(trimethylsilylpropyne)
Matrimid
Robeson upper bound

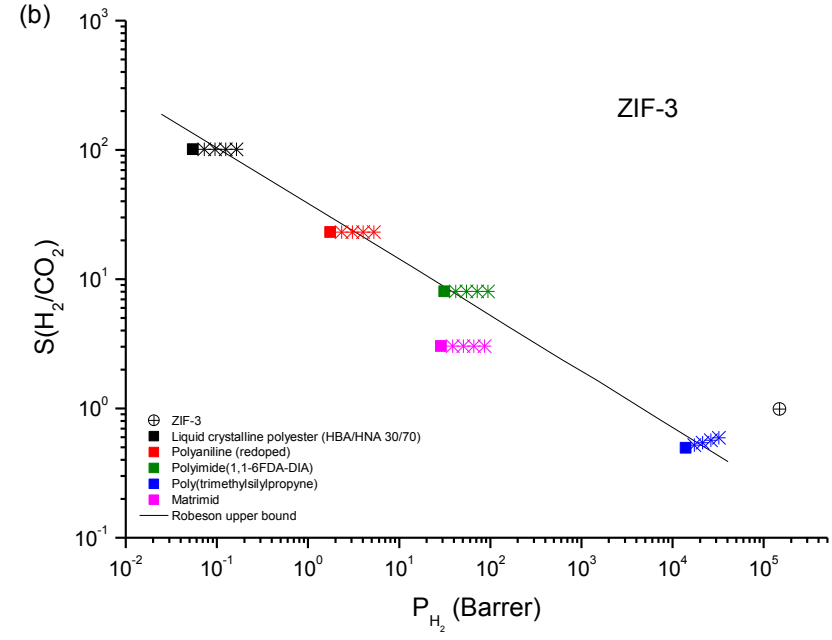
(b)
ZIF-3
S(H2/CO2)
P H2 (Barrer)
ZIF-3
Liquid crystalline polyester (HBA/HNA 30/70)
Polyaniline (redoped)
Polyimide(1,1-6FDA-DIA)
Poly(trimethylsilylpropyne)
Matrimid
Robeson upper bound

(c)

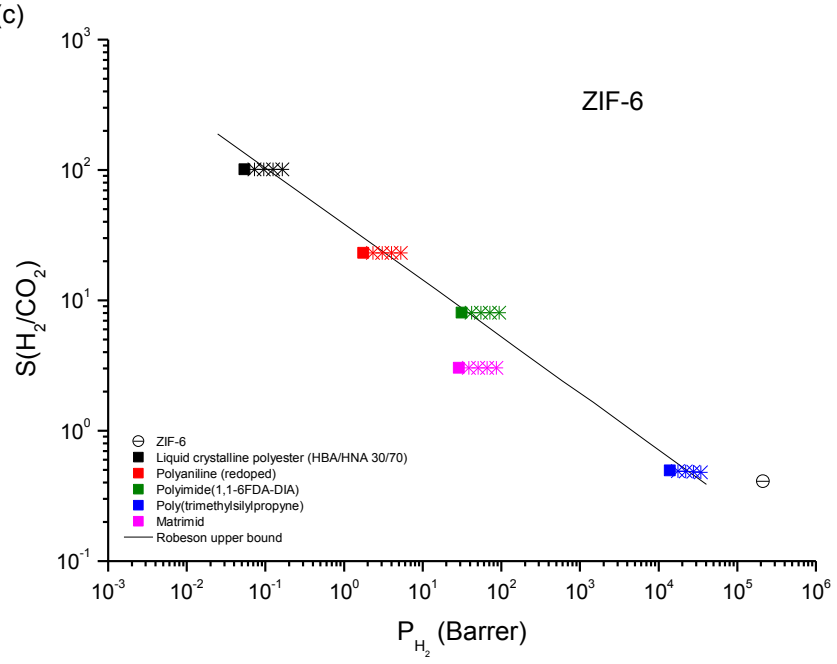
ZIF-6
S(H2/CO2)
PH2 (Barrer)
ZIF-6
Liquid crystalline polyester (HBA/HNA 30/70)
Polyaniline (redoped)
Polyimide(1,1-6FDA-DIA)
Poly(trimethylsilylpropyne)
Matrimid
Robeson upper bound

(d)

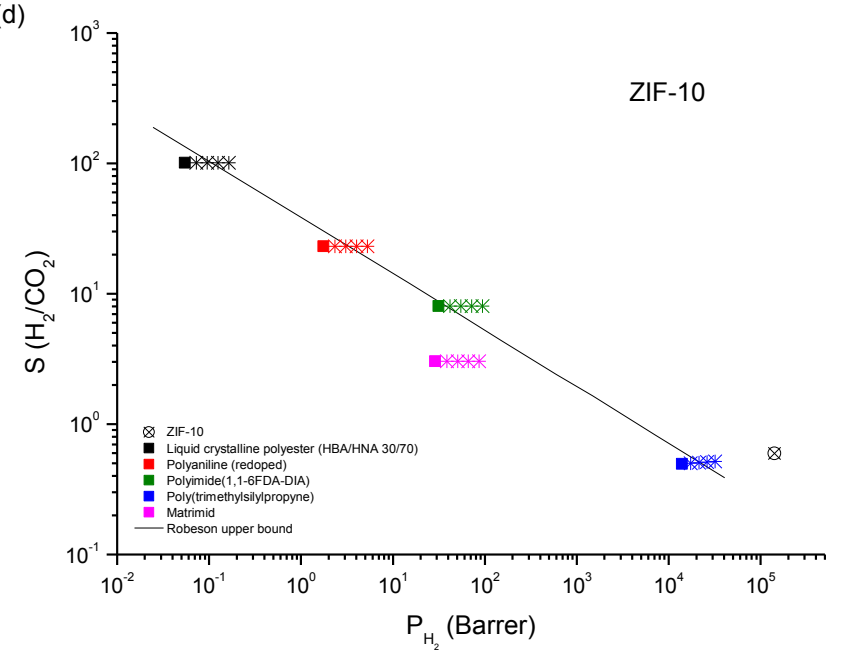
ZIF-10
S (H2/CO2)
PH2 (Barrer)
ZIF-10
Liquid crystalline polyester (HBA/HNA 30/70)
Polyaniline (redoped)
Polyimide(1,1-6FDA-DIA)
Poly(trimethylsilylpropyne)
Matrimid
Robeson upper bound

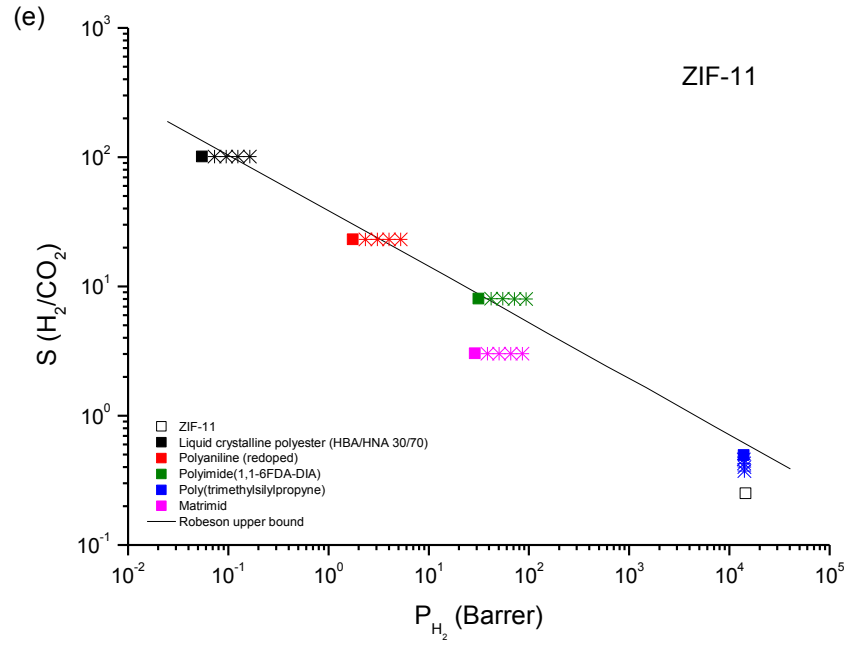
(e)
ZIF-11
S (H2/CO2)
PH2 (Barrer)
ZIF-11
Liquid crystalline polyester (HBA/HNA 30/70)
Polyaniline (redoped)
Polyimide(1,1-6FDA-DIA)
Poly(trimethylsilylpropyne)
Matrimid
Robeson upper bound

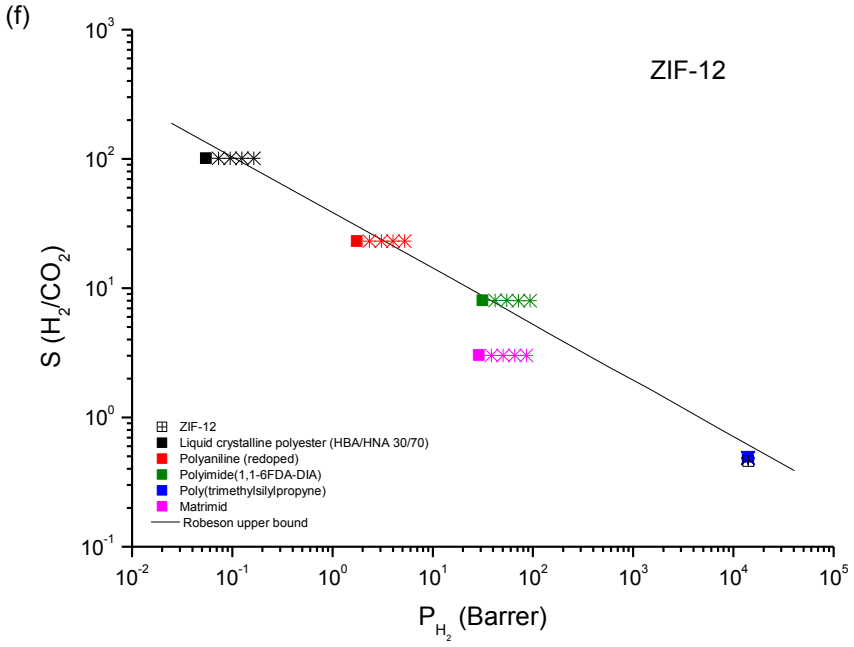
(f)
ZIF-12
S (H2/CO2)
PH2 (Barrer)
ZIF-12
Liquid crystalline polyester (HBA/HNA 30/70)
Polyaniline (redoped)
Polyimide(1,1-6FDA-DIA)
Poly(trimethylsilylpropyne)
Matrimid
Robeson upper bound

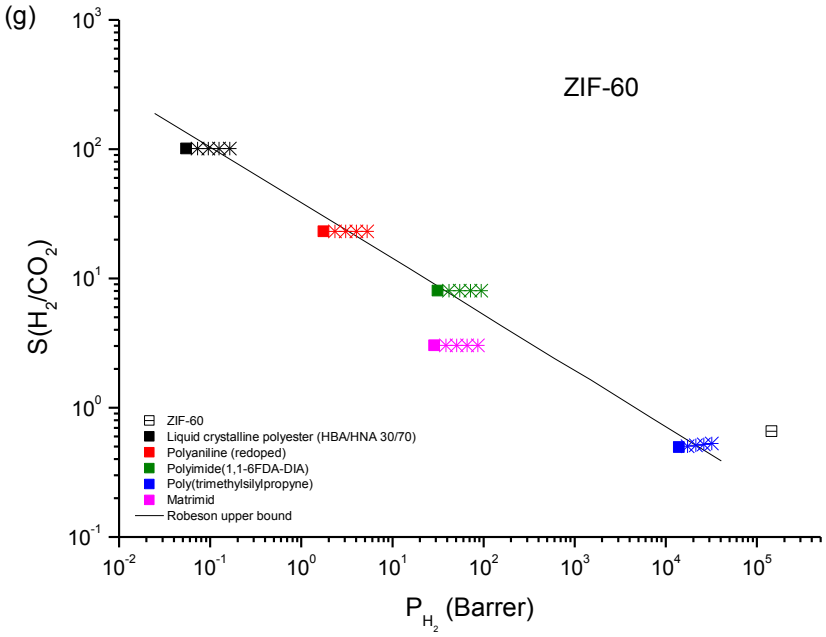
(g)
ZIF-60
S(H2/CO2)
PH2 (Barrer)
ZIF-60
Liquid crystalline polyester (HBA/HNA 30/70)
Polyaniline (redoped)
Polyimide(1,1-6FDA-DIA)
Poly(trimethylsilylpropyne)
Matrimid
Robeson upper bound

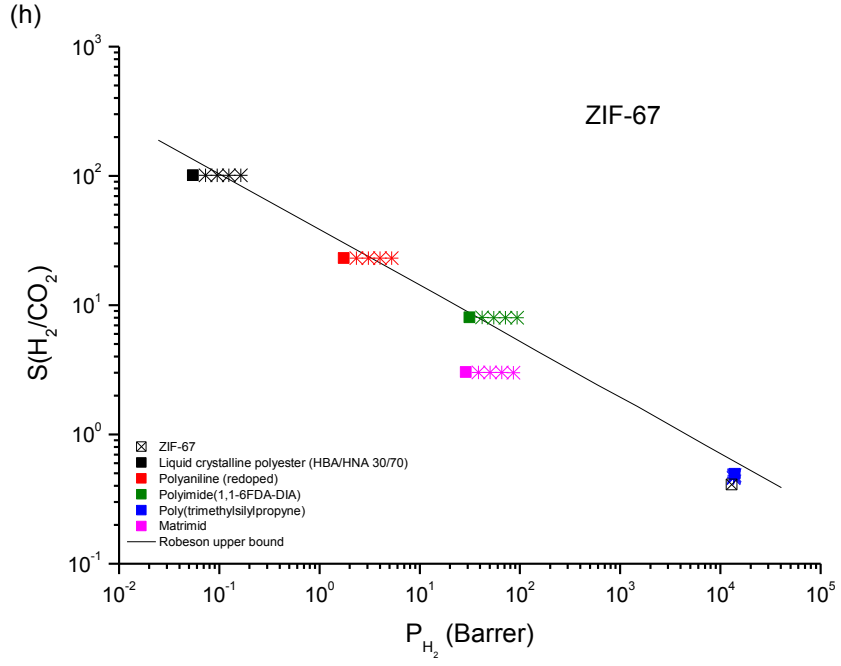
(h)
ZIF-67
S(H2/CO2)
PH2 (Barrer)
ZIF-67
Liquid crystalline polyester (HBA/HNA 30/70)
Polyaniline (redoped)
Polyimide(1,1-6FDA-DIA)
Poly(trimethylsilylpropyne)
Matrimid
Robeson upper bound

(i)

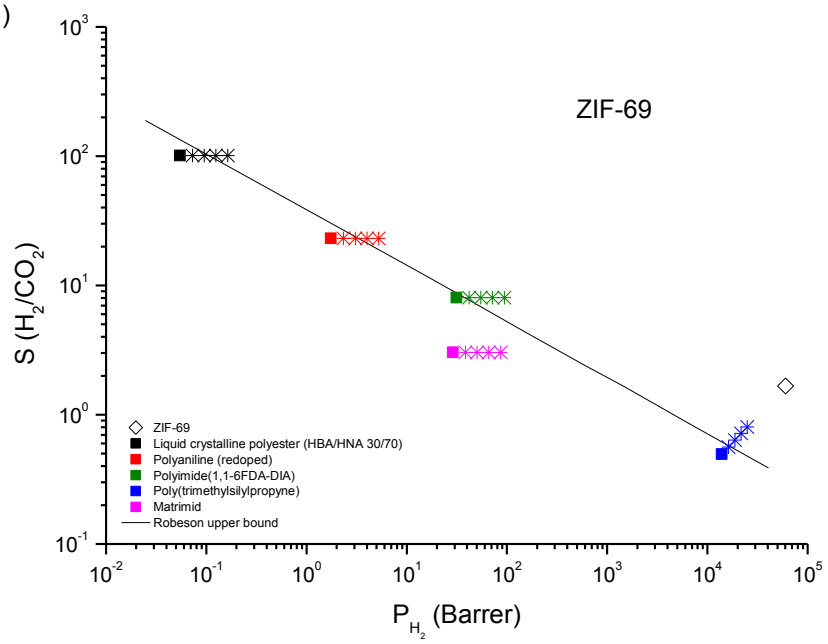
ZIF-69
S (H2/CO2)
PH2 (Barrer)
ZIF-69
Liquid crystalline polyester (HBA/HNA 30/70)
Polyaniline (redoped)
Polyimide(1,1-6FDA-DIA)
Poly(trimethylsilylpropyne)
Matrimid
Robeson upper bound

(j)

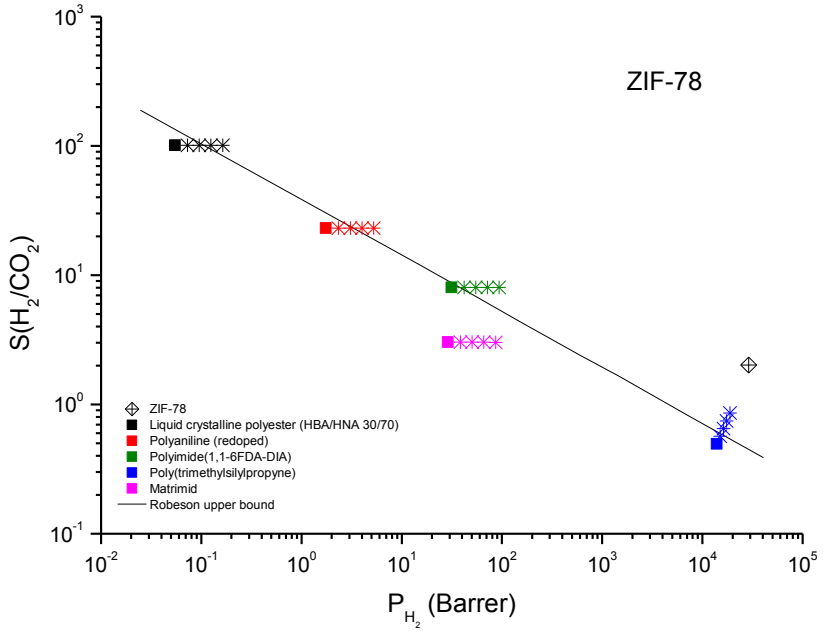
ZIF-78
S(H2/CO2)
PH2 (Barrer)
ZIF-78
Liquid crystalline polyester (HBA/HNA 30/70)
Polyaniline (redoped)
Polyimide(1,1-6FDA-DIA)
Poly(trimethylsilylpropyne)
Matrimid
Robeson upper bound

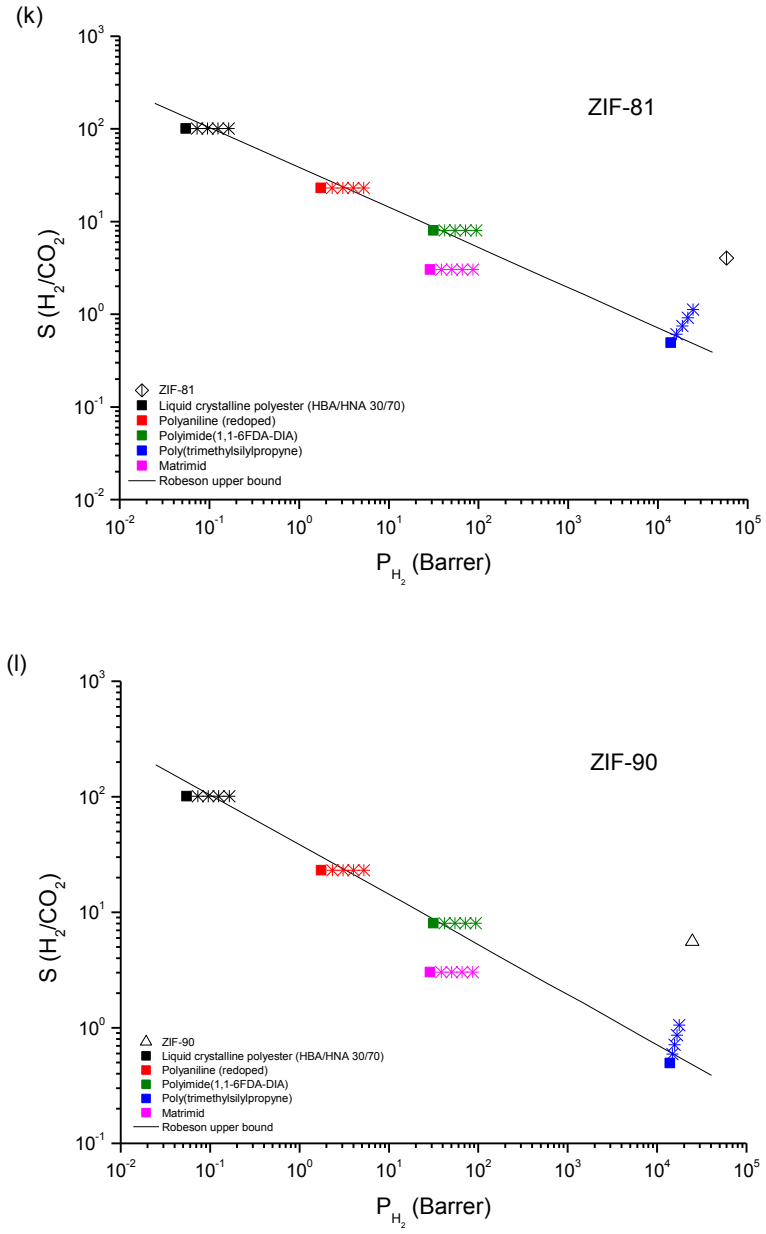

Figure D2: Performance of ZIF-based MMMs for H_2/CO_2 separation. Squares represent the performance of pure polymers and stars represent the performance of MMMs where the volume fraction of the fillers increases from 0.1 to 0.4.

(a)

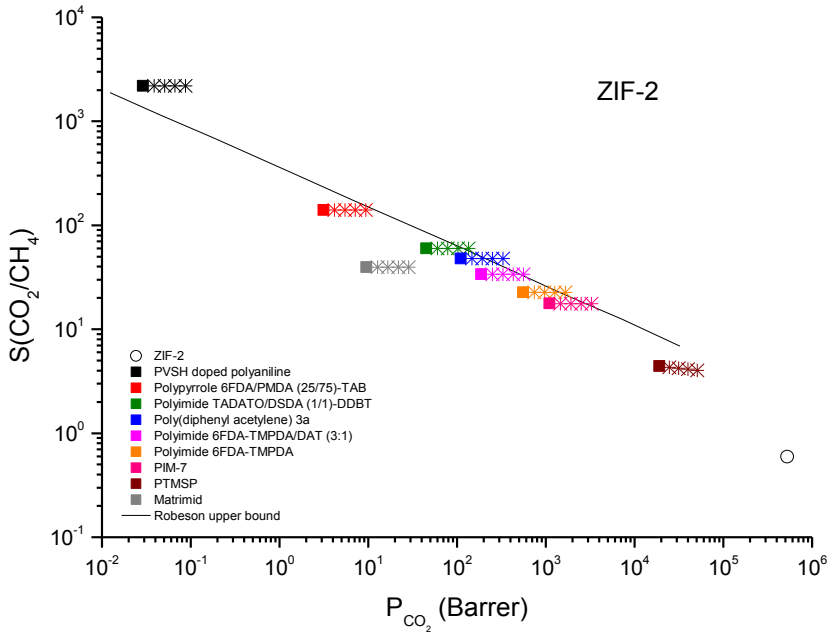
ZIF-2
ZIF-2
PVSH doped polyaniline
Polypyrrole 6FDA/PMDA (25/75)-TAB
Polyimide TADATO/DSDA (1/1)-DDBT
Poly(diphenyl acetylene) 3a
Polyimide 6FDA-TMPDA/DAT (3:1)
Polyimide 6FDA-TMPDA
PIM-7
PTMSP
Matrimid
Robeson upper bound
S(CO2/CH4)
PCO2 (Barrer)

(b)

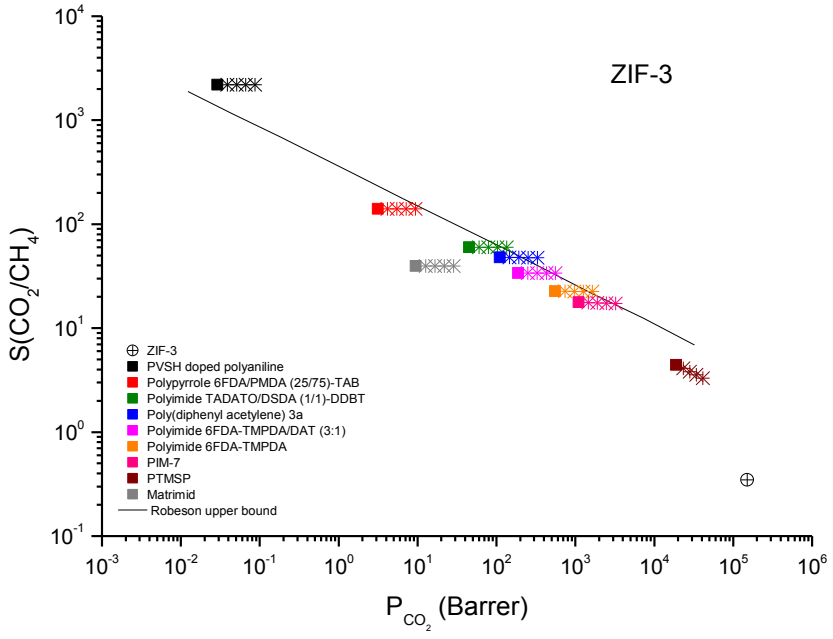
ZIF-3
ZIF-3
PVSH doped polyaniline
Polypyrrole 6FDA/PMDA (25/75)-TAB
Polyimide TADATO/DSDA (1/1)-DDBT
Poly(diphenyl acetylene) 3a
Polyimide 6FDA-TMPDA/DAT (3:1)
Polyimide 6FDA-TMPDA
PIM-7
PTMSP
Matrimid
Robeson upper bound
S(CO2/CH4)
PCO2 (Barrer)

(c)

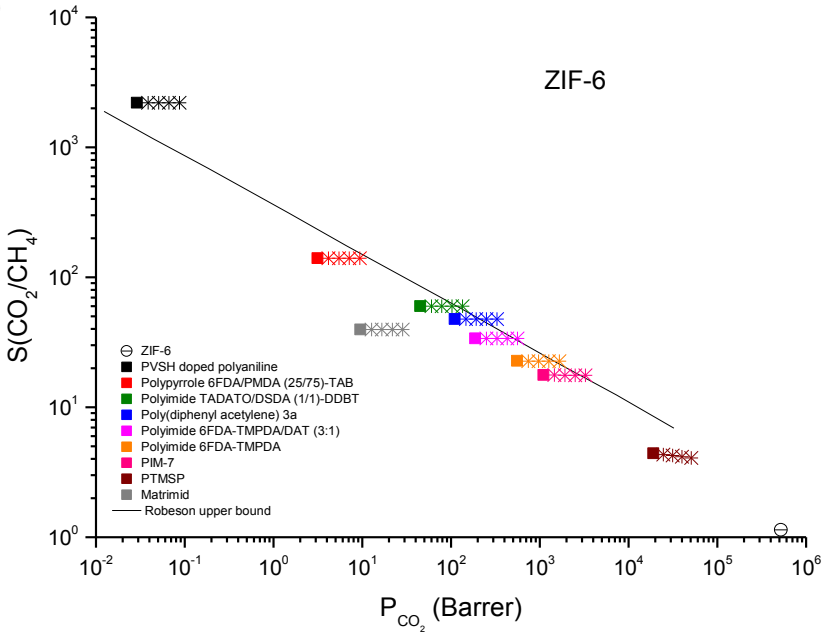
ZIF-6
S(CO2/CH4)
PCO2 (Barrer)
ZIF-6
PVSH doped polyaniline
Polypyrrole 6FDA/PMDA (25/75)-TAB
Polyimide TADATO/DSDA (1/1)-DDBT
Poly(diphenyl acetylene) 3a
Polyimide 6FDA-TMPDA/DAT (3:1)
Polyimide 6FDA-TMPDA
PIM-7
PTMSP
Matrimid
Robeson upper bound

(d)

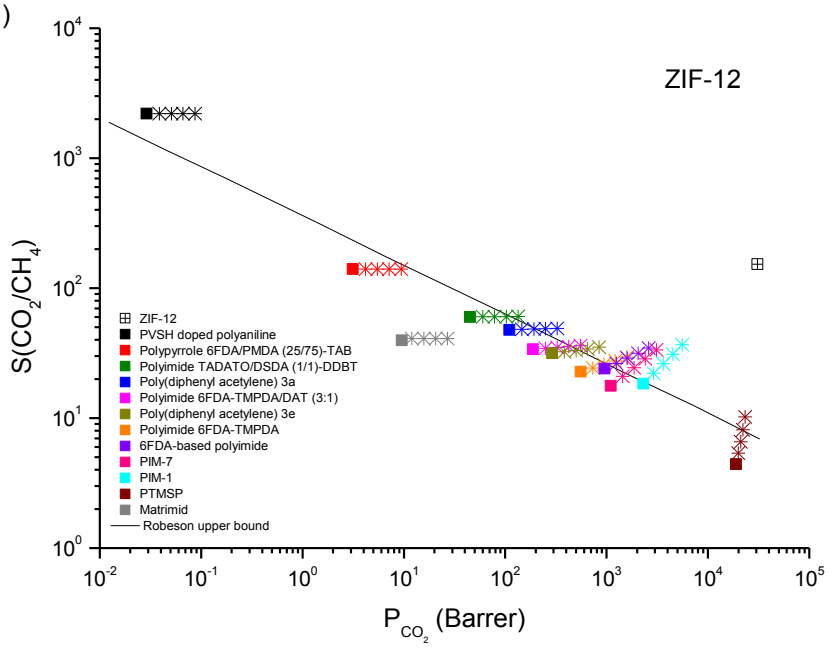
ZIF-12
S(CO2/CH4)
PCO2 (Barrer)
ZIF-12
PVSH doped polyaniline
Polypyrrole 6FDA/PMDA (25/75)-TAB
Polyimide TADATO/DSDA (1/1)-DDBT
Poly(diphenyl acetylene) 3a
Polyimide 6FDA-TMPDA/DAT (3:1)
Poly(diphenyl acetylene) 3e
Polyimide 6FDA-TMPDA
6FDA-based polyimide
PIM-7
PIM-1
PTMSP
Matrimid
Robeson upper bound

(e)

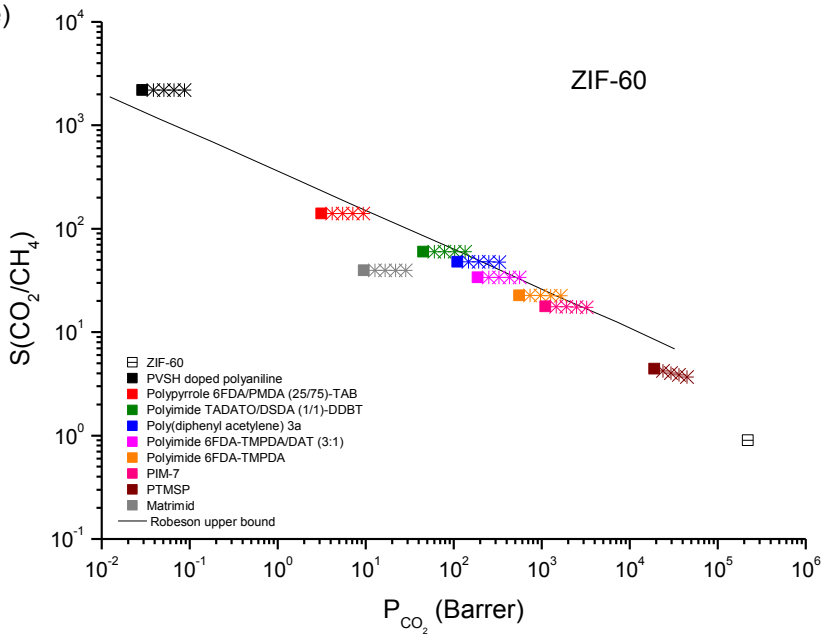
ZIF-60
S(CO2/CH4)
PCO2 (Barrer)
ZIF-60
PVSH doped polyaniline
Polypyrrole 6FDA/PMDA (25/75)-TAB
Polyimide TADATO/DSDA (1/1)-DDBT
Poly(diphenyl acetylene) 3a
Polyimide 6FDA-TMPDA/DAT (3:1)
Polyimide 6FDA-TMPDA
PIM-7
PTMSP
Matrimid
Robeson upper bound

(f)

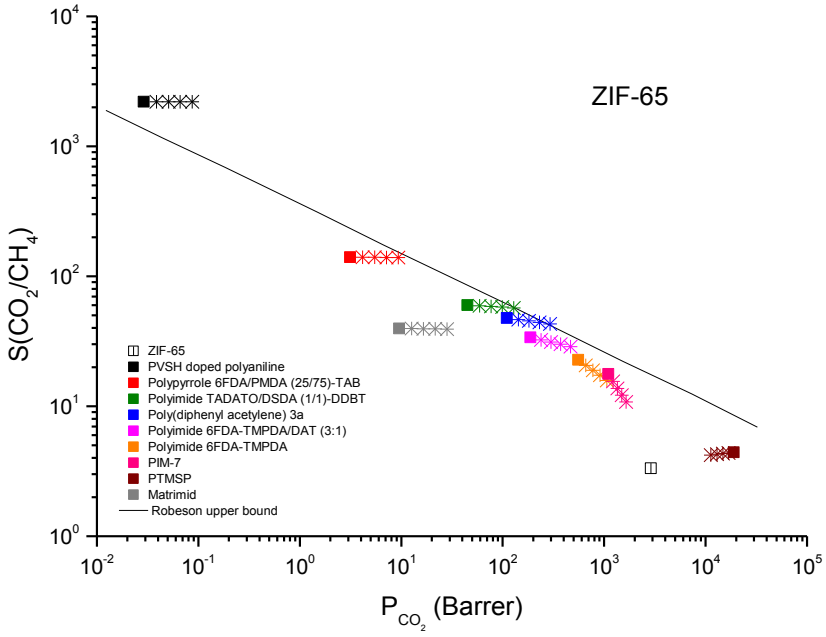
ZIF-65
S(CO2/CH4)
PCO2 (Barrer)
ZIF-65
PVSH doped polyaniline
Polypyrrole 6FDA/PMDA (25/75)-TAB
Polyimide TADATO/DSDA (1/1)-DDBT
Poly(diphenyl acetylene) 3a
Polyimide 6FDA-TMPDA/DAT (3:1)
Polyimide 6FDA-TMPDA
PIM-7
PTMSP
Matrimid
Robeson upper bound

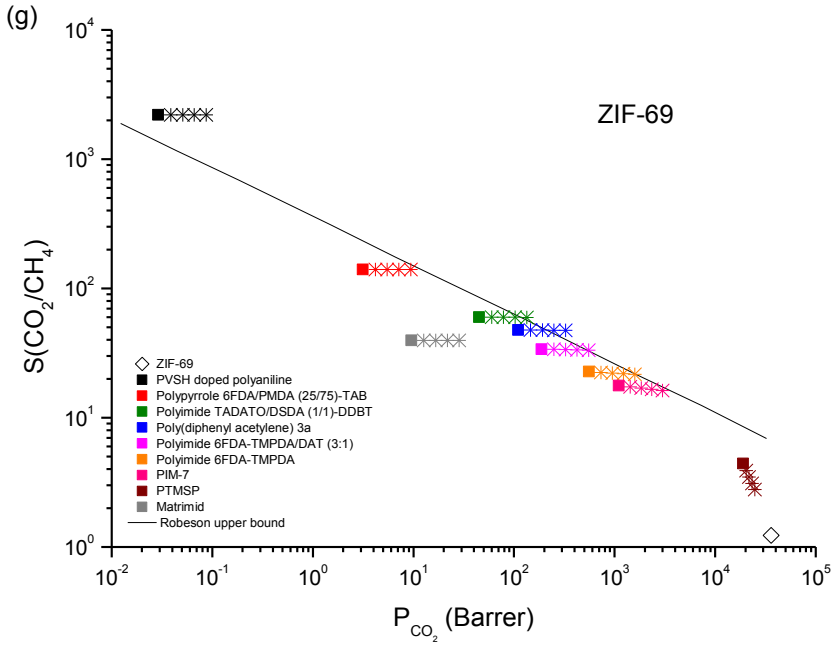
(g)
ZIF-69
S(CO2/CH4)
PCO2 (Barrer)
ZIF-69
PVSH doped polyaniline
Polypyrrole 6FDA/PMDA (25/75)-TAB
Polyimide TADATO/DSDA (1/1)-DDBT
Poly(diphenyl acetylene) 3a
Polyimide 6FDA-TMPDA/DAT (3:1)
Polyimide 6FDA-TMPDA
PIM-7
PTMSP
Matrimid
Robeson upper bound

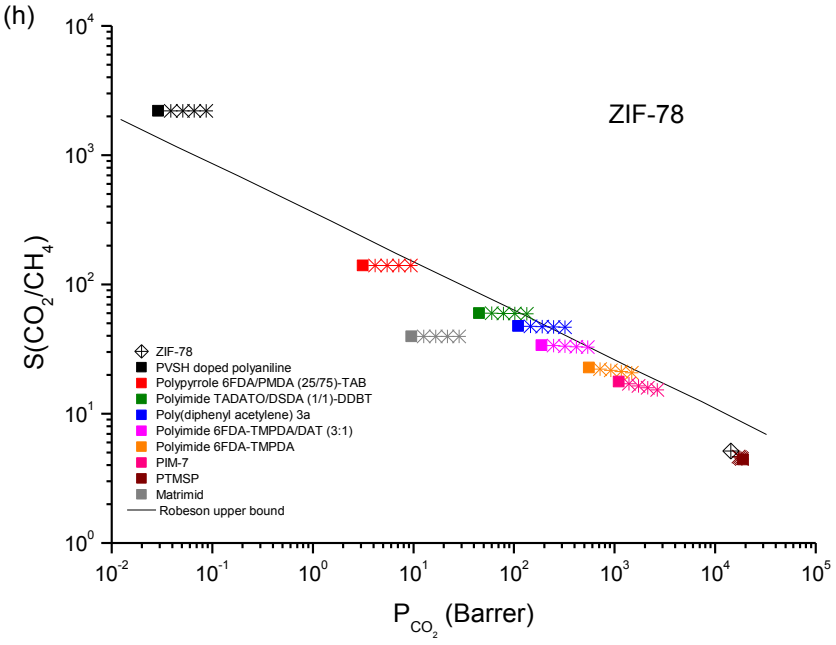
(h)
ZIF-78
S(CO2/CH4)
PCO2 (Barrer)
ZIF-78
PVSH doped polyaniline
Polypyrrole 6FDA/PMDA (25/75)-TAB
Polyimide TADATO/DSDA (1/1)-DDBT
Poly(diphenyl acetylene) 3a
Polyimide 6FDA-TMPDA/DAT (3:1)
Polyimide 6FDA-TMPDA
PIM-7
PTMSP
Matrimid
Robeson upper bound

(i)

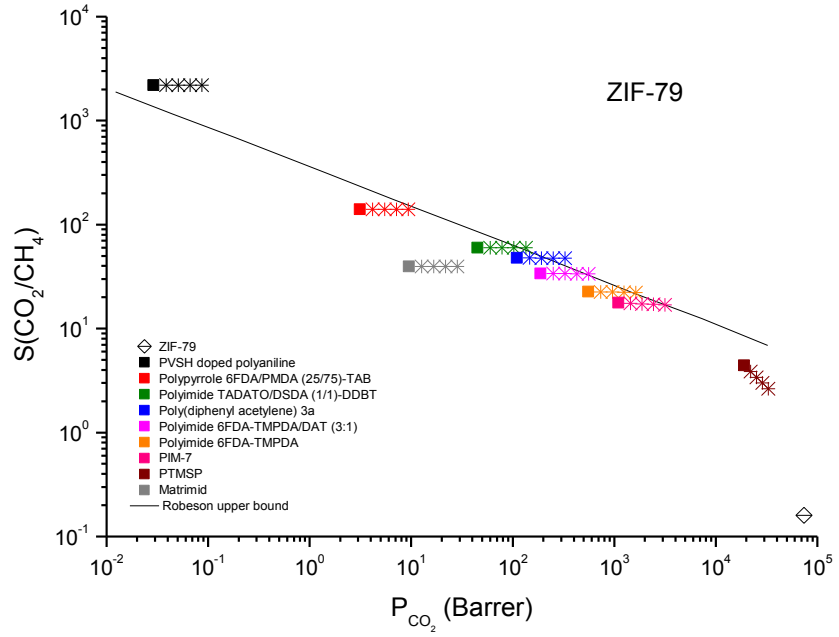
ZIF-79
ZIF-79
PVSH doped polyaniline
Polypyrrole 6FDA/PMDA (25/75)-TAB
Polyimide TADATO/DSDA (1/1)-DDBT
Poly(diphenyl acetylene) 3a
Polyimide 6FDA-TMPDA/DAT (3:1)
Polyimide 6FDA-TMPDA
PIM-7
PTMSP
Matrimid
Robeson upper bound
S(CO2/CH4)
PCO2 (Barrer)

(j)

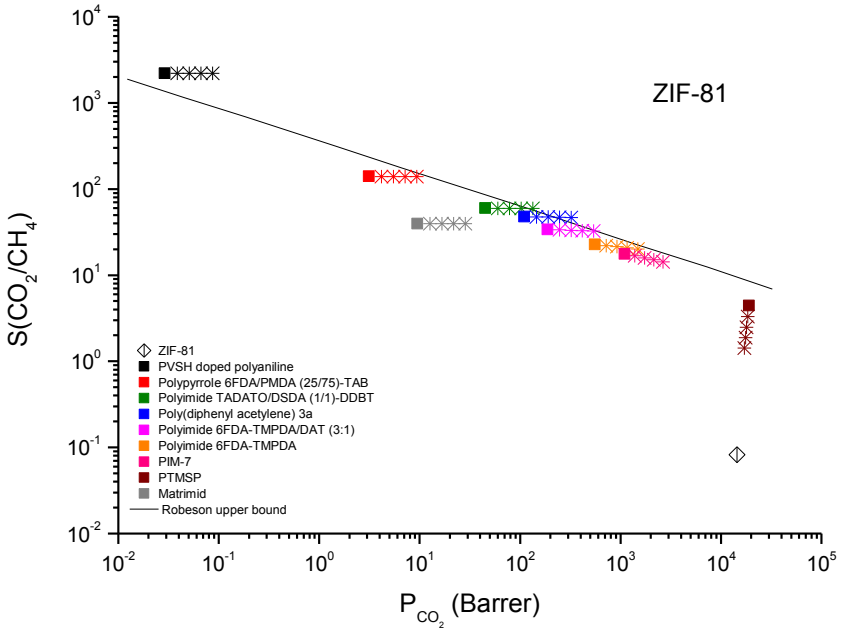
ZIF-81
ZIF-81
PVSH doped polyaniline
Polypyrrole 6FDA/PMDA (25/75)-TAB
Polyimide TADATO/DSDA (1/1)-DDBT
Poly(diphenyl acetylene) 3a
Polyimide 6FDA-TMPDA/DAT (3:1)
Polyimide 6FDA-TMPDA
PIM-7
PTMSP
Matrimid
Robeson upper bound
S(CO2/CH4)
PCO2 (Barrer)

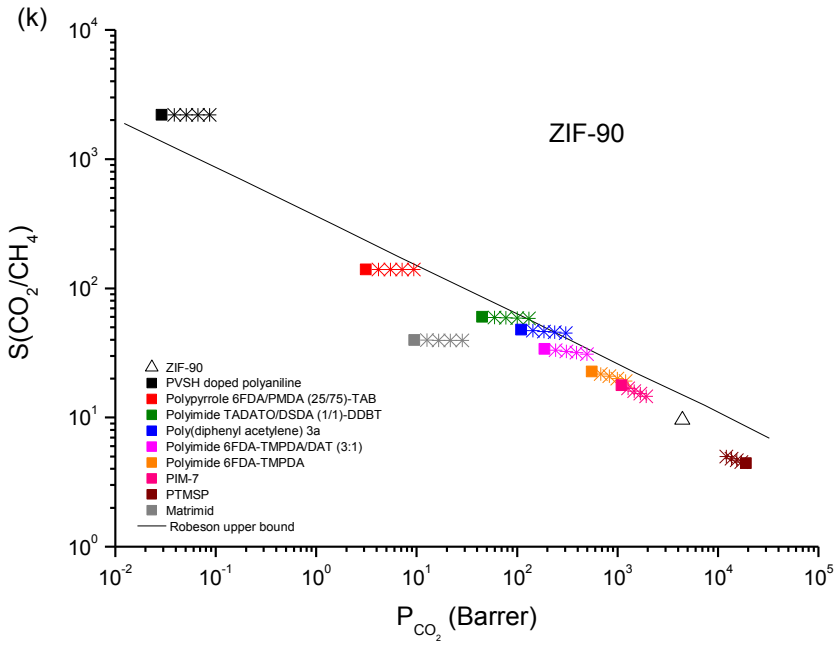

Figure D3: Performance of ZIF-based MMMs for CO_2/CH_4 separation. Squares represent the performance of pure polymers and stars represent the performance of MMMs where the volume fraction of the fillers increases from 0.1 to 0.4.

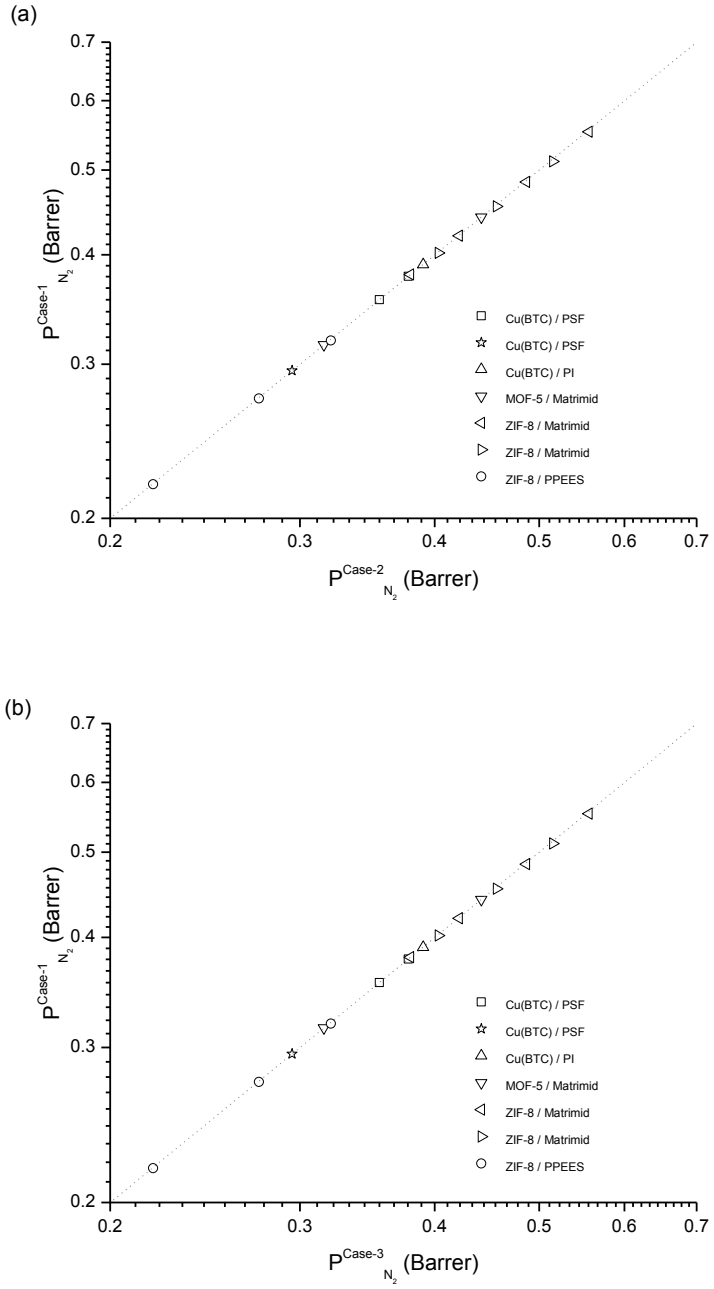

Figure D4: Predicted N_2 permeabilities in CuBTC, MOF-5 and ZIF-8-based MMMs for (a) Case-1 vs. Case-2 and (b) Case-1 vs. Case 3.

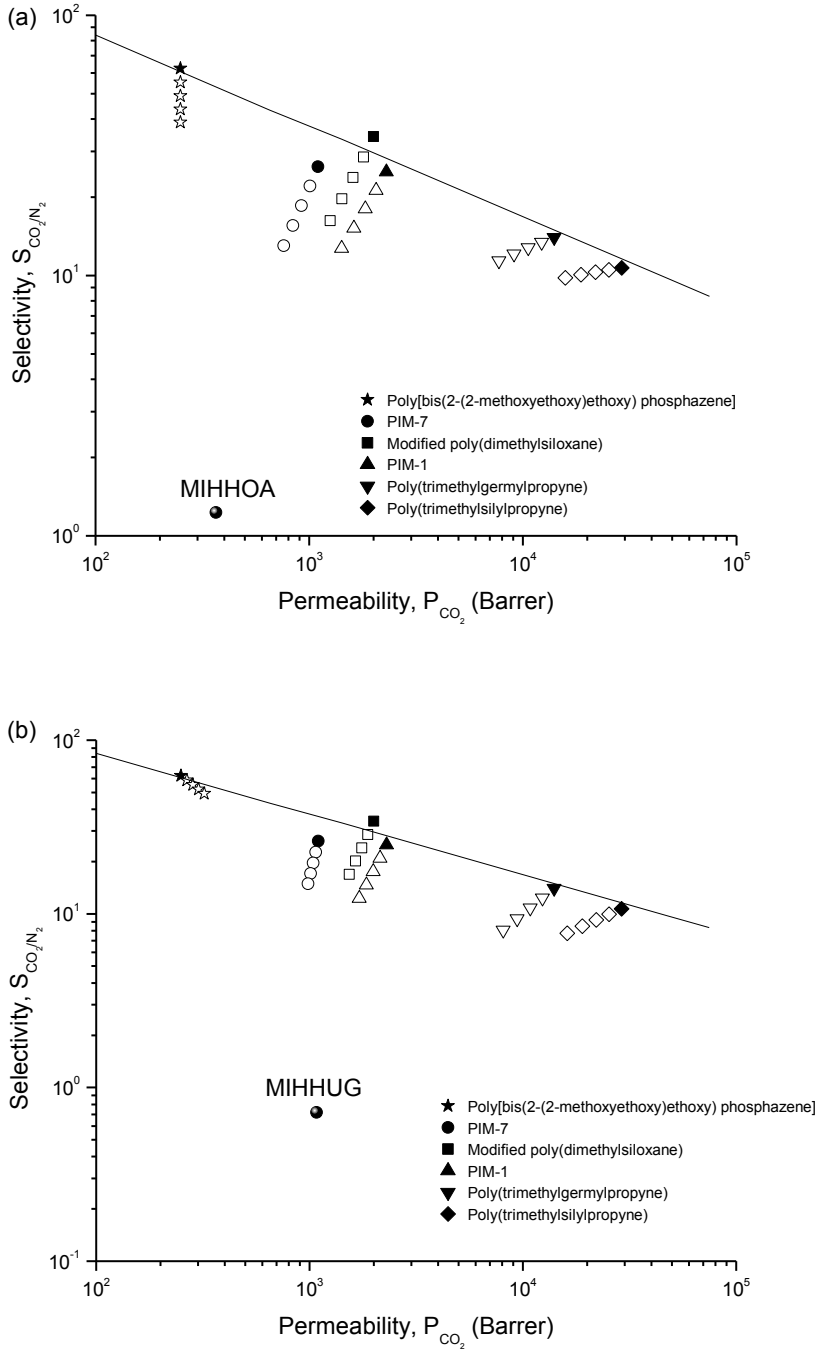
(a)
Selectivity, S_{CO_2/N_2}
Permeability, P_{CO_2} (Barrer)
MIHHOA
Poly[bis(2-(2-methoxyethoxy)ethoxy) phosphazene]
PIM-7
Modified poly(dimethylsiloxane)
PIM-1
Poly(trimethylgermylpropyne)
Poly(trimethylsilylpropyne)
(b)
Selectivity, S_{CO_2/N_2}
Permeability, P_{CO_2} (Barrer)
MIHHUG
Poly[bis(2-(2-methoxyethoxy)ethoxy) phosphazene]
PIM-7
Modified poly(dimethylsiloxane)
PIM-1
Poly(trimethylgermylpropyne)
Poly(trimethylsilylpropyne)

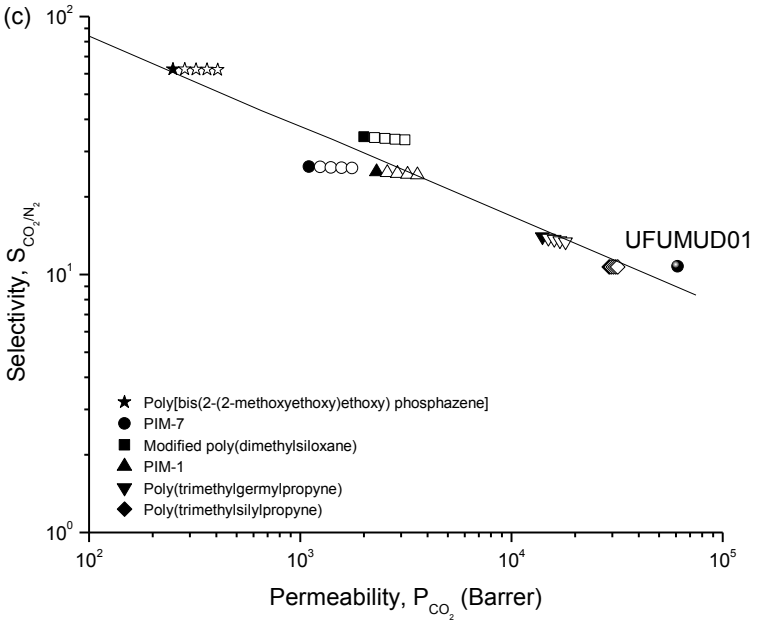
(c)
Selectivity, S_{CO_2/N_2}
Permeability, P_{CO_2} (Barrer)
UFUMUD01
Poly[bis(2-(2-methoxyethoxy)ethoxy) phosphazene]
PIM-7
Modified poly(dimethylsiloxane)
PIM-1
Poly(trimethylgermylpropyne)
Poly(trimethylsilylpropyne)

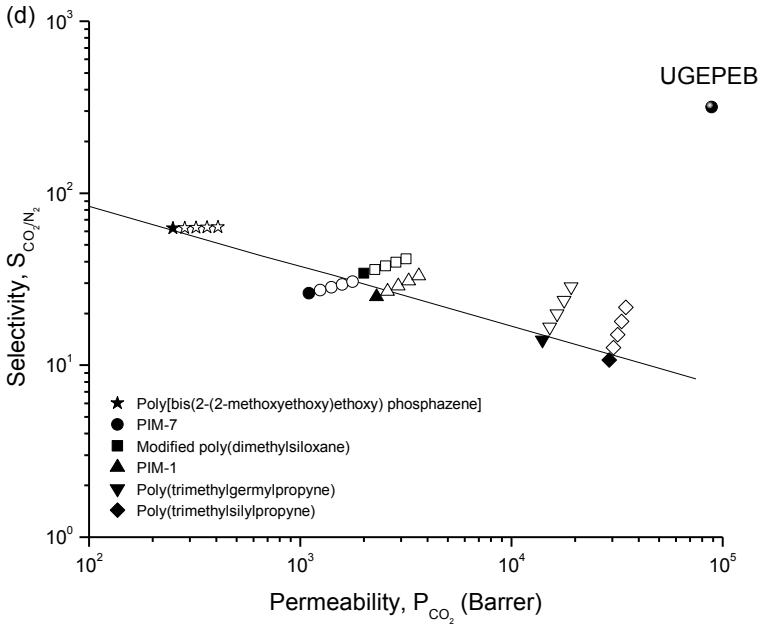
(d)
Selectivity, S_{CO_2/N_2}
Permeability, P_{CO_2} (Barrer)
UGEPEB
Poly[bis(2-(2-methoxyethoxy)ethoxy) phosphazene]
PIM-7
Modified poly(dimethylsiloxane)
PIM-1
Poly(trimethylgermylpropyne)
Poly(trimethylsilylpropyne)

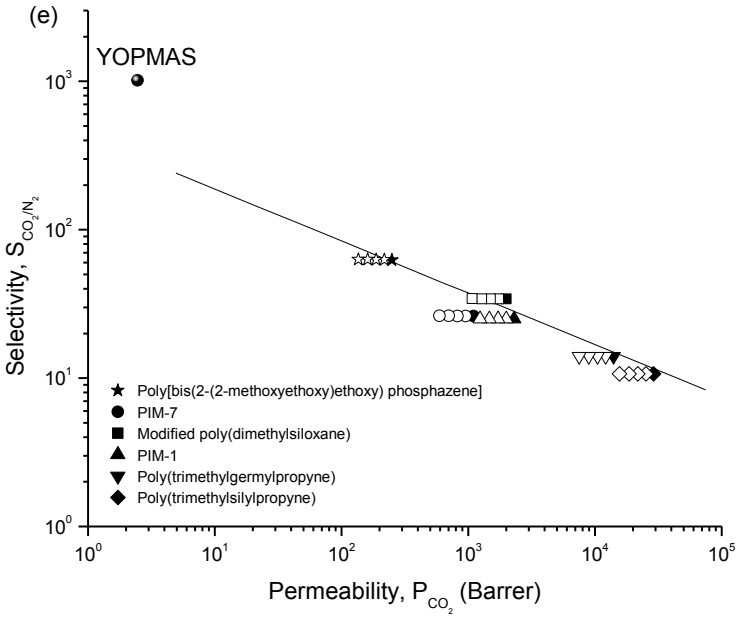
(e)
YOPMAS
Selectivity, S_{CO_2/N_2}
Permeability, P_{CO_2} (Barrer)
Poly[bis(2-(2-methoxyethoxy)ethoxy) phosphazene]
PIM-7
Modified poly(dimethylsiloxane)
PIM-1
Poly(trimethylgermylpropyne)
Poly(trimethylsilylpropyne)

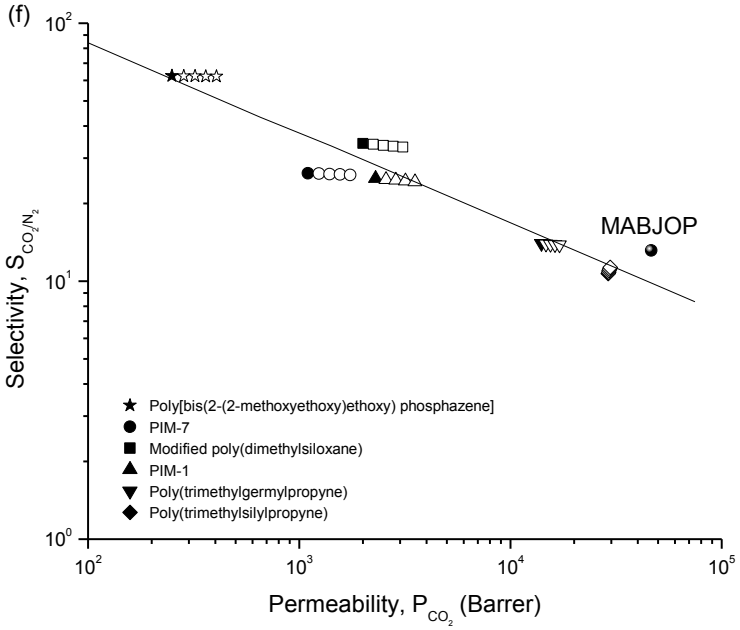
(f)
MABJOP
Selectivity, S_{CO_2/N_2}
Permeability, P_{CO_2} (Barrer)
Poly[bis(2-(2-methoxyethoxy)ethoxy) phosphazene]
PIM-7
Modified poly(dimethylsiloxane)
PIM-1
Poly(trimethylgermylpropyne)
Poly(trimethylsilylpropyne)

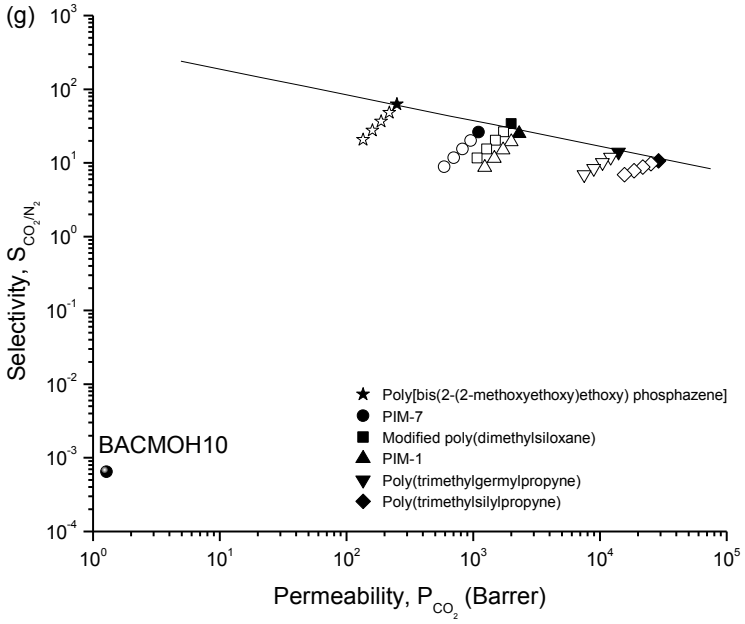
(g)
Selectivity, S_{CO_2/N_2}
Permeability, P_{CO_2} (Barrer)
BACMOH10
Poly[bis(2-(2-methoxyethoxy)ethoxy) phosphazene]
PIM-7
Modified poly(dimethylsiloxane)
PIM-1
Poly(trimethylgermylpropyne)
Poly(trimethylsilylpropyne)

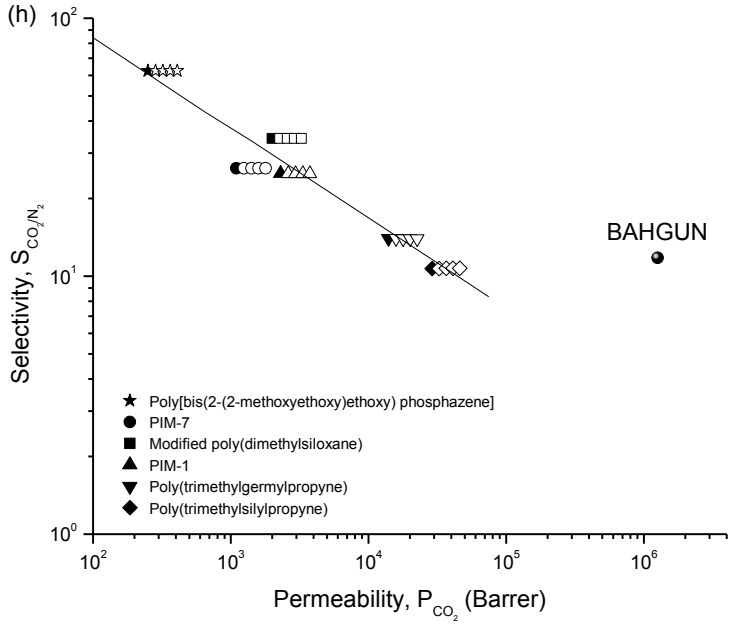
(h)
Selectivity, S_{CO_2/N_2}
Permeability, P_{CO_2} (Barrer)
BAHGUN
Poly[bis(2-(2-methoxyethoxy)ethoxy) phosphazene]
PIM-7
Modified poly(dimethylsiloxane)
PIM-1
Poly(trimethylgermylpropyne)
Poly(trimethylsilylpropyne)

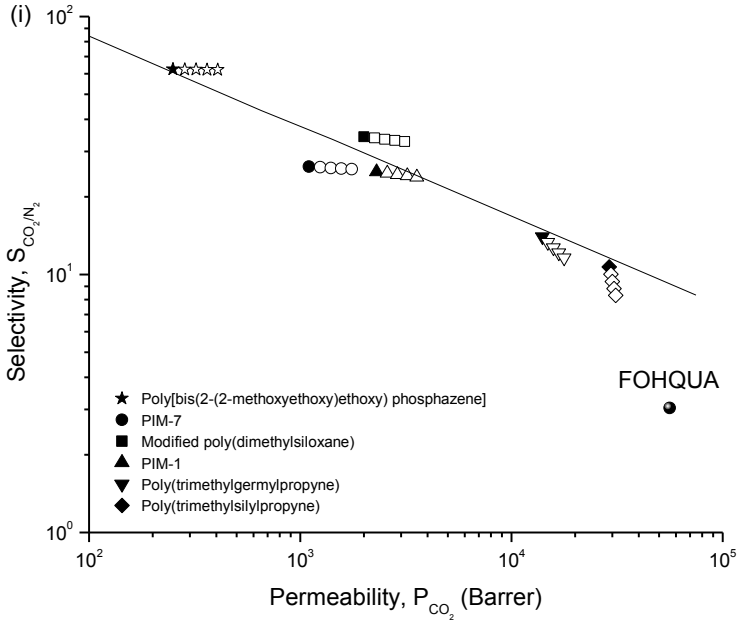
(i)
Selectivity, S_{CO_2/N_2}
Permeability, P_{CO_2} (Barrer)
FOHQUA
Poly[bis(2-(2-methoxyethoxy)ethoxy) phosphazene]
PIM-7
Modified poly(dimethylsiloxane)
PIM-1
Poly(trimethylgermylpropyne)
Poly(trimethylsilylpropyne)

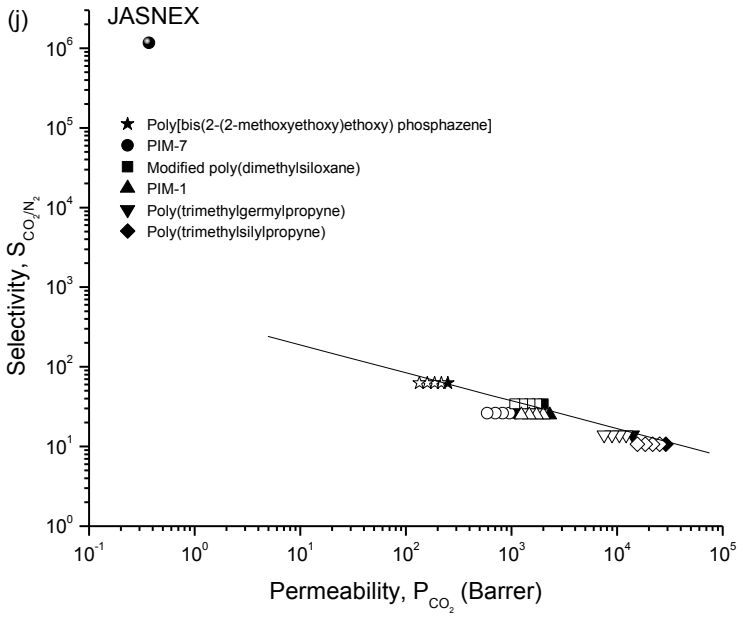
(j)
JASNEX
Selectivity, S_{CO_2/N_2}
Permeability, P_{CO_2} (Barrer)
Poly[bis(2-(2-methoxyethoxy)ethoxy) phosphazene]
PIM-7
Modified poly(dimethylsiloxane)
PIM-1
Poly(trimethylgermylpropyne)
Poly(trimethylsilylpropyne)

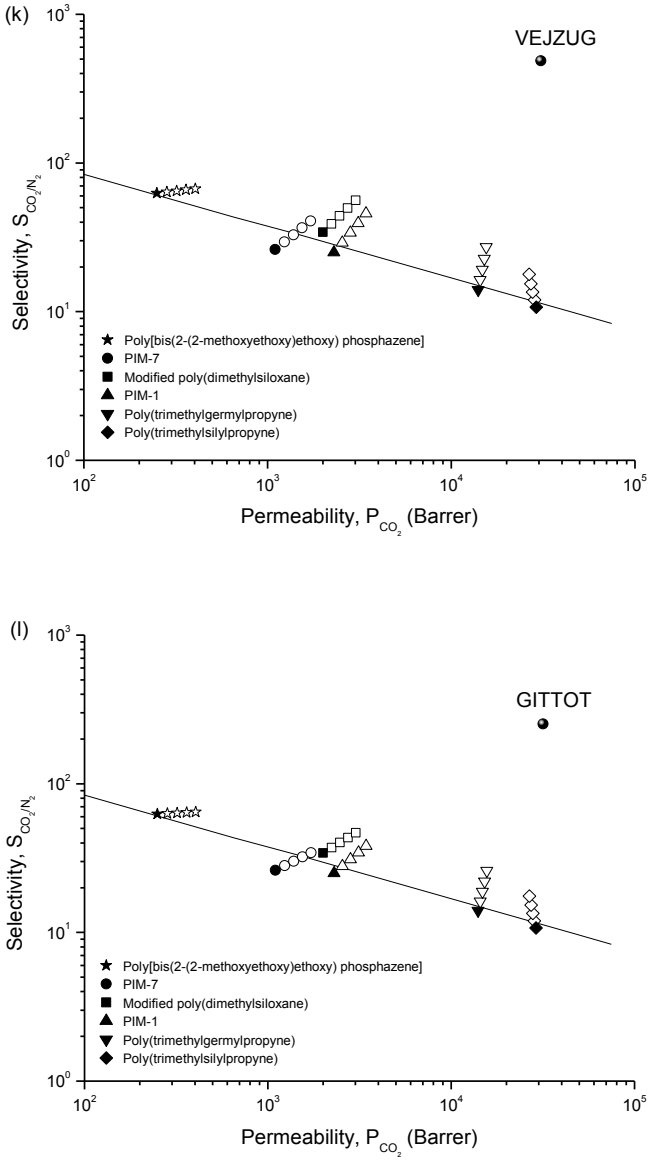

Figure D5: Performances of ZIF and MOF-based MMMs for CO_2/N_2 separation. The closed symbols represent the performance of pure polymers. The open symbols represent the performance of MOF-based MMMs where the volume fraction of the fillers increases from 0.1 to 0.4.

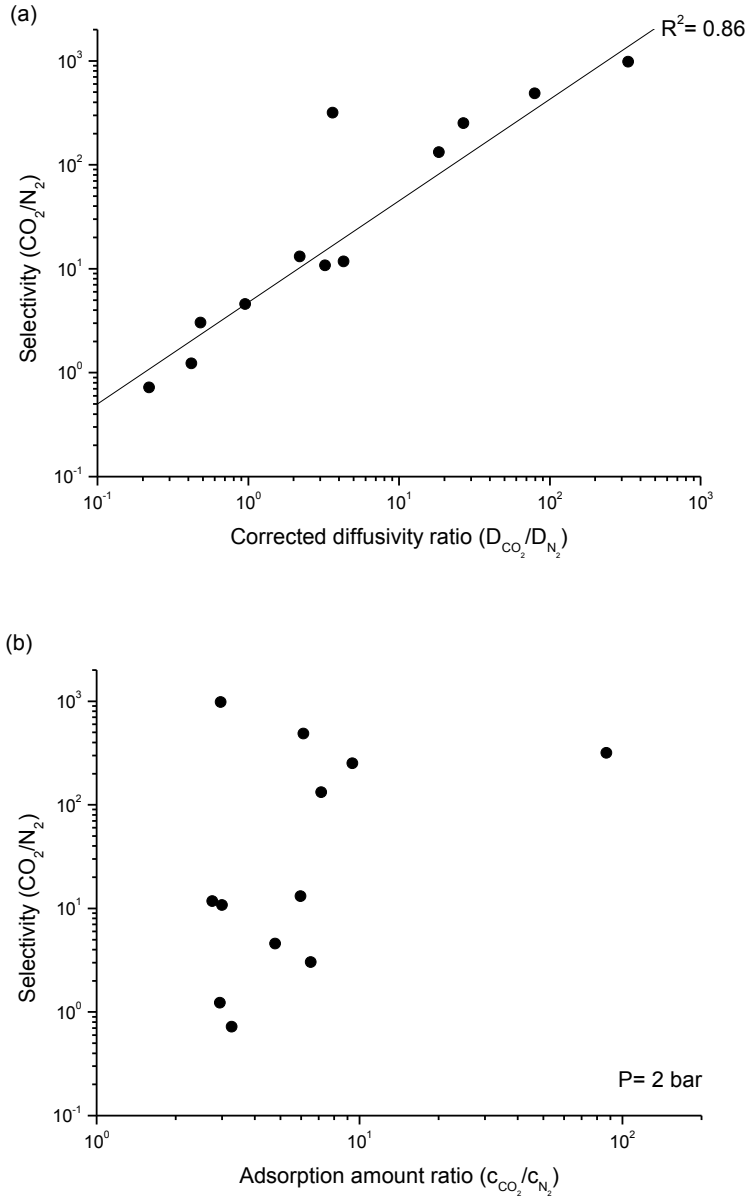

Figure D6: Relation between the selectivity of MOFs and (a) ratio of corrected diffusivity of gases, (b) ratio of loading of gases.